CORSO DI DOTTORATO DI RICERCA IN

“GENETICA E BIOLOGIA CELLULARE”

XXII CICLO

Cell growth density affects the structural and functional properties of Caco-2 differentiated monolayer

BIO/11

Coordinatore: Prof. Giorgio PRANTERA
(Dip. Agrobiologia e Agrochimica, Univ. La Tuscia, Viterbo)

Tutor: Dr. Armando FELSANI
(CNR - INMM, Roma).

Dottorando:
Manuela NATOLI

Table of content

Abstract

The human intestinal Caco-2 cell line has been extensively used as a model of the intestinal barrier. However, it is widely reported in literature that culture-related conditions, as well as the different Caco-2 cell lines utilized in different laboratories, often lead to problems of reproducibility making difficult to compare results. We developed a new cell-growth protocol in which Caco-2 cells were subcultured at 50% of confluence (Low Density, LD) instead of 90% of confluence, as usually reported in literature (High Density, HD). Using this new protocol, Caco-2 cells retained a higher proliferation potential resulting in a cell population, which, reaching confluence was able to differentiate almost synchronously, forming a more homogeneous and perfectly polarized cell monolayer, as compared to that obtained with the HD cells. This comparison has been done by analyzing the gene expression and the structural characteristics of the 21-days differentiated monolayers by microarrays hybridization and by confocal microscopy.

We then investigated if these differences could also modify the effects of toxicants on 21-days-differentiated LD and HD cells. We analyzed the 2 hours-acute toxicity of $CuCl_2$ in terms of actin depolymerization and MT2A (metallothionein 2A) and HSPA1A (heat shock protein 70) genes induction. Copper treatment resulted in different levels of actin depolymerization and gene expression induction in relationship with the culture protocol, the LD cells showing a more homogeneous and stronger response. Our results suggest that cell growth density could influence a number of morphological and physiological properties of differentiated Caco-2 cells and these effects must be taken in account when these cells are used as intestinal model.

Sommario

Le cellule intestinali umani Caco-2 sono largamente utilizzate come modello *in vitro* della barriera intestinale negli studi di farmacocinetica e farmacodinamica; tuttavia in letteratura è riportata l'alta variabilità di questo modello riguardo alle condizioni di coltura cellulare e i cloni di Caco-2 che sono utilizzati. In questo lavoro è stato sviluppato un nuovo protocollo di mantenimento della linea cellulare che prevede la sottocoltura delle cellule quando nella piastra di coltura si raggiunge il 50% di confluenza (Low Density, LD) piuttosto che il consueto 90% (High Density, HD) riportato in letteratura.

Utilizzando questo protocollo (LD) le cellule Caco-2 mantengono un alto potenziale proliferativo che produce un'omogeneità nell'inizio del differenziamento e quindi una strutturazione più omogenea del monostrato cellulare durante e alla fine del differenziamento. Abbiamo quindi condotto uno studio di comparazione delle cellule Caco-2 LD e HD a livello morfologico tramite microscopia confocale e a livello genico tramite la tecnologia microarray.

In seguito abbiamo condotto uno studio fisiologico di risposta tossica andando ad analizzare le differenze tra le cellule HD e LD durante e dopo l'esposizione del monostrato differenziato a concentrazioni crescenti di cloruro di rame. Abbiamo analizzato nelle due ora la depolimerizzazione dell'actina filamentosa tramite microscopia e l'induzione genica di metallotioneina 2A (MT2A) e heat shock protein 70 (HSPA1A). Il trattamento con rame ha evidenziato una differente sensibilità del modello alle concentrazioni utilizzate con una risposta fisiologica più omogenea nelle cellule LD.

In conclusione i nostri risultati suggeriscono una diretta influenza delle procedure di mantenimento della linea cellulare sulle caratteristiche morfologiche e fisiologiche delle cellule Caco-2; queste differenze non possono quindi essere trascurate nel momento in cui questa linea cellulare è utilizzata come modello intestinale umano in vitro negli studi di predittività dei farmaci.

To my family

Edoardo and my cats…

Introduction

In the last twenty years animal experimentation has been supplemented and in some cases replaced with *in vitro* models in particular in the branch of pharmacokinetics and pharmacodynamics. Advances in combinatorial chemistry have revolutionized the field of drug discovery, producing an increasing number of compounds which need to be tested. In this context, the US Food and Drug Administration (FDA) developed a new guideline for bioequivalence studies based on the biopharmaceutical classification system (BCS) in which solubility and permeability are considered fundamental properties to define the rate of absorption of the active ingredient of a drug product (van de Waterbeemd, 1998).

To define these two parameters, many studies on intestine *in vitro* models have been done in the context of the FDA directive and many cell lines are still under investigation to define the best predictive models for biopharmaceutical studies.

The human Caco-2 cell line is one of the most used cell model to study absorption, metabolism and bioavailability of drugs and xenobiotics (Artursson et al., 2001). Notwithstanding it represents a well established and accepted in vitro model for the human intestinal epithelium and its use is recognized by the FDA (Kim et al., 2006; van de Waterbeemd, 1998), many papers claim that cell culture conditions, such as the composition of the medium and the culturing system adopted, as well as the passage number, could affect Caco-2 cells differentiation and transport properties (Sambuy et al., 2005; Briske-Anderson et al., 1997). The Caco-2 cell population maintained in culture is characterized by an intraclonal variability revealed by the presence of subpopulations with different morphologies (Vachon and Beaulieu, 1992) and different physiological characteristics (Vachon et al., 1996; Mahraoui et al., 1992).This property of Caco-2 cells led to the existence of different clones maintained in different laboratories. This fact plus the variability of culture protocols often makes the comparison of results obtained in different laboratories particularly difficult.

In the last few years many studies have been focused on the inter-laboratories variability produced by the cell-culture related factors such as the animal serum used, the supplements added to the culture media, the passage number and the source of the clones (Zucco et al., 2005; Briske-Anderson et al., 1997). Although all these studies underlined the importance of the cell-culture related factors for the reproducibility between

laboratories, up to date, there are no studies that focused on the necessity to standardize the protocols used to manage the propagation of this cell line.

Caco-2 cells differentiate spontaneously in culture without supplementation of differentiating factors and, usually, standard protocols recommend to split cell cultures when they have almost reached the confluence. In a cell model in which the start of differentiation is not under the operator control, it is probable that the intraclonal variability could be strongly influenced by the degree of confluence decided in that particular laboratory.

Since the Caco-2 cell line still remains one of the best choices to study the intestinal physiology, the aim of this study is to define how the splitting confluence could influence the capability of this cell line to differentiate correctly in a structurally and functionally mature enterocyte.

The intestine: morphology and functions

The intestine is a highly coiled muscular tube secured to the peritoneum in the abdominal cavity; in humans we can divide the intestine in two portions: small (6-7 meters) and large (1.5 meters). In the small intestine the whole process of nutrient absorption is carried out, while in the large intestine occurs the recovery of water and minerals that serves the digestion.

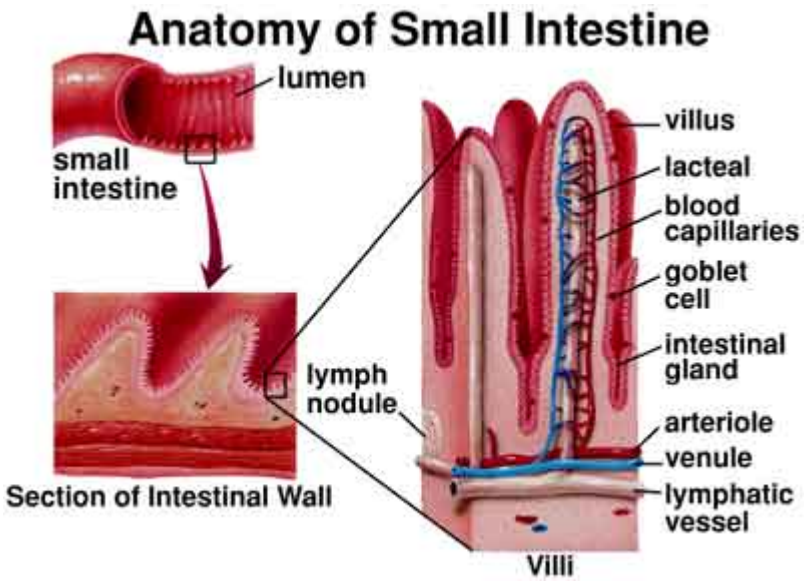

Fig 1 *Anatomy of small intestine*

The small intestine is further divided in three segments according to the functions they perform: *duodenum* (in which are conveyed secretions of liver and pancreas), *jejunum* (in which nutrients are digested to small organic molecules and absorbed into the bloodstream) and *ilium* (where the absorbing processes are completed).

The entire luminal surface of the small intestine has **villi**, small projections of mucosa. The villi are lined with simple columnar epithelial cells, also called **enterocytes**.

The enterocytes are tall cells with middle to basal nuclei and have an apical brush border, also known as microvilli. Both villi and microvilli function to increase the surface area for greater absorption.

Between each villus there are the crypts of Leiberkuhn, also known as intestinal glands, another component of the mucosa. These empty at the base of the villi and extend into the lamina propria. The crypts are lined with the same columnar epithelial cells (enterocytes) and goblet cells as the surface and also house stem cells for the replication of

all intestinal cell types. In the staminal compartment stem cells divide to generate two daughter cells of which the first will continue its staminal life while the latter will differentiate in the constituent cells of the villus.

Concerning the enterocytes they divide, differentiate and migrate up towards the tip of the villus, where they eventually exfoliate.

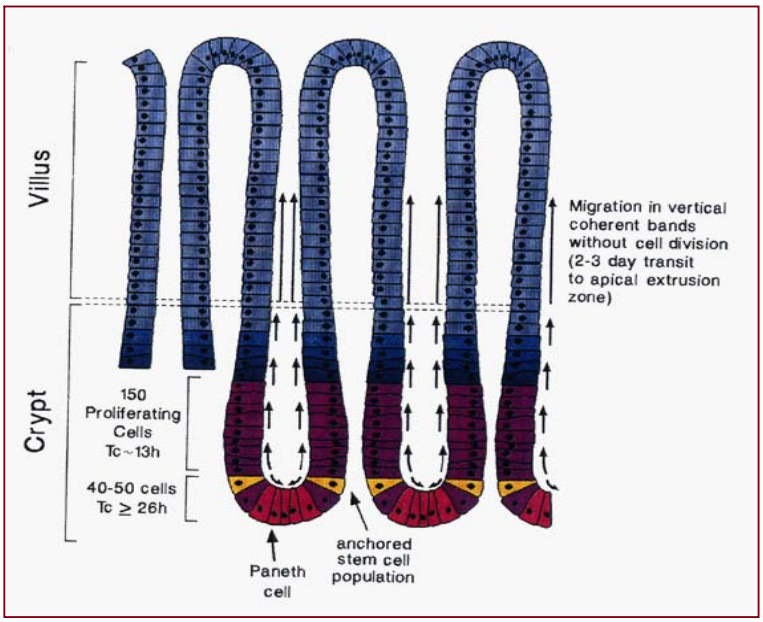

Fig 2 *Schematic representation of the migration of the ienterocyte along the cripta-villus direction (Gordon 1989*

Enteroendocrine paracrine cells are also located in the crypts. They secrete hormones into the capillaries that run through the lamina propria to locally regulate intestinal activity.

The enterocyte

Enterocytes are polarized prism-like cells with the apical compartment faced toward the lumen of the intestine and the basolateral compartment connected with the bloodstream.

The polarization of these cells is guaranteed by a well organized and structured network of intercellular junctions such as tight junctions, adherens junctions and desmosomes that divide the apical domain from the basolateral domain of the cell.

The nucleus is located at the base of the cell whereas the golgi apparatus and lysosomes are positioned in the supernuclear portion of the enterocyte.

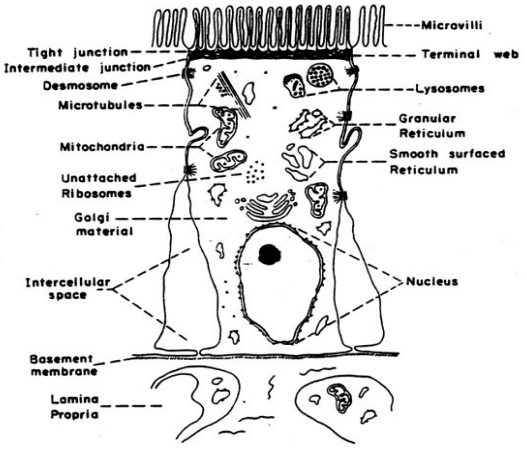

Fig 3 *Schematic representation of a mature enterocyte*

The apical domain of the enterocyte is distinguished by the presence of microvilli (that constitute the brush-border) and by the presence of the structural connecting tight junctions between cells.

The microvilli are constituted with an internal cytoskeleton of actin that run all over the length of the microvillus. This cytoskeleton is connected with its terminal web of intermediate filaments to a net of microtubules at the base of the microvillus.

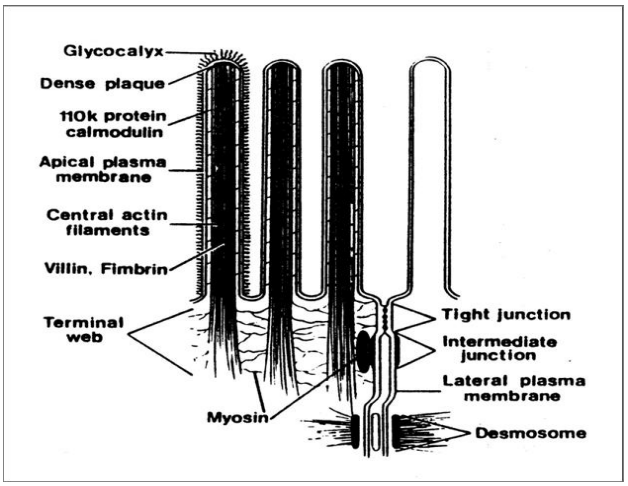

Fig 4 *cytosckeleton of the brush border*

The terminal web of the intermediate filaments is further connected to the entire enterocyte by proteic bridges between myosin type I and calmodulin (Cheney and

Mooseker, 1992); moreover filaments of actin are also connected to proteins villin and fimbrin (Mooseker, 1985). In particular villin is part of the microtubules and constitutes the internal portion of the microvillus.

The apical membrane of the enterocyte is directly involved in the interactions between cells and intestinal lumen and most of the enzymes and transporters crucial for the intestinal absorption are on the microvilli.

The enzymes can be divided according to their activity as: glicosidases (sucrase-isomaltase, lactase, maltase-glucoamidase, trealase); peptidases (aminopeptidase-N and A, dipeptil-peptidase IV) and the lipases.

The tight junctions

Tight junctions (TJ) form a continuous, circumferential, belt like structure at the luminal end of the intercellular space, where it serves as a gatekeeper of the paracellular pathway.

On the cytoplasmic side of the TJ, the TJ plaque is the site of a growing number of TJ-associated protein complexes. Within the confines of the TJ, the cell membranes of adjacent epithelial cells are brought into intimate focal contact sites in which the intercellular space is obliterated. Freeze-fracture electron microscopy reveals these to be a network of strands within the plane of the plasma membranes of neighboring cells.

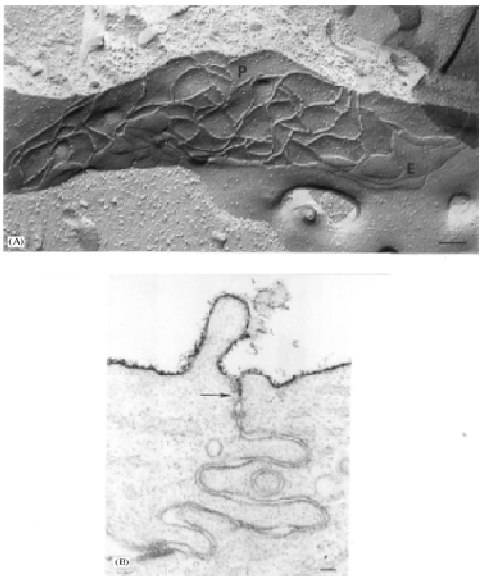

Fig 5 *Structure of tight junctions. A) electron microscopy image of tight junctions after freeze-fracture. B) Tight junction section*

The components constituting the multimolecular TJ complex may be divided into three groups: 1) integral TJ proteins that bridge the apical intercellular space and form a regulated permeability barrier; 2) TJ plaque proteins, many of which express PDZ domains (Psd/SAP90, Disc Large, ZO-1) that serve as links between the integral TJ proteins and the actin cytoskeleton and as adapters for the recruitment of cytosolic molecules implicated in cell signaling; 3) a miscellaneous group of cytosolic and nuclear proteins, tumor suppressor, transcriptional and post-transcriptional factors that interact directly or indirectly with TJ plaque proteins to coordinate such diverse functions as the regulation of paracellular solute permeability, cell proliferation, and cell polarity.

Belong to the first group: occludin, the family of claudins and the junctional adhesion molecules (JAM) that are a member of the immunoglobulin superfamily.

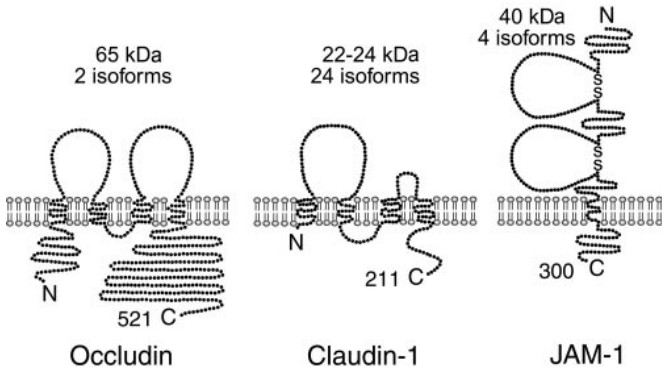

Fig 6 *Schematic representation of the molecular structure of trans-membrane domains of the tight junction proteinsOccludin, Claudin-1 and JAM-1*

The second group consists of a large family of proteins that share in their molecular structure a PDZ domain. Belong to this set of proteins: ZO 1 - 3 (zonula occludens 1 - 3), mDlg (mammalian disc large), MAGI 1 – 3 (membrane associated guanyl kinase inverted protein), MUPP1 (multi-PDZ domain protein 1), PAR (partitioning-defective protein), PALS (protein associated with Lin-7) and Scribb (Scribble).

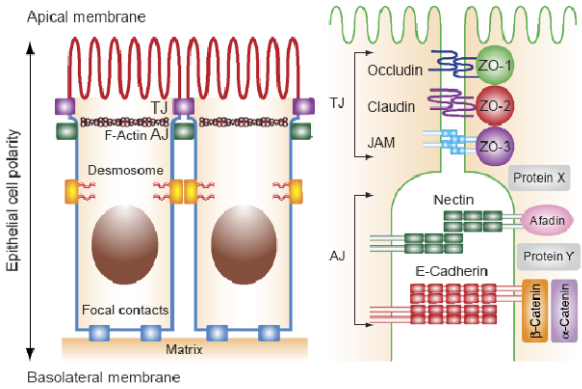

Fig 7 *Organization of junctional proteins in epithelial cells*

The Caco-2 intestinal cell line

Caco-2 cell line derives from a human colon adenocarcinoma and in standard condition of culture expresses spontaneously several morphological and functional characteristics of the enterocytes of the small intestine (Artursson, 1991).

During the growing phase Caco-2 cells remain undifferentiated and immediately after they reach the status of confluence, cells start the differentiation program that will be finished 18-21 days later.

According to the morphological and functional grade of differentiation that Caco-2 cell have during the 21 days from seeding we can divide the cell population into three subgroups: 1) cells homogeneously undifferentiated (sub confluent population); 2) cells heterogeneously polarized and differentiated (intermediate phase); 3) cells homogeneously polarized and differentiated (>15 days after seeding) (Delie and Rubas, 1997).

To better reproduce the steric conditions existing in the intestine *in vivo*, Caco-2 cells are generally cultured on permeable filter supports that allow free access of ions and nutrients to the two sides of the cell monolayer.

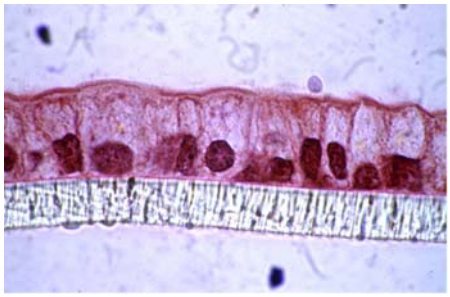

Fig 8 *Cross section of Caco-2 cells seeded and differentiated on PET filter supports*

Since these conditions led to improved morphological and functional differentiation, they have been proposed, and since then extensively utilized, as a more physiological model for intestinal transports and toxicity studies (Artursson, 1991; Hidalgo et al., 1989; Hilgers et al., 1990; Wilson, 1990).

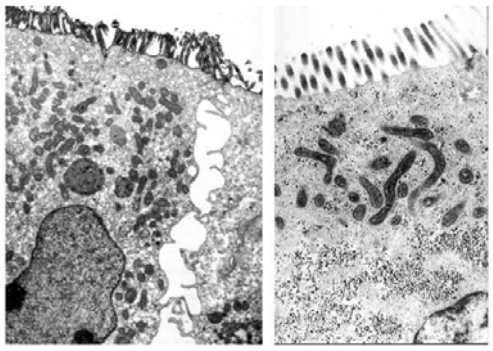

Fig 9 *electron microscopy image of Caco-2 brush border*

If we look at the morphology of Caco-2 cells, we can see that these cells organize as a polarized monolayer with tight junctions and microvilli, mimicking the *in vivo* enterocyte (Pinto et al., 1983). The functional polarity of the differentiated Caco-2 cells is further indicated, when cells are grown on plastic dishes, by the formation of domes in the monolayer due to the detachment from the plastic surface caused by the unidirectional fluxes of ions and water from the apical to the basolateral compartment..

On the microvilli forming the brush border are located a number of enzymes typical of the mature enterocyte such as: sucrase-isomaltase, lactase, aminopeptidase N, dipeptilpeptidane IV and alkaline phosphatase. The level of expression of these enzymes

are comparable to the *in vivo* level and also the activity of these enzymes increases with the different stages of differentiation as in the human small intestine (Delie and Rubas, 1997).

Finally, other functions of the enterocyte that are expressed in Caco-2 cells are the polarized membrane receptors for growth factors and a number of transport activities located either on apical or basolateral membrane.

The cell line variability

The Caco-2 population in culture, even in the stationary differentiated phase, is characterized by the presence of subpopulations with different morphologies. The mosaic expression of brush border enzymes in confluent Caco-2 cells has been previously described and cells with different level of sucrase-isomaltase activity has been sub-cloned (Beaulieu and Quaroni, 1991). Transient mosaic patterns of specific functional intestinal markers and lack of coordination between proliferation and differentiation related genes was also reported (Vachon and Beaulieu, 1992; Vachon et al., 1996), suggesting that the morphological and functional differentiation were not coupled in parental Caco-2 cells.

To improve the homogeneity and the stability of the Caco-2 cell population, clonal cell lines has been isolated and characterized by several groups. The existence of Caco-2 cell lines maintained in different laboratories and/or of different clonal origin, in addition to the effects of different culture protocols, often has made the comparison of results particularly difficult.

Since its original isolation (Fogh et al., 1977), the Caco-2 cell line has been propagated in several laboratories around the world, giving origin to cell populations of different "age" or passage number in culture.

The expression of typical differentiation markers of intestinal enterocytes, such as sucrase-isomaltase and the glucose transporter GLUT-5, has been shown to increase from early to late passages (Chantret et al., 1994; Mahraoui et al., 1992). Passage number can also influence metabolic activities: variability of CYP3A4 mRNA expression level has been reported, and it has been explained as an effect of passage number and/or culture conditions (Nakamura et al., 2002). The variations with increasing passage numbers in the expression level of the differentiation markers have been ascribed to the intrinsic heterogeneity of the parental Caco-2 cell population, leading to the selection during repeated culture passages of faster growing cell sub-populations, expressing different sub-

sets of characteristics (Briske-Anderson et al., 1997; Walter and Kissel, 1994; Walter et al., 1995; Yu et al., 1997).

Another parameter that can be responsible of variations in the expression level of transporters is the cell seeding density before starting cell differentiation. In literature a wide range of seeding densities on permeable filters is reported, but several studies demonstrated that this parameter could influence the structure of monolayer producing cell multilayers and inhibiting carrier mediated transport (Behrens and Kissel, 2003). In particular, the expression of the active peptide transporter HPT1 and of the efflux pump ABCB1 (P-gp) were down-regulated when Caco-2 cells were seeded with a cell density higher than 6×10^5 cells/cm^2.

Materials and Methods

Caco-2 cell line maintanence and differentiation

The human intestinal Caco-2 cell line was originally obtained from Prof. Alan Zweibaum (INSERM, Villejuif, France). To carry out the LD and HD protocols cells were split at 50% and 90% of confluence respectively at least for 10 passages; subsequently a large batch of cells was produced to perform all the experiments and a range of 4 passages after the cells thawing was used to limit passage number inter-variability.

Both LD and HD cells were maintained at 37°C in a 90% air /10% CO_2 atmosphere in DMEM containing 25 mM glucose, 3.7 g/L $NaHCO_3$ and supplemented with 4 mM L-glutamine, 1% non essential amino acids, 100 U/L penicillin, 100µg/L streptomycin, and 10% heat-inactivated foetal calf serum (Hyclone) (complete medium).

For the differentiation experiments, cells were seeded on polyethylene-terephtalate (PET) filter inserts (0.4 µm pore diameter, 4.71 cm^2; Falcon Becton-Dickinson) at a density of 3×10^5 cell/cm^2 and maintained for 21 days in complete medium; the medium was changed three times a week.

Plating efficiency assay

One thousand LD or HD Caco-2 cells were seeded on a 35 mm ∅ dish in complete medium. After 1 week from seeding cells were washed twice with PBS buffer supplemented with 1 mM $CaCl_2$ and $MgCl_2$ respectively (PBS^{++}) and fixed for 30 min with a solution of absolute methanol and 0.001% crystal violet. Dishes were then accurately washed with double distilled H_2O and colonies were counted. The number of colonies formed was expressed as percent of colonies with respect of cells seeded. A total of three independent experiments were performed.

Copper toxicity assay

To investigate the effects of copper ions, 21-days differentiated Caco-2 cells were treated for 1 or 2 h at 37°C with increasing concentrations of $CuCl_2$ in Hanks' balanced salt solution (HBSS, 137 mM NaCl, 5.36 mM KCl, 0.44 mM KH_2PO_4, 0.34 mM Na_2PO_4, 1 mM $CaCl_2$, 1 mM $MgCl_2$, and 5.6 mM glucose) with 20 mM MES, pH 6.0 in the apical (AP) compartment. The basolateral (BL) compartment contained HBSS containing 20 mM HEPES at pH 7.4.

Cell cycle

Cell cycle analysis was performed by pulse-chase bromodeoxyuridine (BrdU, Sigma) incorporation and propidium iodide DNA staining, as previously described (Bucci et al., 2005)

For the BrdU incorporation, 30 min before starting the experiment a pulse of 20 μM BrdU was given to the cell culture. Afterwards, BrdU-free medium was added to the cell culture and samples were taken every 2 h for further 24 h. Mouse anti-BrdU (Becton-Dickinson) and FITC-conjugated F(Ab') rabbit anti-mouse IgG (DAKO) antibodies were used to detect the BrdU incorporation. Twenty thousand events per sample were acquired by using a FACScan cytofluorimeter. The top region of the cytograms represents BrdUrd-positive cells. The percentages of the cell cycle distribution were estimated on linear PI histograms by using the MODFIT software.

Western Blot analysis

LD and HD Caco-2 cells were seeded on PET filters at the density of $3 \cdot 10^5$ cells/cm^2 and harvested at different days of differentiation (cycling cells C, 1, 3, 6, 9, 12, 15, 21 days after seeding). Cells were then incubated in urea buffer (8 M urea, 100 mM NaH_2PO_4, 10 mM Tris pH 8), for 30 min on ice and then briefly sonicated. Proteins were subjected to SDS–polyacrylamide gels electrophoresis. The resolved proteins were blotted overnight to nitrocellulose membranes, which then were blocked in PBS 1X containing 5% non-fat milk for at least 1 h. Blots were incubated with the following primary anti-human antibodies: anti-cyclin A polyclonal antibody (C-19), anti-p27Kip1 polyclonal antibody (C-19), anti-SI polyclonal antibody (T-17), all from Santa Cruz Biotechnology; anti-pRB monoclonal antibody (clone G3-245; BD-Pharmigen) and anti-ezrin monoclonal antibody (clone 3C12; Zymed). The membranes were then incubated 45 min with the relevant secondary antibody (anti mouse, anti-rabbit or anti-goat IgG (H+L)) conjugated with Alexa fluor 680 (Invitrogen) or IRDye 800 (LI-COR Biosciences) and analyzed with the Licor Odyssey Infrared Image System in the 700 or 800 nm channel.

Total RNA preparation

Total cellular RNA was isolated using standard Trizol (Invitrogen) protocol and subsequently purified and DNAse treated on RNAeasy Qiagen columns. Alternatively, total cellular RNA was isolated using NucleoSpin RNA II silica columns (Macherey-

Nagel). RNA quantity was determined by absorbance at 260 nm using a NanoDrop UV-VIS spectrophotometer. Each sample was then quality checked using the RNA 6000 Nano kit with a BioAnalyzer 2100 (Agilent): samples with a RIN index lower than 8.0 were discarded (Schroeder et al., 2006)

Real-time RT-PCR analysis

500 ng RNA was retro-transcribed using standard conditions and the cDNA was then subjected to real time PCR analysis with an Applied Biosystems 7900HT thermal cycler, using the SensiMix SYBR Kit (Bioline) and the following specific primers: PPARG (sense [s]: GACCTGAAACTTCAAGAGTACCAAA, antisense [as]: TGAGGCTTATTGTAGAGCTGAGTC), CDX2 (s: GAGCTGGAGAAGGAGTTTCACTA, as: GCGGTTCTGAAACCAGATTTT), CLDN4 (s: TCCGCCAAGTATTCTGCTG, as: CGTGGCACCTTACACGTAGTT), MYO1A (s: TGGCAGATTTCATCTACAAGAGC, as: GTTTGTGGATGGCAAATTGTT), ANPEP (s: CATCCATCAGAGATGGCAGAC, as: TGCTGAAGAGATCGTTCTGG), SLC11A2 (s: CACCGTCAGTATCCCAAGGT, as: CCGATGATAGCCAACTCCAC), SI (s: AATCCTTTTGGCATCCAGATT, as: GCAGCCAAGAATCCCAAAT), ALPI (s: CATACCTGGCTCTGTCCAAGA, as: GTCTGGAAGTTGGCCTTGAC), CYP3A4 (s: GATGGCTCTCATCCCAGACTT, as: AGTCCATGTGAATGGGTTCC), MT2A (s: CTCTAGCCGCCTCTTCAGC, as: ACTCTTTGCATTTGCAGGAAC), HSPA1A (s: AAGGACCGAGCTCTTCTCG, as: GCTCGGCTCTGAGATTGG), PPIA (s: ATGCTGGACCCAACACAAAT, as: TCTTTCACTTTGCCAAACACC) and TBP (s: GAACATCATGGATCAGAACAACA, as: ATAGGGATTCCGGGAGTCAT). Experiments were done in technical quadruplicates. Expression data were normalized using the Ct values of the internal controls PPIA and TBP.

Whole genome expression profiling

The gene expression profiling was performed using the Agilent two-color microarray system (http://www.chem.agilent.com/enUS/Products/Instruments/dnamicroarrays/Pages/default.aspx). Two different experiments have been performed, with a total of 10 samples: the first one (called "Diff/Cycl") to compare Caco-2 LD cells in the proliferating phase with Caco-2 LD cells at the end of 21-days differentiation period; the second one (called "LD/HD") to compare Caco-2 LD with Caco-2 HD differentiated cells. In the "Diff/Cycl" experiment

two different pairs of biological replicates (isolated from two different LD cell passages) were analyzed, while in the "LD/HD" experiment only one pair of samples was used. In both experiments, for each pair of sample a technical dye-swap replicate was included (see Supplementary Figure 1 for a scheme of the experiments).

500 ng of total RNA were retrotranscribed using oligo-dT primers linked to the T7-promoter and the resulting cDNA was used as a template for cyanine 3-CTP or cyanine 5-CTP labelled cRNA preparation, using the Agilent Low Input Linear Amplification Kit. The labeled cRNA were purified with Qiagen's RNeasy mini spin columns. To monitor both the labelling reactions and the microarray performance, Agilent Spike-In Mix was added to the mRNA samples prior to labelling reactions according the RNA Spike-In protocol.

Two-color mixes of labelled cRNA pairs were hybridized either to 44K ("Diff/Cycl" experiment) or 4x44K ("LD/HD" experiment) whole human genome oligonucleotide microarray (Agilent G4112A and G4112F respectively, 41000 unique probes) at 65°C for 17 hours using Agilent's Gene Expression Hybridization Kit. The hybridized microarrays were disassembled at room temperature in Agilent Gene Expression Wash Buffer 1. After the disassembly, the microarrays were washed in Gene Expression Buffer 1 for one minute at room temperature, followed by washing with Gene Expression Wash Buffer 2 for one minute at 37°C. The microarrays were then treated with acetonitrile for one minute at room temperature.

Post-hybridization image acquisition was accomplished using the Agilent Scanner G2564B, equipped with two lasers (532 nm and 635 nm) and a 48 slide auto-sampler carousel. The "extended range" scanning protocol was used for the 4x44K chip, where the output of two following scannings at 10% and 100% of laser power are numerically combined. Data extraction from the images was accomplished by Agilent Feature Extraction 9.1 software using the standard Agilent two-color gene expression extraction protocol (GE2-v4_91).

Raw data filtering was performed in Microsoft Excel using any of the following criteria to discard spots: spots with more than 5% of saturated pixel in any of the two channels, spots flagged as "not found" by the Feature Extraction software in any of the two channels, spots with a Signal/Noise ratio smaller than 3 in any of the two channels, where Signal = (median of the spot - median spot background level) and Noise is the IQR

(interQuantileRange) of the median spot background. Basic data analysis was perfomed on filtered data using Agilent GeneSpring GX 7.3 and Microsoft Excel. In every array the normalized channel ratio Nr was normalized by the Lowess algorithm within GeneSpring, using 20% of data as smoothing window. In the cluster of Figure 3, the separated Lowess normalized Red (R_norm) and Green (G_norm) channels are obtained by the formulas Log2(R_norm) = (Log2(Nr)+Log2(R*G))/2 and Log2(G_norm) = (-Log2(Nr)+Log2(R*G))/2, where R and G are the non-normalized channel values. For the "Diff/Cycl" experiment two separate normalization procedures were used, the Lowess and the dye-swap method, that combines and averages two dye-swapped replicates. Differentially expressed genes were identified as those showing an average fold change larger than 1.5 and lower than 1.5 in the "LD/HD" experiment, in the linear scale. In the "Diff/Cycl" experiment differential genes were identified with a more stringent criteria, as those showing an average fold change larger than 2.0 or lower than 1/2.0 in the linear scale but in both sets of normalized data, Lowess and dye-swap, except for Figure 5 where the threshold was 1.5. The analysis of over- and under- represented functional annotations was performed, pooling up- and down- regulated genes, using the DAVID web tool (http://david.abcc.ncifcrf.gov/) (Huang et al., 2009), selecting the following categories both for functional clustering (high stringency) and charts: goterm_bp_4, goterm_bp_5, goterm_cc_4, goterm_cc_5, goterm_mf_4, goterm_mf_5, panther_bp_all, panther_mf_all, interpro, pir_superfamily, smart, panther_family, panther_subfamily, kegg_pathway, panther_pathway, chromosome, cytoband, cog_ontology, sp_pir_keywords, up_seq_feature. Gene clustering analysis was done using MeV 4.4 (MultiExperiment Viewer, TM4 suite , http://www.tm4.org/mev/)(Saeed et al., 2006).

Fluorescence and immunofluorescence microscopy

Caco-2 cells were seeded on PET inserts in complete medium and cultured for the time indicated in the legend of the figures. For-F-actin localization cells were fixed in 2% paraformaldehyde in PBS^{++} containing 2% sucrose for 30 min, washed with PBS^{++} , blocked with 5% non-fat dry milk in PBS^{++} and incubated for 30 min with 0.33 mg/ml TRITC-phalloidin (0.25 mm) in PBS^{++} containing 0.2% BSA; double-labeling of the nuclei was performed with 1µg/ml DAPI for 30 sec in PBS. Finally, cells were washed in PBS, briefly rinsed in ddH2O and glasses were mounted with ProLong Gold anti-Fade Reagent (Molecular Probes).

To study the localization of ZO-1 protein and the colocalization of ZO-1 with Claudin 4 or Villin 1, we used a confocal laser scanning microscope (Leica Confocal Microsystem TCS SP5). ZO-1 was detected using the polyclonal anti-ZO-1 antibody purchased by Zymed while for Claudin4 and Villin 1 the antibodies were from Santa Cruz.

The secondary antibodies were: Alexa Fluor 594 Goat anti-mouse IgG, Alexa Fluor 555 Donkey anti-rabbit IgG and Alexa Fluor 488 Goat antirabbit $F(ab')_2$ fragment antibodies. In order to avoid any possible cross-talk between secondary antibodies we chose antibodies generated in Donkey, a species known to show negligible cross-reactivity, or $F(ab')_2$ fragments. Each image represented the maximal projection of 100-frames z-stack; images were processed using Leica Application Suite 6000. Brightness and contrast were adjusted.

Results

The "Low Density" (LD) cell-line maintaining protocol

Caco-2 cells in the growing phase tend to generate islets, showing a core constituted by prismatic epithelial-like more differentiated cells surrounded by large flattened growing cells at the border. When cells approach confluence, the proportion of the prismatic epithelial-like cells increases, up to a point in which these cells represent the large majority of the population. Obviously, each time cells are trypsinized and passed to another plate, the number of growing cells increases, but actually not all the replated cells enter the cell cycle.

We tested a novel cell-line-maintaining protocol, (Low Density protocol or LD protocol) where cells are split when they reach just 50% of confluence with an approximately density of 5 x 10^4 cells/cm^2. Using this protocol we avoid heterogeneous cell-growth conditions in which a subpopulation of cells start to differentiate during the line maintenance procedure. In this paper, we used this protocol in comparison with the standard Caco-2 maintenance protocol in which cells are subcultured at 80-90 % of confluence (High Density protocol or HD protocol).

To form the differentiated monolayer, LD and HD cells were both seeded at the same density of 3 x 10^5 cells/cm^2 on PET inserts (Falcon) and let to differentiate spontaneously into mature enterocytes over 21 days.

LD cells have a higher cell proliferation rate

To explore differences in proliferation of Caco-2 cells maintained either with LD or HD protocol, we first investigated the cell cycle phase's distribution after propidium iodide staining. In Figure 1A is shown the ratio of cell cycle phases percentages evaluated in growing LD and HD cells. A significant increase in the proliferative compartment was observed in LD vs HD cells (S phase = 60 % and G2/M = 30% increase), indicating that in LD cells a higher number of cells was in the proliferative phases.

To investigate whether the increase in LD cell proliferation was due to a faster cell cycle transition we have performed a pulse-chase BrdU incorporation experiment by flow cytometry. Cells were exposed to BrdU for a pulse of 30 min. In order to calculate the cell-cycle phase length, BrdU incorporation was monitored immediately at the end of the BrdU

pulse and every 2 h during the subsequent 24 h. In Figure 1B are shown the BrdU cytograms in LD and HD cells at 0, 6 and 12 h after the pulse. The calculation of the cell-cycle phase length indicated that both S and G1 phases in LD cells were shorter than in HD cells (S-phase length = 12 vs 17 h; G1 phase length = 4 vs 6.5 h), thus resulting in a reduced total cell cycle duration (LD cells = 19 h vs HD cells = 25 h). It was therefore evident that LD cells entered and completed the cell cycle faster than HD cells. The colony formation assay (Figure 1C, right and left panel) also demonstrated that the LD cells have a higher proliferative potential than the HD ones: cycling LD cells show 60% of colonies formed compared to the 29% of the HD ones (Figure 1C, left panel) and this difference is still maintained after 21-days of differentiation, when LD cells show 45% of colony formed compared to the 15 % of HD cells (Figure 1C, right panel).

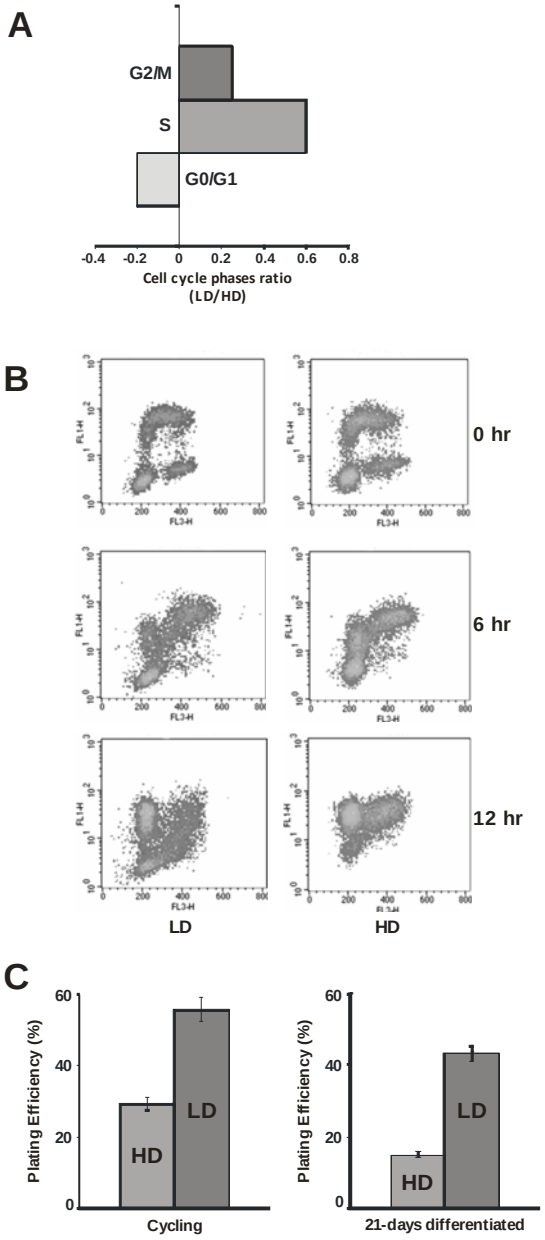

Figure 1. Effects of cell-growth density on cell-cycle length and plating efficiency.

(A) Cell cycle phase ratios of growing LD versus HD cells. (B) Representative cytograms of BrdU pulse-chase experiments. Each cytogram shows the different distribution of LD and HD cells 0, 6 and 12 hours after the BrdU pulse. (C) Plating efficiency of growing (left panel) and differentiated (right panel) LD and HD cells referred as percent of colony formed after plating.

LD cells show a slower exit from cell cycle but express the same level of differentiation markers as compared to the HD cells

To determine if cells with different proliferative potential were equally able to exit from the cell cycle and differentiate spontaneously in mature enterocytes, we followed the expression levels of some cell-cycle regulating proteins and intestine differentiation markers during 21 days of differentiation. Both LD and HD cells were seeded at the density of 3 x 10^5 cells/cm^2 on PET inserts and harvested at the indicated days of cell differentiation. As visible in Figure 2A, consistent with a faster exit from the cell cycle, the HD Caco-2 cells showed, earlier than the LD cells, modifications in some cell cycle-related molecules such as dephosphorylation of the retinoblastoma gene product (pRB; day 3 vs day 9 in LD cells), down-regulation of cyclin A (day 6 vs day 9 in LD cells) and accumulation of p27 (day 1 vs day 3 in LD cells). Correspondingly, a significant increase of the differentiation protein marker sucrate-isomaltase was already evident in HD cells at day 9, while LD cells showed an equivalent amount of SI only at day 15. Such differences between LD and HD cells can be explained by hypothesizing that the Caco-2 cells maintained at high density of culture have already entered the differentiation program beforehand cell seeding on the PET inserts.

Differences between the LD and the HD cell were also evident examining the trend of expression during the differentiation process of genes involved in the intestinal development. As shown in Figure 2B, we analyzed during the 21 days of differentiation by qRT-PCR the expression of genes encoding for intestinal enzymes, such as CYP3A4 (cytochrome P450), ALPI (phosphatase alkaline), ANPEP (aminopeptidase N) and SI (sucrase-isomaltase); for brush border transporters, such as SLC11A2 (or DMT1, divalent metal transporter 1); for structural proteins, such as CLDN4 (Claudin 4), MYO1A (Villin1); for transcriptional factor essential in the cripta-villus transition, such as PPARG (peroxisome proliferative activated receptor gamma) and CDX2 (caudal-type homeobox transcription factor 2). The general trend of induction of CDX2 and PPARG genes was almost the same in LD and HD cells whereas the value of fold increase is clearly higher in LD cells. The pattern of expression did not significantly vary also for the structural genes CLDN4 and MYO1A and the transporter SLC11A2. On the contrary the genes coding for brush- border enzymes ANPEP, SI and ALPI showed the largest differences both in trend of expression and fold increase. A significant difference between LD and HD cells was also suggested by the substantial induction of CYP3A4 gene in LD cells.

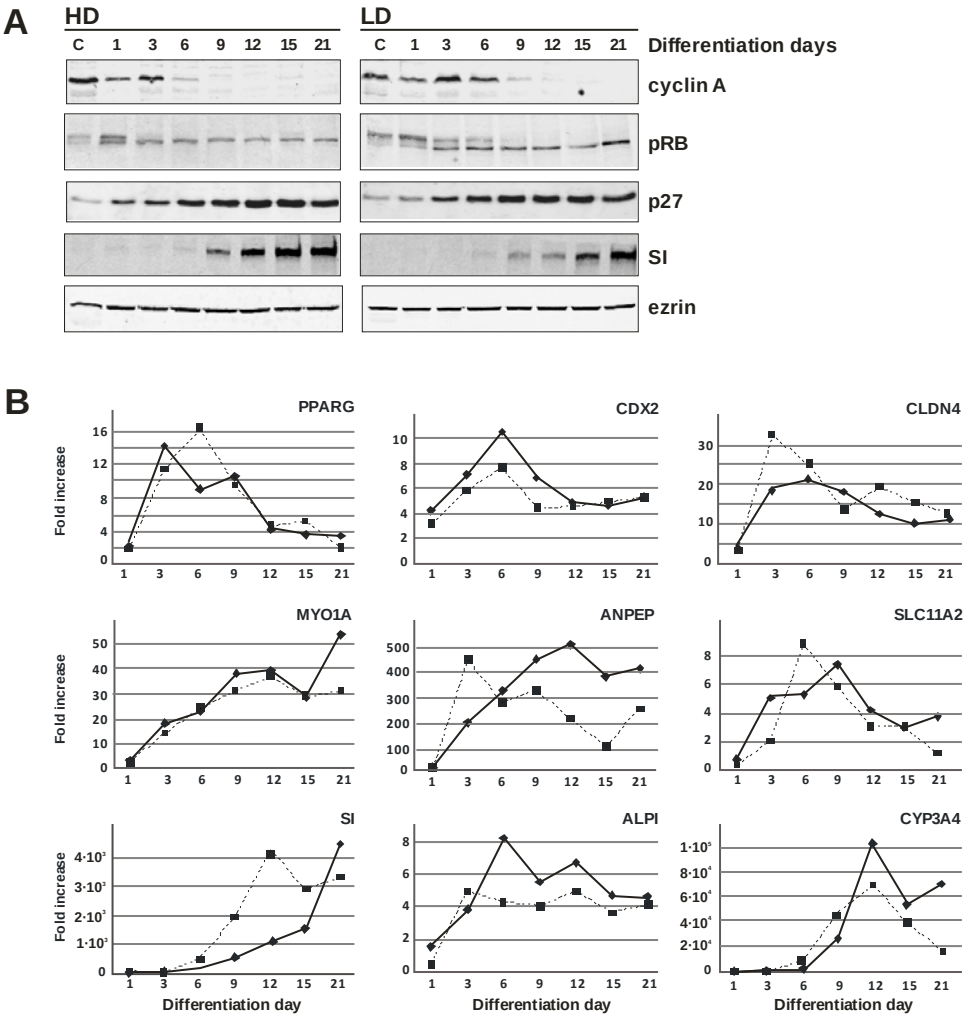

Figure 2. Effects of cell-growth density on the time-courses of the expression of cell cycle regulatory proteins and intestine differentiation key genes during 21 days of LD and HD cell differentiation.

(A) Western blot time course analysis on total cell lysates of some cell-cycle regulatory proteins and differentiation markers of the intestinal maturation of Caco-2 cells. Each lane was loaded with 80 µg of proteins from cell lysate. Ezrin was used as a loading control. The experiment was repeated three times showing similar results. A representative blot is presented. C: cycling cells (B) Quantitative RT-PCR time-course of genes involved in the enterocyte development. The values are expressed as fold induction respect to cycling LD cells.

The differentiated LD Caco-2 cells possess a well-defined enterocyte-like gene expression profile

To investigate the effects of the alternative line-maintenance protocol on the terminal differentiation of the Caco-2 cells, we used the Agilent microarray technology to compare the whole gene expression profiles of (i) 21-days differentiated LD cells versus LD cycling cells; and (ii) 21-days differentiated LD cells versus 21-days differentiated HD cells. The first experiment, called "Diff/Cycl", was designed in the two-color dye-swap configuration with biological duplicates of the samples (as schematized in supplementary Figure S1), the data were normalized using the Lowess and the dye-swap methods and differential genes were selected by filtering a combination of both normalized datasets as shown in supplementary Figure S2.

Figure 3 shows the hierarchical cluster of the filtered normalized expression data obtained from the two-color microarray "Diff/Cycl" experiment. The 8 columns correspond to the red and the green separated Lowess-normalized channels (see methods) for each of the four arrays. In this cluster it is possible to discriminate sets of genes that are up or down regulated in terms of absolute values; on the top of the cluster the biological replicates and technical replicates cluster together as expected indicating a good reproducibility between duplicate samples.

Supplementary Figure 3 shows another hierarchical cluster diagram obtained using the same filtered normalized expression data from the "Diff/Cycl" experiment. In red are grouped the genes at least 2 fold up-regulated while in green are grouped the genes at least 2 fold down-regulated in differentiated cells. The four columns correspond to the $\log_2$ ratio differentiated/cycling cells for the 4 arrays (two biological replicates and the corresponding 2 dye-swapped technical replicates). The sample tree on the top of the diagram shows that the technical replicates cluster together as expected.

On the right of the figure there is a list of the statistically significant functional categories ($10^{-2}<p<10^{-15}$) obtained submitting the 2-fold filtered genes to the DAVID Bioinformatics Database (http://david.abcc.ncifcrf.gov/) (Sherman et al., 2007). The black marks below each category indicate the position in the hierarchical cluster on the left of the genes belonging to that category. The median position of genes along the Y-axis of the cluster has been computed for each category and the list of categories has been sorted according to this value, for a better discrimination of categories containing more down-regulated genes from those containing a majority of up-regulated genes.

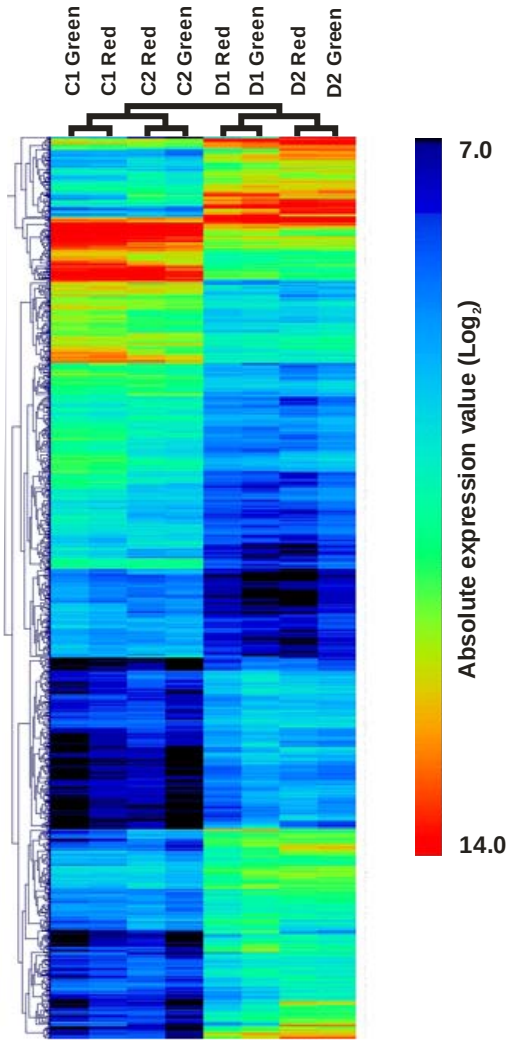

Figure 3. Hierarchical clustering, with Euclidean distance, of filtered normalized expression data obtained from the two-color microarray experiment "Diff/Cycl" where the Caco-2 LD differentiated cells are screened versus the Caco-2 LD cycling cells.

Log_2 of absolute expression values are shown. The set used for clustering is composed by the 1183 genes that show an average ratio Differentiated/Cycling greater than 2.0 or smaller than 1/2.0 (in the linear scale) in normalized data, where the normalization procedure included both the Lowess and dye-swap methods (see Materials and Methods). The 8 columns correspond to the Red and Green separate Lowess normalized channels for each of the 4 arrays; 2+2 biological replicates and the corresponding technical 2+2 dye-swapped replicates (one per sample) are shown. The column headers have the following meaning: C, cycling cells; D, differentiated cells, 1 and 2 refers to the biological replicate samples; Red and Green, refers to the cyanine label (either Red, cyanine 5 or Green, cyanine 3). It is clear from the sample tree on the top of the diagram that the chosen gene set is very effective in discriminating cycling and differentiated cells, since the biological replicates cluster together, cycling samples on the left and differentiated ones on the right, moreover within each of these two groups the technical replicates also cluster together.

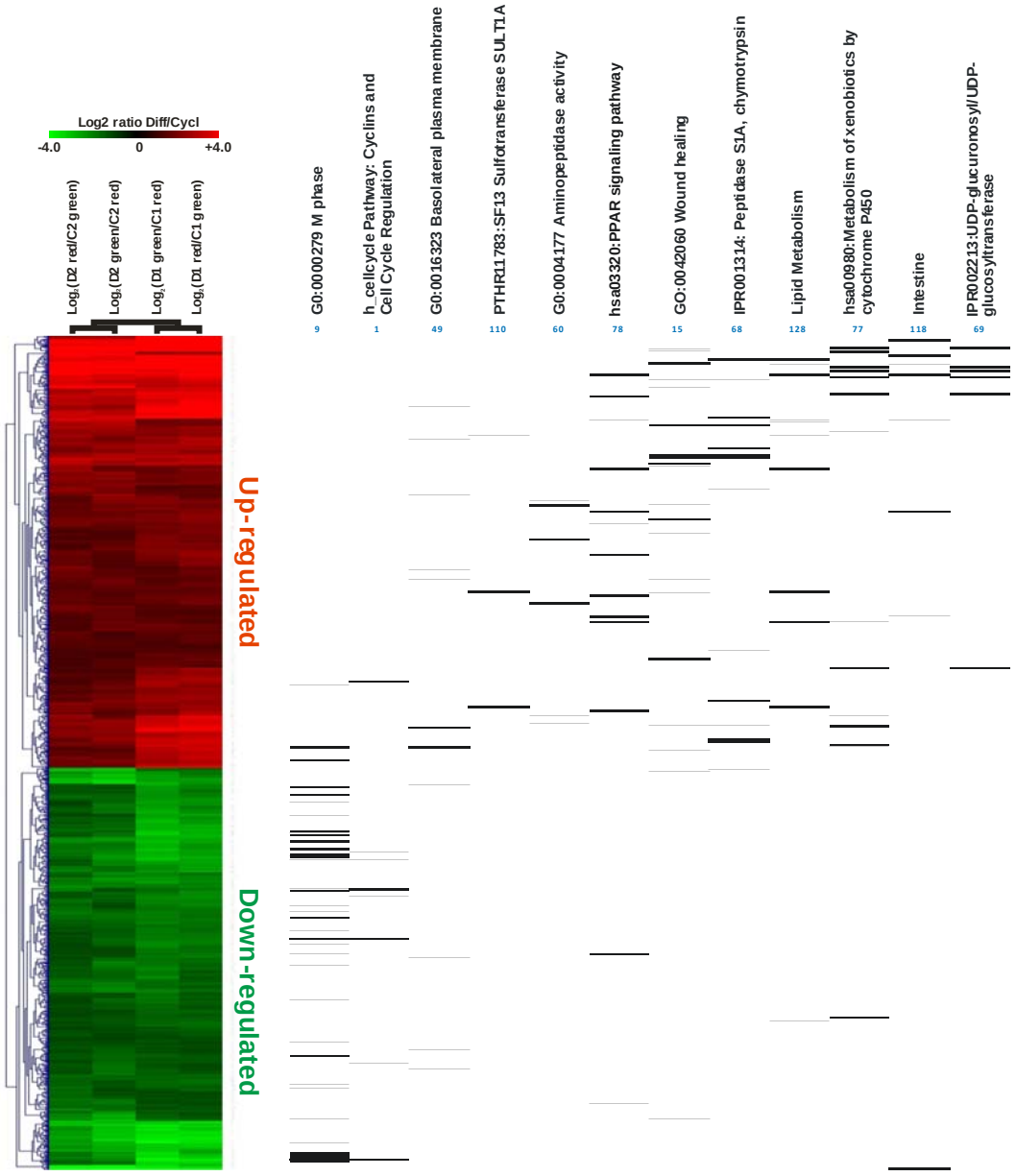

Figure 4. Hierarchical clustering, with Euclidean distance, of filtered nornalized expression data obtained from the two-color microarray experiment "Diff/Cycl" where the Caco-2 LD proliferating cells are screened versus the Caco-2 LD cycling cells.

Log_2 of relative expression values are shown. The set used for clustering is composed by the 1183 genes that show an average ratio Differentiated/Cycling greater than 2.0 or smaller than 1/2.0 (in the linear scale) in normalized data, where the normalization procedure included both the Lowess and dye-swap methods (see Materials and Methods). The 4 columns correspond to the Log_2 ratio Differentiated/Cycling for the 4 arrays: 2 couples of biological replicates and the corresponding 2 dye-swapped technical replicates. The column headers have the following meaning: C, cycling cells; D, differentiated cells, 1 and 2 refers to the biological replicate samples; Red and Green, refers to the cyanine label (either Red, cyanine 5 or Green, cyanine 3). The sample tree on the top of the diagram

shows that the technical replicates cluster together as expected. The gene annotation using the DAVID system is shown to the right: on the top are listed the main statistically significant functional categories (under- or over-represented in the gene set), below every black mark indicates that the corresponding gene belongs to the category on the top. The categories definitions and the genes belonging to them are listed in Supplementary Table 1.

A short and sorted list of non biologically redundant categories is reported in Figure 4 together with the hierarchical cluster diagram. Analyzing the genes comprised in the more up-regulated categories, they were typical genes of the intestine differentiation, while the down-regulated categories include cell cycle progression and regulation genes. The up-regulated genes belong to the PPAR-signaling pathway, the intestine, the lipid metabolism, the xenobiotics metabolism by CYP450 and the UDP-glucoronosyl/UDP-glucosyl transferases. The down-regulated genes are represented mainly by those belonging to the pathways controlling cell cycle progression and regulation. In Supplementary Table 1 is reported a list of the categories and the corresponding p-values shown in Figure 4.

Then we compared the whole gene expression profile of 21-days differentiated LD cells versus 21-days differentiated HD cells, obtaining the list of the genes whose level of expression was different between LD and HD cells: we called this the "LD/HD" experiment. Supplementary Table 2 reports the 163 genes of LD cells showing at least 1.5-fold increase or decrease with respect to the HD cells. Among these listed genes, relevant ones are involved in the function of the absorbing enterocyte, such as those coding for transporters (SLCO4A1, SLC12A2, SLC2A14 etc.) and enzymes (GSTM3, GPX7, CP), and others implicated in the cell polarization processes (PBK, DLG7, LAMA1).

Figure 5A shows the intersection of two sets of differential expressed genes obtained from the above described microarray experiments: the set of genes increasing or decreasing at least 1.5 fold in the Diff/Cycl" experiment and the set of genes increasing or decreasing at least 1.5-fold in the "LD/HD" experiment. It is quite surprising that out of the 163 genes differentially espressed between LD and HD cells, 56 also belong to the set of 2888 genes differentially expressed between differentiated and cycling LD cells. We have thus analyzed the distribution of these genes as shown in Figure 5B plotting the Log_2 ratios of each gene. This scatter plot shows both the extent and direction of gene expression variations. About 50% of the genes in common between the two sets are located into the right quadrants (b and c), representing genes up-regulated at the end of differentiation and

more expressed in LD (b quadrant) or in HD differentiated cells (c quadrant). These genes are reported in Supplementary Table 3. The left quadrants (a and d) of the plot contain the genes that are down-regulated at the end of differentiation. Interestingly, the other 50% of the genes in common between the two sets form a cluster only in the (a) quadrant, and include those that are more expressed in LD cells and down-regulated during differentiation. Among these genes (also reported in Supplementary Table 3) most are related with apoptosis, cell cycle and DNA repair

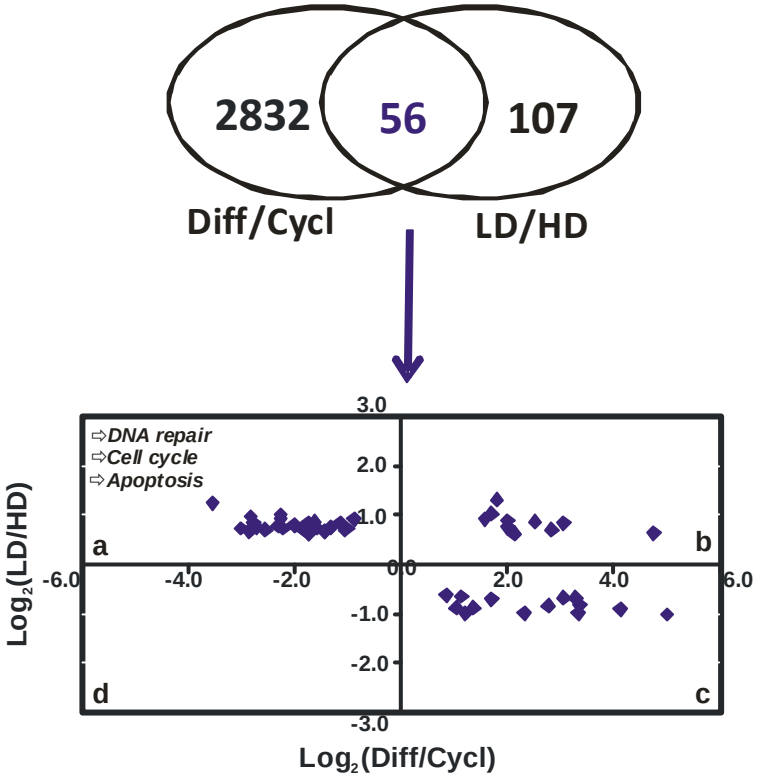

Figure 5. Intersection of the sets of differentially expressed genes obtained from the Diff/Cycl" experiment and from the "LD/HD" experiment.

From Lowess normalized data a total of 2888 genes ("Diff/Cycl" experiment) and 163 genes ("LD/HD" experiment) were selected, showing an average relative ratio greater than 1.5 or smaller than 1/1.5 in the linear scale. The relative Log_2 ratios of genes belonging to both sets, {Diff/Cycl ∩ LD/HD} in blue in the Venn diagram, are shown in the scatter plot. The three gene sets located in the quadrants (a), (b) and (c) of the plot are listed in the Supplementary Table 3, functionally annotated using the DAVID system. The 163 genes belonging to the LD/HD set, {LD/HD}, were also functionally annotated using the DAVID system and are reported in Supplementary Table 2. The most significant DAVID keywords are shown for the subset in quadrant (a).

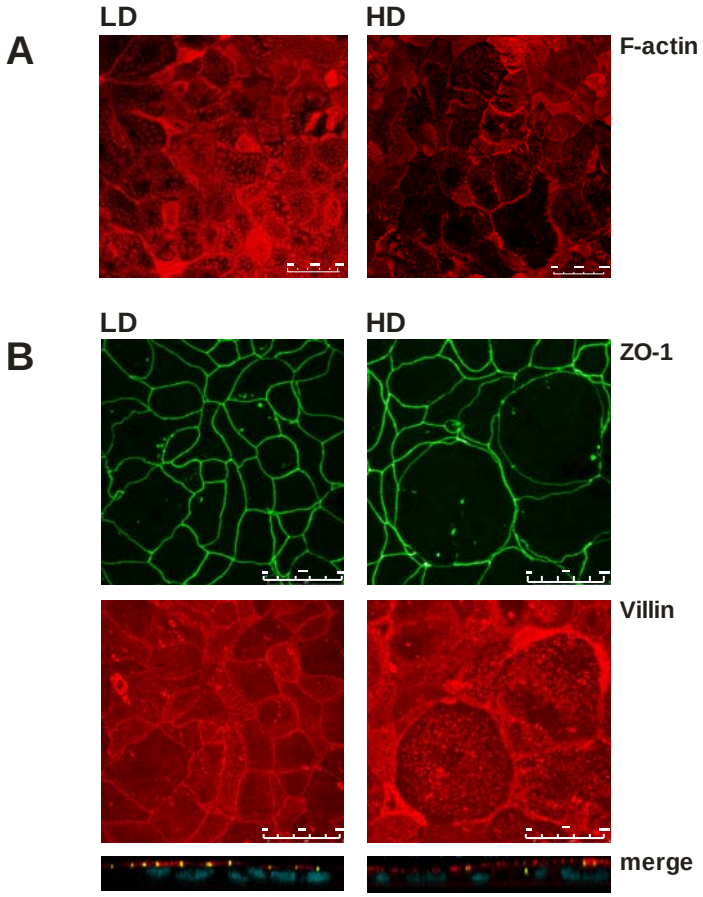

Figure 6. Localization by confocal microscopy of Caco-2 brush border proteins.

(A) Phalloidin-TRITC staining of F-actin of 21-days differentiated LD and HD cells. Each image is the orthogonal maximum projection of a 100-frames z-stack. (B) ZO-1 and villin co-immunofluorescence staining of 21-days differentiated LD and HD cells. Upper panel: orthogonal maximum projection (100-frames z-stack) of ZO-1 protein; medium panel: orthogonal maximum projection (100-frames z-stack) of villin protein; lower panel: perpendicular projection (100-frames z-stack) of merged ZO-1 (green) and villin (red) proteins with nuclei (cyan). Scale bars: 25 micron.

Cell-growth density deeply influence the architecture of polarized monolayer

We then investigated the effects of the two alternative cell-line culture protocol on the characteristics of differentiated cell monolayer, and in particular on the organization of proteins participating to the tight junction complex (Paris et al., 2008) and the structure of the brush border (Khurana and George, 2008).

Figure 6A shows representative images obtained by confocal microscopy of 21-days differentiated LD and HD cells stained with phalloidin-TRITC. This staining is specific for the fraction of actin present in polymerized form (F-actin), which in the intestinal epithelium constitutes the cytoskeleton that runs all over the length of the microvilli, anchoring them to the terminal web located at the base (Friederich et al., 1990). The LD cells show a regular brush border, in which the microvilli are well distributed all over the monolayer surface and clearly defined by their content of F-actin, while the monolayer formed by HD cells was characterized by scarce amount of polymerized actin, showing large unstained regions.

Figure 6B shows the localization of the protein villin, one of the main structural component of the microvilli (Khurana and George, 2008). The co-staining with the tight-junction protein zonula occludens 1 (ZO-1) allowed identifying the apical domain of the cells (Fanning et al., 1998). In this case, the amount of villin was comparable between the two samples and its localization was correct in relation to the ZO-1 position. This result indicates that the morphological difference between the brush-border of the two cell types was mainly due to the different level of actin polymerization.

To further investigate the effects of the cell-line maintenance protocols on the structure and organization of the cell monolayer, we analyzed the localization of the tight junction proteins ZO-1 and claudin 4. These proteins are key components for the assembly and functionality of the tight junction barrier, and normally they possess a well defined localization along the perimeter of the cells. ZO-1 surrounds the upper side of the cell, defining the border of apical domain, while claudin 4 runs all over the lateral domain (Acharya et al., 2004).

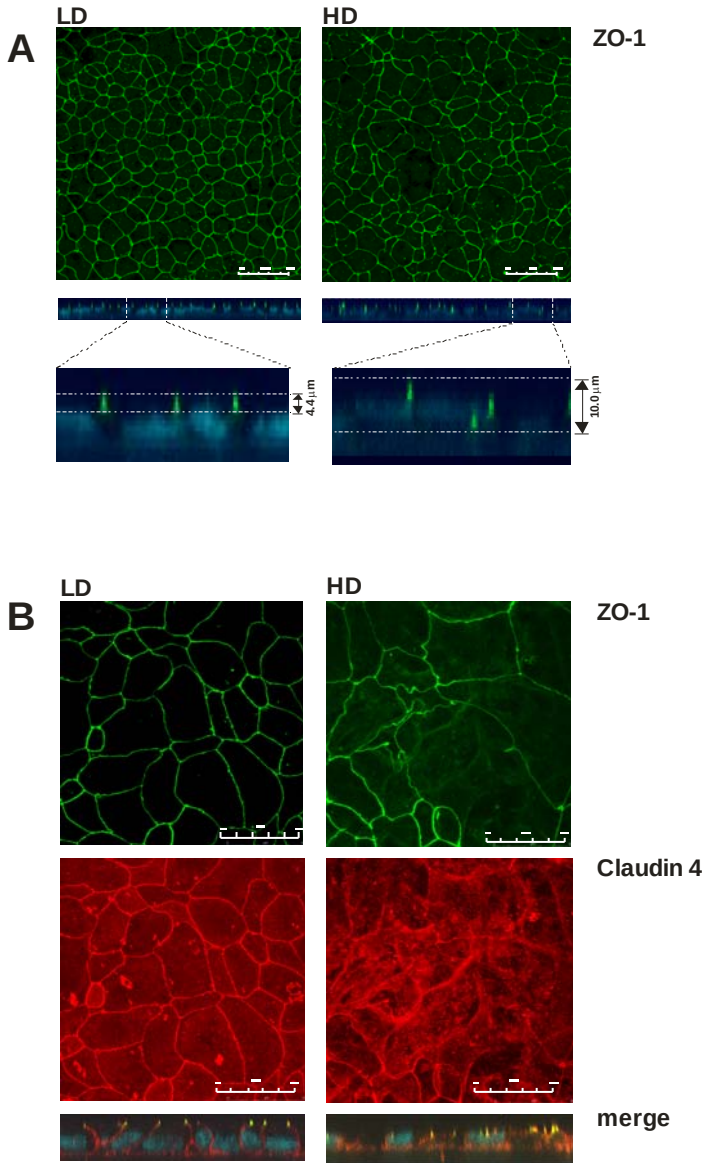

Figure 7. Localization by confocal microscopy of Caco-2 tight junction proteins.

(A) ZO-1 and claudin-4 co-immunofluorescence staining of 21-days differentiated LD and HD cells. Each image is the orthogonal maximum projection of a 100-frames z-stack. Upper panel: orthogonal maximum projection of ZO-1 protein; medium panel: orthogonal maximum projection of claudin-4 protein; lower panel: perpendicular projection of merged ZO-1 (green), claudin-4 (red) and nuclei (cyan). Scale bar is 25 micon(B) ZO-1 immunofluorescence staining of 21-days differentiated LD and HD cells. Each image is the orthogonal maximum projection of a 50-frames z-stack. Upper panel: orthogonal maximum projection of ZO-1 protein; medium panel: perpendicular projection of merged ZO-1 protein (green) and nuclei (cyan); lower panel: detail of the distribution of ZO-1 protein along the z-axis. Scale bar: 50 micron.

Figure 7A shows the immunostaining of ZO-1 in differentiated LD and HD cells. The ZO-1 localization in the orthogonal projection of the LD monolayer appears very regular, defining an homogeneous pattern of cell boundaries, further confirmed by the perpendicular projection, in which ZO-1 fluorescence is aligned in a narrow (about 4 μm) and well defined region. On the contrary, HD cells form a much more irregular monolayer, both in orthogonal and perpendicular view. The region containing the ZO-1 signals is wider (about 10 μm) and the signals are scattered and not aligned.

Figure 7B shows the consequences of the perturbed ZO-1 distribution on the localization of claudin-4. While in the LD monolayer both proteins are regularly aligned around the boundaries of the cells, in the HD one the correct localization of claudin 4 is completely lost, both in the orthogonal and the perpendicular projection.

Cell-growth density affects the Caco-2 response to toxic injury

On the basis of the above described differences in the structure of the junctional complex and in the aspect of the brush border, we asked whether the changes observed between LD and HD cells could also result in a different cellular response to toxic injury

To address this question, we carried out an acute treatment with increasing concentrations of copper chloride, a compound that enters into the Caco-2 cells mainly by its apical transporter DMT1 (SLC11A2) (Arredondo et al., 2003) and whose effects on the cells structure in terms of polymerization of the actin are well documented in literature (Ferruzza et al., 2002; Ferruzza et al., 1999b; Ferruzza et al., 1999a). In Figure 8A, the effect of 2 hours treatment with 100 and 300 μM $CuCl_2$ on the actin grade of polymerization is shown. We observed an increasing depolymerization of F-actin both in LD and HD cells, but the dose-effect ratio was not comparable between cell types. In HD cells the treatment with 100 μM $CuCl_2$ had substantially no effect on the polymerizated fraction of actin, while the effect of the same concentration on LD cells were extremely evident, resulting in the actin almost complete depolymerization. Only at 300 μM $CuCl_2$ actin was completely depolymerizated in both cell types and no difference was evident between them.

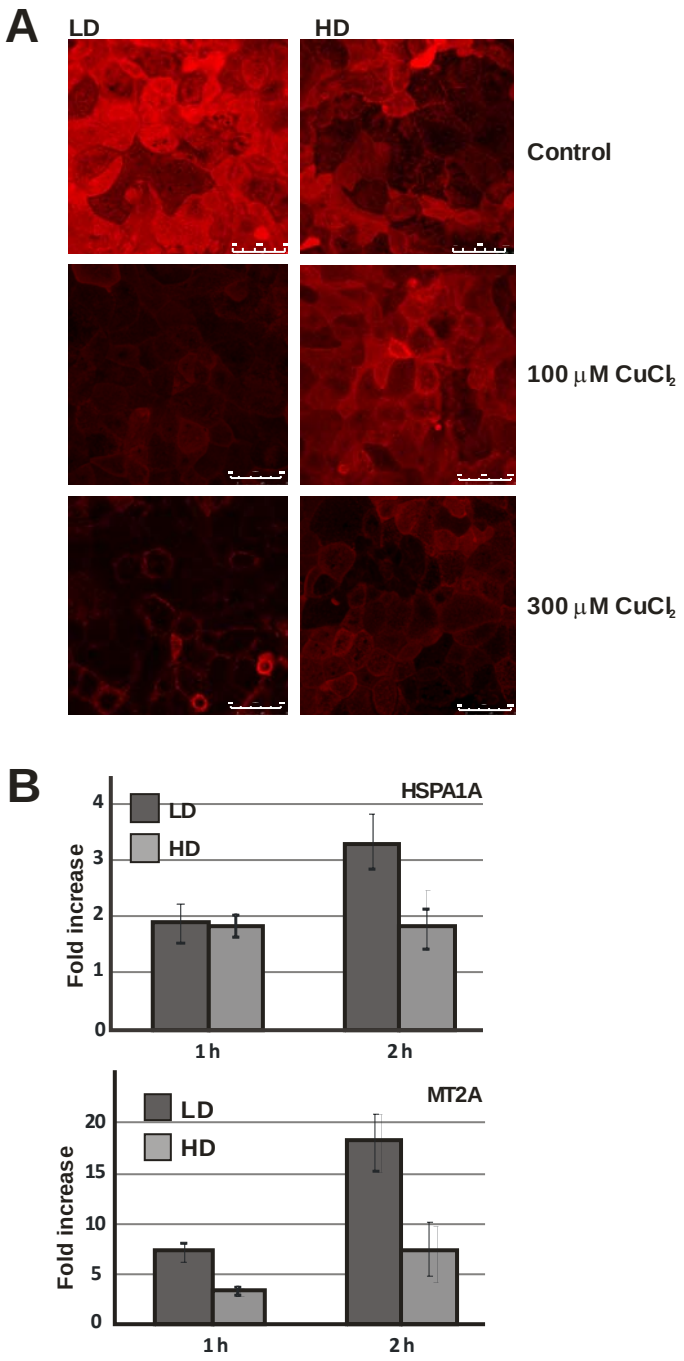

Figure 8. Response of LD and HD Caco-2 cells to copper chloride treatment.

(A) Phalloidin-TRITC staining of F-actin of 21-days differentiated LD and HD cells treated for 2 hours with increasing concentrations of copper chloride. Each image is the orthogonal maximum projection of a 100-frames z-stack. Scale bar: 25 micron. (B) Relative expression by quantitative RT-PCR of two genes involved in the response to copper toxicity, MT2A and HSPA1A, in 21-days differentiated LD and HD cells treated with 100 μM $CuCl_2$ for 1 or 2 hours. The values are expressed as fold induction respect to untreated LD or HD differentiated cells.

To see if the different response of the two cell types was also reflected at the gene expression level, we measured by real-time RT-PCR the expression level of two genes involved in copper metabolism and toxicity response: the heath shock protein 70 (HSPA1A) and the metallothionein 2A (MT2A) (Song and Freedman, 2005). Figure 8B shows that after 1 and 2 hours of 100 μM $CuCl_2$ treatment, the expression of MT2A was significantly higher in LD compared with HD cells. In the same experimental conditions, the increase of HSPA1A was time-dependent and more pronounced in LD cells, with a strong increase after 2 hours of treatment. Moreover, it is worthwhile to note, that in all these experiments, which have been repeated many times, the response of LD cells were always more reproducible and constant compared to the HD ones.

Discussion

We studied the effects elicited by Caco-2 cell line growth-density on the formation of the differentiated monolayer. To minimize the effects of any other difference, the experiments have been carried out using cells derived from the same source and applying rigorously standardized times of culture and differentiation, type of plastics, quality of animal serum and cell handling. Our results demonstrated how a simple modification of the routine manipulation of this cell line is sufficient to deeply influence the characteristics of the differentiated cells.

The general idea behind the new LD growth-differentiation protocol was to apply the differentiation-inducing conditions to totally undifferentiated actively-growing cells, avoiding as much as possible the intermediate stage of a partially differentiated inhomogeneous cell population. The cell cycle time of LD cells was shorter, suggesting that LD growing cell were more active and in healthier conditions. Moreover, comparing the cell cycle profiles of growing LD and HD cells, we found a higher number of LD cells in the proliferative compartment of the cell cycle, suggesting a more synchronous state of the cell population. The colony formation assay demonstrated how the HD cells have a reduced ability to attach to the plate (almost 50% less than LD ones), probably due to a selective pressure that acts against cells that have already started the differentiation program. On the contrary the LD cells were less subjected to this type of selection, because only a small subpopulation of these cells reached a degree of confluence sufficient to trigger the differentiation process.

The analysis of proteins involved in the exit from the cell cycle during 21 days of differentiation has been very informative. Results about pRB protein dephosphorilation (Tamrakar et al., 2000) showed that the HD cells withdraw from cell cycle at least 3-6 days before LD cells. The same time delay was confirmed analyzing the time-course of the levels of cyclin A and kinase inhibitor $p27^{Kip}$ (Reed, 1997). The early exit from cell cycle showed by the HD cells can be a consequence of the higher degree of confluence in which these cells were maintained and it is consistent with their reduced ability to attach to the plate. Notwithstanding the delay in the onset of sucrase-isomaltase (Beaulieu et al., 1989) accumulation was in accord with the general delay in the exit from cell cycle of LD cells, its value level at plateau confirmed the capability of LD cells to differentiate at the same extent of the HD ones.

Analyzing the RT-qPCR time-course of LD and HD cells, we found that two genes encoding for transcription factors controlling intestinal cells differentiation, PPARG (Huin et al., 2002) and CDX2 (Walters, 2005), display similar trend and timing of transcript accumulation. Our interpretation is that both regulatory genes were induced by the same mechanism and with the same timing after cell seeding, starting the differentiation process. The other genes examined by RT-PCR are structural and functional differentiation markers, presumably controlled directly or indirectly by the two above-mentioned transcription factors. These genes could be grouped into two categories according to the trend and timing of their expression: the genes of the first category (MYO1A, SLC11A2, ALPI and CYP3A4) behaved almost in the same way in LD and HD cells, while the expression of the genes belonging to the second category (SI, ANPEP and CLDN4) increased significantly earlier in HD cells, in some case even before the peak of induction of CDX2 and PPARG. Our explanation of this fact is that HD cells have been subjected to a first round of transcriptional induction before the final seeding on the filters.

Notwithstanding this early induction, the level of SI accumulation in HD cells was lower of that reached at the end of differentiation by the LD cells. Also the induction of CYP3A4 was strong in LD cells both as absolute value and in comparison with the HD cells. It is worthwhile to note that previously in literature a similar variability in the expression of SI and CYP3A4 (this latter often undetectable in Caco-2 clones) was ascribed to interclonal variability and passage numbers (Fogh et al., 1977; Peterson and Mooseker, 1992; Schmiedlin-Ren et al., 1997a; Schmiedlin-Ren et al., 1997b).

The microarray data clearly demonstrated that the LD cell growing protocol was able to produce Caco-2 cells that after 21 days were capable to form a perfectly differentiated monolayer of mature enterocytes. Our data, even if limited to the comparison of growing and differentiated cells, appeared very similar and comparable to those recently published by Brown (Saaf et al., 2007; Halbleib et al., 2007). We found a good clusterization of microarray data with the biological processes involved in differentiation. The annotated gene list obtained using DAVID database tools showed a good correlation between the genes up or down regulated in our model and those expected to be up- or down-regulated in intestinal differentiation.

Analyzing the microarray data obtained comparing the 21-day differentiated LD versus HD cells, we found only a limited number of differences. We found 163 differentially expressed genes, which, since we were comparing two differentiated cultures

obtained from the same original cell clone and differing only for the growth-density conditions, represents a significant number. More interestingly, about one third of these modulated genes correspond to genes that are regulated during the differentiation process. In our opinion, this significant modulation of the gene expression of the differentiated cells supports our hypothesis that the initial growth-density condition of a Caco-2 cell culture affects the quality of the subsequent differentiation process.

Acknowledgements

This work was supported by EU FP6 Project "LIINTOP" Contract number LSHB-CT-2006-037499 to Flavia Zucco, and by grant of FILAS to CNR, Institute of Neurobiology and Molecular Medicine, Rome. The microarray experiments have been done in the EBRI-CNR genomic facility.

We are indebted with Dr. Yula Sambuy and Dr. Maria Laura Scarino for useful discussion. We thank Dr. Yula Sambuy for critical reading of the manuscript.

Bibliography

Acharya,P., Beckel,J., Ruiz,W.G., Wang,E., Rojas,R., Birder,L., and Apodaca,G. (2004). Distribution of the tight junction proteins ZO-1, occludin, and claudin-4, -8, and -12 in bladder epithelium. Am. J. Physiol Renal Physiol *287*, F305-F318.

Arredondo,M., Munoz,P., Mura,C.V., and Nunez,M.T. (2003). DMT1, a physiologically relevant apical Cu1+ transporter of intestinal cells. Am. J. Physiol Cell Physiol *284*, C1525-C1530.

Artursson,P. (1991). Cell cultures as models for drug absorption across the intestinal mucosa. Crit Rev. Ther. Drug Carrier Syst. *8*, 305-330.

Artursson,P., Palm,K., and Luthman,K. (2001). Caco-2 monolayers in experimental and theoretical predictions of drug transport. Adv. Drug Deliv. Rev. *46*, 27-43.

Beaulieu,J.F., Nichols,B., and Quaroni,A. (1989). Posttranslational regulation of sucrase-isomaltase expression in intestinal crypt and villus cells. J. Biol. Chem. *264*, 20000-20011.

Beaulieu,J.F. and Quaroni,A. (1991). Clonal analysis of sucrase-isomaltase expression in the human colon adenocarcinoma Caco-2 cells. Biochem. J. *280 (Pt 3)*, 599-608.

Behrens,I. and Kissel,T. (2003). Do cell culture conditions influence the carrier-mediated transport of peptides in Caco-2 cell monolayers? Eur. J. Pharm. Sci. *19*, 433-442.

Briske-Anderson,M.J., Finley,J.W., and Newman,S.M. (1997). The influence of culture time and passage number on the morphological and physiological development of Caco-2 cells. Proc. Soc. Exp. Biol. Med. *214*, 248-257.

Bucci,B., D'Agnano,I., Amendola,D., Citti,A., Raza,G.H., Miceli,R., De,P.U., Marchese,R., Albini,S., Felsani,A., Brunetti,E., and Vecchione,A. (2005). Myc down-regulation sensitizes melanoma cells to radiotherapy by inhibiting MLH1 and MSH2 mismatch repair proteins. Clin. Cancer Res. *11*, 2756-2767.

Chantret,I., Rodolosse,A., Barbat,A., Dussaulx,E., Brot-Laroche,E., Zweibaum,A., and Rousset,M. (1994). Differential expression of sucrase-isomaltase in clones isolated from early and late passages of the cell line Caco-2: evidence for glucose-dependent negative regulation. J. Cell Sci. *107 (Pt 1)*, 213-225.

Cheney,R.E. and Mooseker,M.S. (1992). Unconventional myosins. Curr. Opin. Cell Biol. *4*, 27-35.

Delie,F. and Rubas,W. (1997). A human colonic cell line sharing similarities with enterocytes as a model to examine oral absorption: advantages and limitations of the Caco-2 model. Crit Rev. Ther. Drug Carrier Syst. *14*, 221-286.

Fanning,A.S., Jameson,B.J., Jesaitis,L.A., and Anderson,J.M. (1998). The tight junction protein ZO-1 establishes a link between the transmembrane protein occludin and the actin cytoskeleton. J. Biol. Chem. *273*, 29745-29753.

Ferruzza,S., Sambuy,Y., Rotilio,G., Ciriolo,M.R., and Scarino,M.L. (1999a). The effect of copper on tight junctional permeability in a human intestinal cell line (Caco-2). Adv. Exp. Med. Biol. *448*, 215-222.

Ferruzza,S., Scacchi,M., Scarino,M.L., and Sambuy,Y. (2002). Iron and copper alter tight junction permeability in human intestinal Caco-2 cells by distinct mechanisms. Toxicol. In Vitro *16*, 399-404.

Ferruzza,S., Scarino,M.L., Rotilio,G., Ciriolo,M.R., Santaroni,P., Muda,A.O., and Sambuy,Y. (1999b). Copper treatment alters the permeability of tight junctions in cultured human intestinal Caco-2 cells. Am. J. Physiol *277*, G1138-G1148.

Fogh,J., Fogh,J.M., and Orfeo,T. (1977). One hundred and twenty-seven cultured human tumor cell lines producing tumors in nude mice. J. Natl. Cancer Inst. *59*, 221-226.

Friederich,E., Pringault,E., Arpin,M., and Louvard,D. (1990). From the structure to the function of villin, an actin-binding protein of the brush border. Bioessays *12*, 403-408.

Halbleib,J.M., Saaf,A.M., Brown,P.O., and Nelson,W.J. (2007). Transcriptional modulation of genes encoding structural characteristics of differentiating enterocytes during development of a polarized epithelium in vitro. Mol. Biol. Cell *18*, 4261-4278.

Hidalgo,I.J., Raub,T.J., and Borchardt,R.T. (1989). Characterization of the human colon carcinoma cell line (Caco-2) as a model system for intestinal epithelial permeability. Gastroenterology *96*, 736-749.

Hilgers,A.R., Conradi,R.A., and Burton,P.S. (1990). Caco-2 cell monolayers as a model for drug transport across the intestinal mucosa. Pharm. Res. *7*, 902-910.

Huang,d.W., Sherman,B.T., and Lempicki,R.A. (2009). Systematic and integrative analysis of large gene lists using DAVID bioinformatics resources. Nat. Protoc. *4*, 44-57.

Huin,C., Schohn,H., Hatier,R., Bentejac,M., Antunes,L., Plenat,F., Bugaut,M., and Dauca,M. (2002). Expression of peroxisome proliferator-activated receptors alpha and gamma in differentiating human colon carcinoma Caco-2 cells. Biol. Cell *94*, 15-27.

Khurana,S. and George,S.P. (2008). Regulation of cell structure and function by actin-binding proteins: villin's perspective. FEBS Lett. *582*, 2128-2139.

Kim,J.S., Mitchell,S., Kijek,P., Tsume,Y., Hilfinger,J., and Amidon,G.L. (2006). The suitability of an in situ perfusion model for permeability determinations: utility for BCS class I biowaiver requests. Mol. Pharm. *3*, 686-694.

Mahraoui,L., Rousset,M., Dussaulx,E., Darmoul,D., Zweibaum,A., and Brot-Laroche,E. (1992). Expression and localization of GLUT-5 in Caco-2 cells, human small intestine, and colon. Am. J. Physiol *263*, G312-G318.

Mooseker,M.S. (1985). Organization, chemistry, and assembly of the cytoskeletal apparatus of the intestinal brush border. Annu. Rev. Cell Biol. *1*, 209-241.

Nakamura,T., Sakaeda,T., Ohmoto,N., Tamura,T., Aoyama,N., Shirakawa,T., Kamigaki,T., Nakamura,T., Kim,K.I., Kim,S.R., Kuroda,Y., Matsuo,M., Kasuga,M.,

and Okumura,K. (2002). Real-time quantitative polymerase chain reaction for MDR1, MRP1, MRP2, and CYP3A-mRNA levels in Caco-2 cell lines, human duodenal enterocytes, normal colorectal tissues, and colorectal adenocarcinomas. Drug Metab Dispos. *30*, 4-6.

Paris,L., Tonutti,L., Vannini,C., and Bazzoni,G. (2008). Structural organization of the tight junctions. Biochim. Biophys. Acta *1778*, 646-659.

Peterson,M.D. and Mooseker,M.S. (1992). Characterization of the enterocyte-like brush border cytoskeleton of the C2BBe clones of the human intestinal cell line, Caco-2. J. Cell Sci. *102 (Pt 3)*, 581-600.

Pinto ,M., Robine-Leon,S., Appay,M., Kedinger,M., Triadou,N., and Dussaulx,E. (1983). Enterocyte-like differentiation and polarization of the human colon carcinoma cell line Caco-2 in culture. Biology of the cell.

Reed,S.I. (1997). Control of the G1/S transition. Cancer Surv. *29*, 7-23.

Saaf,A.M., Halbleib,J.M., Chen,X., Yuen,S.T., Leung,S.Y., Nelson,W.J., and Brown,P.O. (2007). Parallels between global transcriptional programs of polarizing Caco-2 intestinal epithelial cells in vitro and gene expression programs in normal colon and colon cancer. Mol. Biol. Cell *18*, 4245-4260.

Saeed,A.I., Bhagabati,N.K., Braisted,J.C., Liang,W., Sharov,V., Howe,E.A., Li,J., Thiagarajan,M., White,J.A., and Quackenbush,J. (2006). TM4 microarray software suite. Methods Enzymol. *411*, 134-193.

Sambuy,Y., de,A., I, Ranaldi,G., Scarino,M.L., Stammati,A., and Zucco,F. (2005). The Caco-2 cell line as a model of the intestinal barrier: influence of cell and culture-related factors on Caco-2 cell functional characteristics. Cell Biol. Toxicol. *21*, 1-26.

Schmiedlin-Ren,P., Edwards,D.J., Fitzsimmons,M.E., He,K., Lown,K.S., Woster,P.M., Rahman,A., Thummel,K.E., Fisher,J.M., Hollenberg,P.F., and Watkins,P.B. (1997a). Mechanisms of enhanced oral availability of CYP3A4 substrates by grapefruit constituents. Decreased enterocyte CYP3A4 concentration and mechanism-based inactivation by furanocoumarins. Drug Metab Dispos. *25*, 1228-1233.

Schmiedlin-Ren,P., Thummel,K.E., Fisher,J.M., Paine,M.F., Lown,K.S., and Watkins,P.B. (1997b). Expression of enzymatically active CYP3A4 by Caco-2 cells grown on extracellular matrix-coated permeable supports in the presence of 1alpha,25-dihydroxyvitamin D3. Mol. Pharmacol. *51*, 741-754.

Schroeder,A., Mueller,O., Stocker,S., Salowsky,R., Leiber,M., Gassmann,M., Lightfoot,S., Menzel,W., Granzow,M., and Ragg,T. (2006). The RIN: an RNA integrity number for assigning integrity values to RNA measurements. BMC. Mol. Biol. *7*, 3.

Sherman,B.T., Huang,d.W., Tan,Q., Guo,Y., Bour,S., Liu,D., Stephens,R., Baseler,M.W., Lane,H.C., and Lempicki,R.A. (2007). DAVID Knowledgebase: a gene-centered database integrating heterogeneous gene annotation resources to facilitate high-throughput gene functional analysis. BMC. Bioinformatics. *8*, 426.

Song,M.O. and Freedman,J.H. (2005). Expression of copper-responsive genes in HepG2 cells. Mol. Cell Biochem. *279*, 141-147.

Tamrakar,S., Rubin,E., and Ludlow,J.W. (2000). Role of pRB dephosphorylation in cell cycle regulation. Front Biosci. *5*, D121-D137.

Vachon,P.H. and Beaulieu,J.F. (1992). Transient mosaic patterns of morphological and functional differentiation in the Caco-2 cell line. Gastroenterology *103*, 414-423.

Vachon,P.H., Perreault,N., Magny,P., and Beaulieu,J.F. (1996). Uncoordinated, transient mosaic patterns of intestinal hydrolase expression in differentiating human enterocytes. J. Cell Physiol *166*, 198-207.

van de Waterbeemd,H. (1998). The fundamental variables of the biopharmaceutics classification system (BCS): a commentary. Eur. J. Pharm. Sci. *7*, 1-3.

Walter,E. and Kissel,T. (1994). Transepithelial transport and metabolism of thyrotropin-releasing hormone (TRH) in monolayers of a human intestinal cell line (Caco-2): evidence for an active transport component? Pharm. Res. *11*, 1575-1580.

Walter,E., Kissel,T., and Raddatz,P. (1995). Transport of peptidomimetic renin inhibitors across monolayers of a human intestinal cell line (Caco-2): evidence for self-enhancement of paracellular transport route. Pharm. Res. *12*, 1801-1805.

Walters,J.R. (2005). Recent findings in the cell and molecular biology of the small intestine. Curr. Opin. Gastroenterol. *21*, 135-140.

Wilson,G. (1990). Cell culture techniques for the study of drug transport. Eur. J. Drug Metab Pharmacokinet. *15*, 159-163.

Yu,H., Cook,T.J., and Sinko,P.J. (1997). Evidence for diminished functional expression of intestinal transporters in Caco-2 cell monolayers at high passages. Pharm. Res. *14*, 757-762.

Zucco,F., Batto,A.F., Bises,G., Chambaz,J., Chiusolo,A., Consalvo,R., Cross,H., Dal,N.G., de,A., I, Fabre,G., Guillou,F., Hoffman,S., Laplanche,L., Morel,E., Pincon-Raymond,M., Prieto,P., Turco,L., Ranaldi,G., Rousset,M., Sambuy,Y., Scarino,M.L., Torreilles,F., and Stammati,A. (2005). An inter-laboratory study to evaluate the effects of medium composition on the differentiation and barrier function of Caco-2 cell lines. Altern. Lab Anim *33*, 603-618.

Appendix I – Supplementary Data

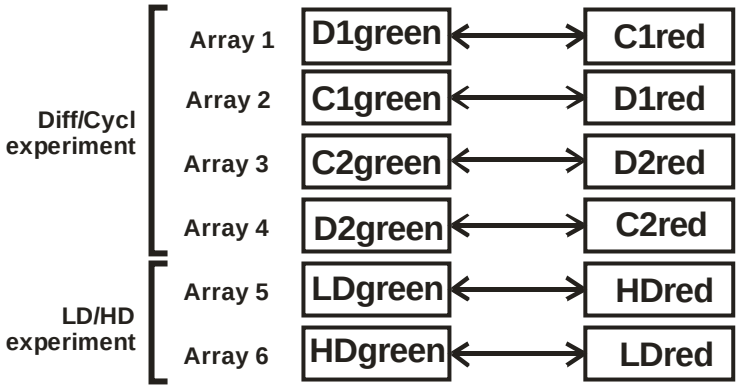

Supplementary Figure S1. Whole genome expression profiling using Agilent two-color microarray platform.

In the figure are schematized the experimental designs of the Diff/Cycl and the LD/HD microarray experiments. Each rectangle represents one labeled cRNA. The headers inside the rectangles have the following meaning: C, cycling cells; D, differentiated cells, 1 and 2 refers to the biological replicate samples; Red and Green, refers to the cyanine label (either Red, cyanine 5 or Green, cyanine 3).

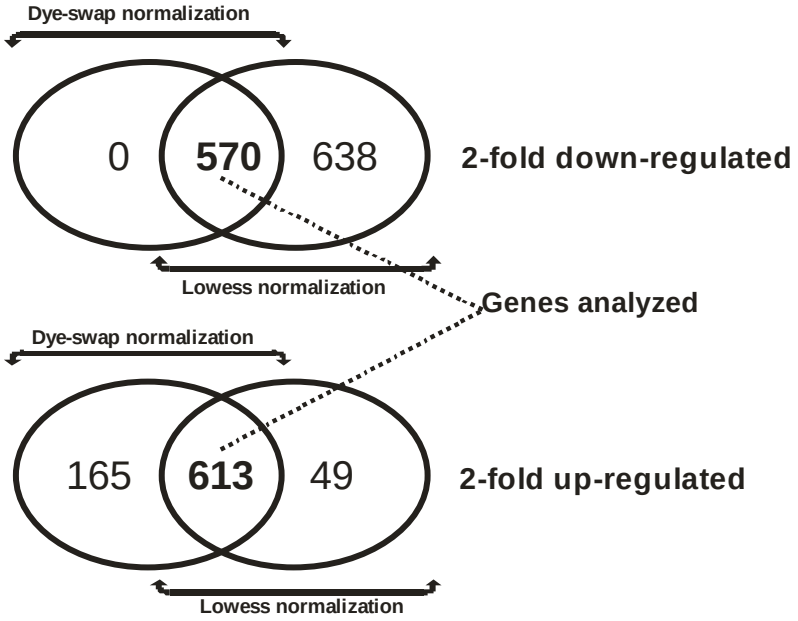

Supplementary Figure S2. Venn diagrams summarizing the results of the normalization and filtering methods applied to the Diff/Cycl row data.

The data from the Diff/Cycl experiment were normalized using both the Lowess and the dye-swap methods and the 2-fold differentially up-regulated and down-regulated genes were selected by filtering a combination of both normalized data sets.

Supplementary Figure S3. Hierarchical clustering, with Euclidean distance, of filtered nornalized expression data obtained from the two-color microarray experiment "Diff/Cycl" where the Caco-2 LD proliferating cells are screened versus the Caco-2 LD cycling cells.

Log_2 of relative expression values are shown. The set used for clustering is composed by the 1183 genes that show an average ratio Differentiated/Cycling greater than 2.0 or smaller than 1/2.0 (in the linear scale) in normalized data, where the normalization procedure included both the Lowess and dye-swap methods (see Materials and Methods and Figure S2). The 4 columns correspond to the Log_2 ratio Differentiated/Cycling for the 4 arrays: 2 couples of biological replicates and the corresponding 2 dye-swapped technical replicates. The column headers have the following meaning: C, cycling cells; D, differentiated cells, 1 and 2 refers to the biological replicate samples; Red and Green, refers to the cyanine label (either Red, cyanine 5 or Green, cyanine 3). The sample tree on the top of the diagram shows that the technical replicates cluster together as expected. The gene annotation using the DAVID system is shown to the right: on the top are listed all the statistically significant functional categories (under- or over-represented in the gene set), below every black mark indicates that the corresponding gene belongs to the category on the top. The categories definitions and the genes belonging to them are listed in Supplementary Table 1.

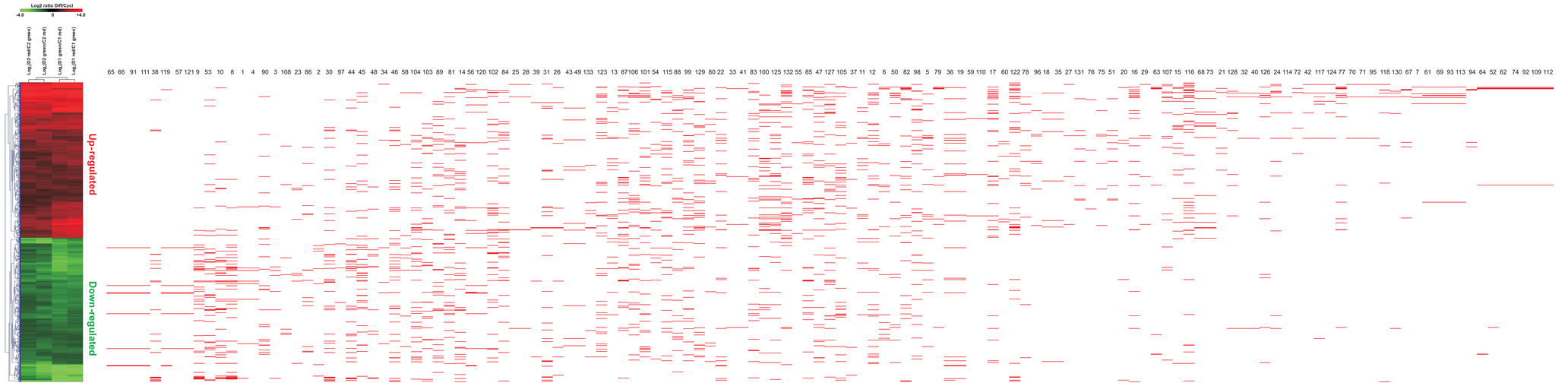
Log2 ratio Diff/Cycl
-4.0
0
+4.0
Log(D2 red/C2 green)
Log(D2 green/C2 red)
Log(D1 green/C1 red)
Log(D1 red/C1 green)
Up-regulated
Down-regulated
65 66 91 111 38 119 57 121 9 53 10 8 1 4 90 3 108 23 86 2 30 97 44 45 48 34 46 58 104 103 89 81 14 56 120 102 84 25 28 39 31 26 43 49 133 123 13 87 106 101 54 115 88 99 129 80 22 33 41 83 100 125 132 55 85 47 127 105 37 11 12 6 50 82 98 5 79 36 19 59 110 17 60 122 78 96 18 35 27 131 76 75 51 20 16 29 63 107 15 116 68 73 21 128 32 40 126 24 114 72 42 117 124 77 70 71 95 118 130 67 7 61 69 93 113 94 64 52 62 74 92 109 112

Figure S2

Supplementary Table 1. List of the statistically significant functional categories obtained submitting to the DAVID web tool the 1183 genes that show an average ratio Differentiated/Cycling greater than 2.0 or smaller than 1/2.0.

First column lists functional category numbers that identify the specific category, corresponding to those reported in Figure 4 and in Figure S3. Second column lists DAVID category type as described in Material and Methods. Third column describes the complete definition of the category term. Fourth column indicates the number of genes of the submitted data set that match the corresponding category. In the fifth column is shown the percent of genes found in the data set that match the category. The sixth column shows the significance of the category in the submitted data set in terms of p-value. Finally are named the genes belonging to that category found in the data set.

Supplementary Table 1

	Category	Term	Count	%	Pvalue	Genes																																							
1	BIOCARTA	h_cellcyclePathway:Cyclins and Cell Cycle Regulation	8	0.0103	0.000549896	CDC25A	E2F1	CDKN1A	CDC2	CDK6	CCNE1	CCND1	CCNB1																																
2	BIOCARTA	h_mcmPathway:CDK Regulation of DNA Replication	5	0.0065	0.001149428	MCM5	KITLG	CCNE1	CDT1	CDC6																																			
3	BIOCARTA	h_g2Pathway:Cell Cycle: G2/M Checkpoint	7	0.009	0.00423918	PLK1	CDKN1A	CHEK1	BRCA1	CDC2	YWHAH	CCNB1																																	
4	BIOCARTA	h_g1Pathway:Cell Cycle: G1/S Check Point	7	0.009	0.00788261	CDC25A	E2F1	CDKN1A	CDC2	CDK6	CCNE1	CCND1																																	
5	COG_ONTOLOGY	Amino acid transport and metabolism	18	0.0233	4.87082E-07	SCRN2	SAT2	ANPEP	ACY1	ODC1	SLC7A6	ALDH18A1	GATM	DDC	PYCR1	ABAT	MAOB	PRSS23	GLULD1	SLC7A5	PAOX	AGXT2	THOP1																						
6	COG_ONTOLOGY	Posttranslational modification, protein turnover, chaperones	14	0.0181	0.044875303	PSAT1	TCP1	STOM	GSTA4	CCT2	ABCB6	TPP1	CCT5	GSTA5	RNF128	PSMD11	GSTA2	PSMD12	GSTA1																										
7	CYTOBAND	4q13	3	0.0039	0.037189479	UGT2B17	UGT2B7	UGT2B15																																					
8	GOTERM_BP_4	GO:0022403~cell cycle phase	53	0.0685	4.96579E-15	CDC25A	ADCY3	RCC2	KPNA2	PAM	PTTG1	CCNE1	ZWINT	EREG	CENPF	ASPM	RAN	BCAT1	MAPRE1	CDCA5	CCNB1	KIF23	ANLN	CDT1	CCNA2	CDCA3	CHEK1	H2AFX	CDK6	HELLS	UBE2C	CCNB2	RAD51	TIMELESS	PLK1	NOLC1	CCNG2	CDCA8	CDC2	TPX2	E2F1	BCL6	SUV39H		
9	GOTERM_BP_4	GO:0000279~M phase	44	0.0568	5.33377E-13	TIMELESS	CDC25A	KPNA2	PLK1	ADCY3	RCC2	NOLC1	CCNG2	CDCA8	CDC2	PAM	PTTG1	ZWINT	EREG	CENPF	TPX2	ASPM	RAN	SUV39H2	CDC20	MAPRE1	CDCA5	CCNB1	KIF23	BIRC5	BUB3	C18orf24	MAD2L1	PKMYT1	ANLN	DLG7	CDC6	CCNA2	YWHAH	KIF2C	CDCA3	CHEK1			
10	GOTERM_BP_4	GO:0000074~regulation of progression through cell cycle	58	0.0749	7.97552E-11	CDC25A	MYBL2	CCNE1	ZWINT	EREG	CENPF	RAN	GTPBP4	PDGFC	RBBP8	MAPRE1	GSG2	CCNB1	SNF1LK	CDT1	ANLN	CCNA2	NME2	PDCD4	CKS1B	CHEK1	CDK6	UBE2C	CCNB2	TIMELESS	PLK1	CCNG2	DKC1	CDC2	CCT2	BCL6	C9orf127	BRCA1	G0S2	CDKN1C	CDC20	MYC	F		
11	GOTERM_BP_4	GO:0009309~amine biosynthetic process	16	0.0207	2.01729E-06	PSAT1	SEPHS2	ODC1	SULT1A2	ASNS	ALDH18A1	BBOX1	DDC	NAGS	PYCR1	MTHFD2	PRODH	GLULD1	BCAT1	CORO2A	C9orf103																								
12	GOTERM_BP_4	GO:0019752~carboxylic acid metabolic process	50	0.0646	2.67502E-06	PSAT1	MARS	AKR1C1	SLC7A1	ASNS	BCAT1	SLC7A5	XPNPEP2	ACOX2	PEPD	SLC27A2	ACY1	EPHX2	SLC7A6	PPARA	ALDOB	ALDH18A1	ASPA	GATM	MTHFD2	GLS	PGM1	OAT	SLC3A1	PTGS2	ATF3	DAO	TARS	CRYL1	FADS1	ME1	FABP1	MCFD2	PYCR1	ABAT	BRCA1	CORO2A			
13	GOTERM_BP_4	GO:0044271~nitrogen compound biosynthetic process	17	0.022	1.51888E-05	PSAT1	SEPHS2	NOS2A	ODC1	SULT1A2	ASNS	ALDH18A1	BBOX1	DDC	NAGS	PYCR1	MTHFD2	PRODH	GLULD1	BCAT1	CORO2A	C9orf103																							
14	GOTERM_BP_4	GO:0042127~regulation of cell proliferation	43	0.0556	2.16155E-05	TIMELESS	S100A11	CDCA7	OSR2	BLM	TOB1	ODC1	VIPR1	ANG	EREG	MXI1	FABP6	NRP1	EMP3	ERBB2	BCL6	GTPBP4	GAL	BRCA1	FTH1	CDKN1C	FGB	PAWR	ANXA1	MYC	CD164	CDKN1A	TGM2	FGA	TBX2	MAGED1	CDC6	GPC3	EDN1	TFF1	EEF1E1	NME2	CHEK1	FGG	TBC
15	GOTERM_BP_4	GO:0042060~wound healing	18	0.0233	3.49873E-05	MST1	KNG1	SERPINA1	FGA	F2	PROCR	TMPRSS6	FBLN5	F10	EREG	ADAMTS13	F7	CD59	FGG	APOH	EVL	FGB	SERPINC1																						
16	GOTERM_BP_4	GO:0008202~steroid metabolic process	22	0.0284	5.10031E-05	SOAT2	SORL1	ACOX2	AKR1C1	AFP	UGT2B17	HSD17B2	SULT1A2	OSBPL3	APOA1	APOB	FABP6	SCARB1	SULT1A4	UGT2B11	UGT2B15	YWHAH	SCP2	APOE	GAL	LDLR	SULT1A1																		
17	GOTERM_BP_4	GO:0044255~cellular lipid metabolic process	49	0.0633	5.71486E-05	AKR1C1	UGT2B17	CHPT1	OSBPL3	SULT1A2	SULT1A4	SCARB1	DGAT2	GPX4	ACOX2	SMPD3	SLC27A2	EPHX2	AFP	HSD17B2	PNLIPRP2	PPARA	APOA1	PPT1	LDLR	PTGS2	SOAT2	DGAT1	CRYL1	FADS1	IPO4	FABP1	ANG	APOB	MTMR11	APOC3	FABP6	UGT2B15	SCP2	ABAT	GA				
18	GOTERM_BP_4	GO:0046486~glycerolipid metabolic process	7	0.009	0.000661216	DGAT1	DGAT2	PNLIPRP2	ANG	DGKD	APOB	APOC3																																	
19	GOTERM_BP_4	GO:0006873~cellular ion homeostasis	20	0.0258	0.002121932	CCL2	TGM2	EPHX2	SLC30A1	SLC9A3R1	KNG1	NEDD4L	ABCB6	EDN1	CCL15	SLC40A1	MT2A	BNIP3	MT1X	PPT1	APOE	CKB	FTH1	RGN	MYC																				
20	GOTERM_BP_4	GO:0030104~water homeostasis	4	0.0052	0.002397011	NPPB	KNG1	NEDD4L	EDN1																																				
21	GOTERM_BP_4	GO:0030168~platelet activation	6	0.0078	0.003044715	FGG	FGA	EVL	F2	FGB	ADAMTS13																																		
22	GOTERM_BP_4	GO:0048878~chemical homeostasis	23	0.0297	0.003633278	CCL2	AKR1C1	TGM2	EPHX2	SLC30A1	SLC9A3R1	KNG1	NEDD4L	ABCB6	EDN1	CCL15	SLC40A1	BNIP3	MT2A	NPPB	MT1X	PPT1	APOE	CKB	FTH1	LDLR	RGN	MYC																	
23	GOTERM_BP_4	GO:0050678~regulation of epithelial cell proliferation	7	0.009	0.003892856	NME2	ERBB2	CDK6	NME1	CDKN1C	MAGED1	EREG																																	
24	GOTERM_BP_4	GO:0006869~lipid transport	12	0.0155	0.005229167	SCP2	SORL1	APOA4	ATP8B2	APOE	LDLR	APOM	APOA1	PPARA	OSBPL3	APOB	APOC3																												
25	GOTERM_BP_4	GO:0030299~cholesterol absorption	4	0.0052	0.007463951	APOA4	AKR1C1	LDLR	APOA1																																				
26	GOTERM_BP_4	GO:0030155~regulation of cell adhesion	9	0.0116	0.008260224	CD164	VAV3	BCL6	GTPBP4	TGM2	PRSS2	PODXL	KNG1	CDK6																															
27	GOTERM_BP_4	GO:0042744~hydrogen peroxide catabolic process	4	0.0052	0.012837895	APOA4	GPX3	CAT	GPX4																																				
28	GOTERM_BP_4	GO:0050892~intestinal absorption	4	0.0052	0.016166934	APOA4	AKR1C1	LDLR	APOA1																																				
29	GOTERM_BP_4	GO:0000302~response to reactive oxygen species	5	0.0065	0.026632541	APOA4	GPX3	APOE	CAT	GPX4																																			
30	GOTERM_BP_4	GO:0007010~cytoskeleton organization and biogenesis	33	0.0426	0.028494493	ANK3	CEBPA	KPNA2	STMN1	UCHL1	ZWINT	ANG	CNN3	TUBB6	RAN	BCL6	RANBP1	BRCA1	ARHGEF10	MAPRE1	TUBAL3	MYL7	KIF3C	KIF23	PRC1	CNN1	ANLN	EPB41L2	ACTB	GSN	YWHAH	KIF2C	APOE	EVL	UBE2C	SPAG5	DBN1	RACGAP1							
31	GOTERM_BP_4	GO:0032989~cellular structure morphogenesis	31	0.0401	0.037938407	IGFBP2	VAV3	UCHL1	CHPT1	POU4F1	EMP3	NRP1	KAZALD1	BCL6	DGKD	EFNA1	TNFRSF12A	CDKN1A	LTBP4	MYO1A	SOCS2	CYR61	YWHAH	NPPB	CD320	APOE	PPT1	PRSS2	NET1	EVL	SEMA3B	ITGA7	NOP5/NOP	DBN1	PALM	VCL									
32	GOTERM_BP_4	GO:0015918~sterol transport	4	0.0052	0.039391304	APOE	LDLR	APOA1	APOB																																				
33	GOTERM_BP_4	GO:0006749~glutathione metabolic process	4	0.0052	0.045334051	GPX3	MGST1	GPX4	GSTA1																																				
34	GOTERM_BP_4	GO:0010038~response to metal ion	5	0.0065	0.046215427	MT1X	NEDD4L	ALDOB	CCND1	ACTB																																			
35	GOTERM_BP_5	GO:0046486~glycerolipid metabolic process	7	0.009	0.000698236	DGAT1	DGAT2	PNLIPRP2	ANG	DGKD	APOB	APOC3																																	
36	GOTERM_BP_5	GO:0050801~ion homeostasis	21	0.0271	0.003184489	CCL2	TGM2	EPHX2	SLC30A1	SLC9A3R1	KNG1	NEDD4L	ABCB6	EDN1	CCL15	SLC40A1	BNIP3	MT2A	NPPB	MT1X	PPT1	APOE	CKB	FTH1	RGN	MYC																			
37	GOTERM_BP_5	GO:0007162~negative regulation of cell adhesion	5	0.0065	0.027542493	CD164	BCL6	GTPBP4	PODXL	KNG1																																			
38	GOTERM_BP_5	GO:0007017~microtubule-based process	17	0.022	0.029487572	KIF3C	KIF23	CEBPA	STMN1	KPNA2	PRC1	UCHL1	ZWINT	KIF2C	TUBB6	RAN	RANBP1	BRCA1	MAPRE1	UBE2C	SPAG5	TUBAL3																							
39	GOTERM_BP_5	GO:0045785~positive regulation of cell adhesion	4	0.0052	0.029577205	VAV3	TGM2	PRSS2	CDK6																																				
40	GOTERM_BP_5	GO:0030301~cholesterol transport	4	0.0052	0.040444583	APOE	LDLR	APOA1	APOB																																				
41	GOTERM_BP_5	GO:0006749~glutathione metabolic process	4	0.0052	0.046531429	GPX3	MGST1	GPX4	GSTA1																																				
42	GOTERM_CC_4	GO:0042627~chylomicron	4	0.0052	0.003600614	APOA4	APOE	APOB	APOC3																																				
43	GOTERM_CC_4	GO:0016323~basolateral plasma membrane	11	0.0142	0.00429675	TJP1	MUC20	MYO1A	TRIP6	AQP3	EVL	SLC39A5	ANXA1	CDH17	VCL	RHBG																													
44	GOTERM_CC_4	GO:0044430~cytoskeletal part	46	0.0594	0.0056666	CEBPA	RCC2	STMN1	PLK1	MYO7B	PTP4A1	CDC2	LMNB2	PROCR	NES	TACC2	CENPF	TPX2	TUBB6	BMF	RANBP1	BRCA1	CDC20	MAPRE1	TUBAL3	CCNB1	MYL7	KIF23	BIRC5	KIF3C	CALD1	PRC1	C18orf24	MAD2L1	MYO1A	TCP1	MYL5	ANLN	DLG7	CDC6	EPB41L2	KIF2C	P		
45	GOTERM_CC_4	GO:0043231~intracellular membrane-bound organelle	336	0.4341	0.005902909	RFC2	TMEM29	MYBL2	CHPT1	RCN1	ORC6L	ABCB6	MCM6	ASPM	NRP1	FJX1	DGAT2	NCOA7	CDCA5	KIAA0101	FOXQ1	GAA	ESCO2	ASAHL	ATP5L	FKBP4	HN1	GUSB	PTRF	NME2	ST6GAL1	GLS	CHEK1	VRK1	OAT	SLC3A1	CDK6	WHSC1	NLE1	MSH6	RAD51	TIMELESS	PLK1	D	
46	GOTERM_CC_4	GO:0005856~cytoskeleton	66	0.0853	0.008310983	ANK3	EPB41L4B	CEBPA	STMN1	RCC2	MYO7B	PTP4A1	STOM	MICAL2	TACC2	NES	CENPF	CTNNAL1	MAPRE1	CCNB1	KIF23	CALD1	PRC1	TCP1	SLC9A3R1	ANLN	MYL5	EPB41L2	MYO15B	GSN	PEA15	SPAG4	AKAP9	CCNB2	PLK1	CDC2	LMNB2	PROCR	FARP1	COTL1	ENC1	TPX			
47	GOTERM_CC_4	GO:0005624~membrane fraction	46	0.0594	0.01137292	SOAT2	SLC26A3	FADS1	UGT2B17	ABCC3	CHPT1	APOB	MAN2A1	SCARB1	UGT2B15	CDH17	CYFIP2	SLC1A1	TJP1	CD68	CD59	OLR1	EMP3	NRP1	MGST1	DGAT2	EBNA1BP2	SYNCRIP	SLC26A2	SLC17A4	CYP2C9	TSPAN12	CYP3A7	FANCG	CD164	CALD1	SLC1A3	SMPD3	UGT2B10						
48	GOTERM_CC_4	GO:0005815~microtubule organizing center	13	0.0168	0.016548047	BIRC5	PLK1	MAD2L1	TCP1	PROCR	DLG7	TACC2	Cep72	RANBP1	BRCA1	AKAP9	BUB1	CCNB1																											
49	GOTERM_CC_5	GO:0016323~basolateral plasma membrane	11	0.0142	0.003843993	TJP1	MUC20	MYO1A	TRIP6	AQP3	EVL	SLC39A5	ANXA1	CDH17	VCL	RHBG																													
50	GOTERM_CC_5	GO:0005792~microsome	16	0.0207	0.006482761	UGT2B10	FADS1	UGT2B17	UGT2B7	CHPT1	APOB	UGT2B11	UGT2B15	PTRF	MGST1	SYNCRIP	GNPTG	PTGS2	CYP2C9	FANCG	CYP3A7																								
51	GOTERM_CC_5	GO:0005777~peroxisome	9	0.0116	0.037790145	SCP2	ACOX2	DAO	SLC27A2	EPHX2	PHYH	CAT	PAOX	ABP1																															
52	GOTERM_MF_4	GO:0004364~glutathione transferase activity	6	0.0078	0.004247365	GSTA5	MGST1	GSTA2	GSTA4	GSTA3	GSTA1																																		
53	GOTERM_MF_4	GO:0016818~hydrolase activity, acting on acid anhydrides, in phosphorus-containing anhydrides	39	0.0504	0.023844634	BLM	RFC2	MCM7	ABCC3	RFC4	EIF4A2	ABCB6	OCA2	GNL2	MCM6	ATAD3A	TUBB6	ATP8B2	RAN	GTPBP4	DDX10	RFC3	FIGNL1	DDX21	RAB35	TUBAL3	EHD4	MYL7	DKFZP564J	TGM2	RAB3B	MCM3	CDC6	ATP5L	MCM4	MCM5	MCM2	CHTF18	DNM1L	HSPA8	ABCA5	MSH6	R		
54	GOTERM_MF_4	GO:0015291~secondary active transmembrane transporter activity	17	0.022	0.024644484	SLC26A3	SLC2A14	SLC1A3	SLC25A22	SLC38A1	SLC5A11	SLC6A4	SLC2A5	SLC6A8	CDH17	SLC1A1	PEA15	SLC19A3	SLC26A2	SLC17A4	SLC2A8	SLC26A6																							
55	GOTERM_MF_4	GO:0016641~oxidoreductase activity, acting on the CH-NH2 group of donors, oxygen as acceptor	4	0.0052	0.025433096	DAO	MAOB	LOX	ABP1																																				
56	GOTERM_MF_5	GO:0005507~copper ion binding	16	0.0207	2.71328E-06	APOA4	SORL1	AFP	PAM	ANG	HEPH	LOX	MT1L	MT2A	PYCR1	MT1H	MT1X	MT1B	ALB	MT1E	ABP1																								
57	GOTERM_MF_5	GO:0046870~cadmium ion binding	5	0.0065	0.000176342	MT1H	MT1X	MT1B	MT1E	MT1L																																			
58	GOTERM_MF_5	GO:0046943~carboxylic acid transmembrane transporter activity	9	0.0116	0.012865527	SLC1A3	SLC25A22	SLC38A1	SLC3A1	SLC7A1	SLC7A6	SLC7A5	OCA2	SLC1A1																															
59	GOTERM_MF_5	GO:0004062~aryl sulfotransferase activity	3	0.0039	0.015682454	SULT1A2	SULT1A1	SULT1A4																																					
60	GOTERM_MF_5	GO:0004177~aminopeptidase activity	6	0.0078	0.02355901	PEPD	DPP4	ANPEP	PGCP	XPNPEP2	TPP1																																		
61	GOTERM_MF_5	GO:0015020~glucuronosyltransferase activity	5	0.0065	0.033691232	UGT2B10	UGT2B17	UGT2B7	UGT2B15	UGT2B11																																			
62	INTERPRO	IPR003080:Glutathione S-transferase, alpha class	5	0.0065	9.4996E-06	GSTA5	GSTA2	GSTA4	GSTA3	GSTA1																																			
63	INTERPRO	IPR010987:Glutathione S-transferase, C-terminal-like	8	0.0103	0.000149658	EEF1E1	GSTA5	CLIC4	MARS	GSTA2	GSTA4	GSTA3	GSTA1																																
64	INTERPRO	IPR004046:Glutathione S-transferase, C-terminal	7	0.009	0.000158638	EEF1E1	GSTA5	MARS	GSTA2	GSTA4	GSTA3	GSTA1																																	
65	INTERPRO	IPR000006:Metallothionein, vertebrate	6	0.0078	0.000160161	MT2A	MT1H	MT1X	MT1B	MT1E	MT1L																																		
66	INTERPRO	IPR003019:Metallothionein superfamily	6	0.0078	0.000160161	MT2A	MT1H	MT1X	MT1B	MT1E	MT1L																																		
67	INTERPRO	IPR000519:P-type trefoil	5	0.0065	0.000212169	TFF3	SI	TFF2	TFF1	GAA																																			
68	INTERPRO	IPR001314:Peptidase S1A, chymotrypsin	12	0.0155	0.002418431	F7	PRSS3	TMPRSS2	MST1	PRSS2	C2	PRSS23	HPN	F2	TMPRSS6	F10	KLK1																												
69	INTERPRO	IPR002213:UDP-glucuronosyl/UDP-glucosyltransferase	5	0.0065	0.007043097	UGT2B10	UGT2B17	UGT2B7	UGT2B15	UGT2B11																																			
70	INTERPRO	IPR000074:Apolipoprotein A1/A4/E	3	0.0039	0.008006812	APOA4	APOE	APOA1																																					
71	INTERPRO	IPR013326:Apolipoprotein/apolipophorin	3	0.0039	0.008006812	APOA4	APOE	APOA1																																					
72	INTERPRO	IPR012290:Fibrinogen, alpha/beta/gamma chain, coiled coil	3	0.0039	0.008006812	FGG	FGA	FGB																																					
73	INTERPRO	IPR001254:Peptidase S1 and S6, chymotrypsin/Hap	12	0.0155	0.008265517	F7	PRSS3	TMPRSS2	MST1	PRSS2	C2	PRSS23	HPN	F2	TMPRSS6	F10	KLK1																												
74	INTERPRO	IPR004045:Glutathione S-transferase, N-terminal	5	0.0065	0.011443824	GSTA5	GSTA2	GSTA4	GSTA3	GSTA1																																			
75	INTERPRO	IPR002347:Glucose/ribitol dehydrogenase	6	0.0078	0.028185938	CBR1	HSD17B2	DECR1	MGC4172	DHRS3	RDH5																																		
76	INTERPRO	IPR001902:Sulphate anion transporter	3	0.0039	0.03381575	SLC26A3	SLC26A2	SLC26A6																																					
77	KEGG_PATHWAY	hsa00980:Metabolism of xenobiotics by cytochrome P450	15	0.0194	7.18779E-05	UGT2B10	AKR1C1	UGT2B17	UGT2B7	GSTA4	AKR1C3	GSTA3	UGT2B11	UGT2B15	GSTA5	MGST1	GSTA2	CYP2C9	GSTA1	CYP3A7																									
78	KEGG_PATHWAY	hsa03320:PPAR signaling pathway	13	0.0168	0.001741434	ACOX2	SLC27A2	ME1	FABP1	PPARA	APOA1	APOC3	FABP6	NR1H3	SCP2	OLR1	CYP27A1	GK																											
79	KEGG_PATHWAY	hsa00480:Glutathione metabolism	9	0.0116	0.002690907	GSTA5	GPX3	ANPEP	MGST1	GSTA2	GSTA4	GPX4	GSTA3	GSTA1																															
80	KEGG_PATHWAY	hsa00561:Glycerolipid metabolism	8	0.0103	0.037655819	DGAT1	PPAP2C	DGAT2	PNLIPRP2	DGKD	GK	LIPA	LIPG																																
81	PANTHER_BP_ALL	BP00286:Cell structure	135	0.1744	8.16928E-06	VAV3	SLC6A8	KIAA1984	ASPM	CD59	HMMR	PDGFC	DDX10	NCOA7	FGB	FOXQ1	NOXA1	NETO2	SMPDL3A	NEDD4L	PPARA	APOA1	NY-SAR-48	ATP5L	EPB41L2	CCT5	TIMP3	ATF3	PAOX	E2F7	THOP1	MPZL1	RAB37	RAD51	MSH6	MORC4	TKT	FLJ21865	ARHGAP11	CCNG2	FAD				
82	PANTHER_BP_ALL	BP00180:Detoxification	27	0.0349	3.16092E-05	ME1	MCF2L	ELL2	FZD4	COTL1	FARP1	GSTA5	SMA5	GSTA2	HMBS	SEZ6L2	HNMT	CES1	TUBAL3	DPYSL3	BPHL	EPHX2	AFP	GSTA4	MAGED1	GSTA3	PON3	KIF2C	AREG	GSTA1	MSH6	RDH5													
83	PANTHER_BP_ALL	BP00026:Cholesterol metabolism	46	0.0594	0.000108771	SOAT2	DUSP14	DGAT1	CCNG2	CDC2	ETHE1	CENPA	OSBPL3	MT1L	BCL6	HMGB2	SUV39H2	BRCA1	P2RX4	DGAT2	HNMT	DGKD	FGB	ERBB3	TSPAN12	GAA	BIRC5	SMPD3	RABEPK	GABRE	PKMYT1	COL6A1	AQP3	TNFSF10	RALGPS1	ALDH18A1	KIAA1191	PEA15	CDCA3	TIMM23					
84	PANTHER_BP_ALL	BP00289:Other metabolism	116	0.1499	0.000114855	FBXL15	AKR1C1	RFC2	PAM	WDR4	ASPM	TNFRSF14	NCOA7	DKK1	SLC7A5	MAPRE1	DEFB1	DPYSL3	PFKFB4	MEP1A	NEDD4L	MYL5	PPARA	NY-SAR-48	EPB41L2	HN1	ASPA	TIMP3	PTRF	MTHFD2	GLS	STMN3	RPL15	LMBRD1	LGI4	TRPM6	CHTF18	MGC4172	PAOX	CCNB2	FADS				
85	PANTHER_BP_ALL	BP00103:Cell surface receptor mediated signal transduction	101	0.1305	0.000253064	VAV3	TFF3	GPA33	RFC2	TMEM29	VIPR1	NBR1	TMC4	SLC6A8	CDH17	KIAA1984	NRP1	CD59	HMGB2	PDGFC	NCOA7	GSG2	UNC93A	UGT2B10	APOA1	KREMEN2	PEA15	STMN3	TRPM6	C20orf108	SDCBP2	CDK6	OS9	GPR160	UBE2C	NLE1	RAD51	DAO	DONSON	FARP1	ABAT	S			
86	PANTHER_BP_ALL	BP00022:Fatty acid beta-oxidation	14	0.0181	0.00062042	ADCY3	ACOX2	PEO1	HDAC7A	TRIP6	SEPHS2	SLC7A6	MCM3	HN1	KREMEN2	DECR1	ARHGEF10	SLC7A5	LRRC19																										
87	PANTHER_BP_ALL	BP00104:G-protein mediated signaling	133	0.1718	0.003325227	VAV3	TFF3	GPA33	VIPR1	CHPT1	TMC4	KIAA1984	PRSS3	NRP1	CD59	TNFRSF14	HMGB2	FJX1	NCOA7	UNC93A	SMPDL3A	UGT2B10	GSTA4	LTB	GEMIN4	APOA1	EPB41L2	PEA15	STMN3	RPL15	PRSS2	TRPM6	SDCBP2	CDK6	WHSC1	OS9	GPR160	UBE2C	RAD51	TKT	MOSC2				
88	PANTHER_BP_ALL	BP00295:Steroid metabolism	27	0.0349	0.004055732	SOAT2	DAO	DGAT1	DUSP14	CDC2	C5orf4	OSBPL3	HSPD1	DGAT2	NUP107	HNMT	TSPAN12	FOXQ1	CYP3A7	BYSL	CDC45L	COL6A1	PKMYT1	HSD17B2	UGT2B11	TIMM23	CBR1	HMGB3	ALB	WNT10A	F11R	AREG													
89	PANTHER_BP_ALL	BP00020:Fatty acid metabolism	36	0.0465	0.007911643	FANCD2	SEMA4G	NOLC1	FABP1	TST	FBLN5	ORC6L	MCFD2	CDH17	SLC1A1	F7	CD68	HMMR	BRCA1	DECR1	FAM64A	WDSOF1	CYP2C9	LRRC19	ANXA1	SLC26A6	CALD1	ACOX2	CDKN1A	LTBP4	CA12	PPARA	MCM3	ACTB	YWHAH	CDH16	MT1X	EIF4EBP1	ACTG2	LETMD1	HMGN2				
90	PANTHER_BP_ALL	BP00112:Calcium mediated signaling	21	0.0271	0.023294121	TIMELESS	DPP4	MRS2L	LYAR	RCN1	EEF1E1	PDCD4	H2AFX	SI	PRSS2	BRCA1	EBNA1BP2	NCOA7	RGN	WDSOF1	MAPRE1	GPX4	MCM10	EHD4	RACGAP1	MOSC2																			
91	PANTHER_FAMILY	PTHR23299:METALLOTHIONEIN	6	0.0078	0.000283662	MT2A	MT1H	MT1X	MT1B	MT1E	MT1L																																		
92	PANTHER_FAMILY	PTHR11571:GLUTATHIONE S-TRANSFERASE	5	0.0065	0.000916544	GSTA5	GSTA2	GSTA4	GSTA3	GSTA1																																			
93	PANTHER_FAMILY	PTHR11926:GLUCOSYL/GLUCURONOSYL TRANSFERASES	5	0.0065	0.004141905	UGT2B10	UGT2B17	UGT2B7	UGT2B15	UGT2B11																																			
94	PANTHER_FAMILY	PTHR13826:INTESTINAL TREFOIL FACTOR-RELATED	3	0.0039	0.005416854	TFF3	TFF2	TFF1																																					
95	PANTHER_FAMILY	PTHR18976:APOLIPOPROTEIN	3	0.0039	0.005416854	APOA4	APOE	APOA1																																					
96	PANTHER_FAMILY	PTHR19410:SHORT-CHAIN DEHYDROGENASES/REDUCTASE FAMILY MEMBER	7	0.009	0.01459605	SCP2	CBR1	HSD17B2	DECR1	MGC4172	DHRS3	RDH5																																	
97	PANTHER_FAMILY	PTHR12081:E2F	3	0.0039	0.035951937	E2F1	E2F2	E2F7																																					
98	PANTHER_MF_ALL	MF00082:Transporter	44	0.0568	3.71944E-07	SLC26A3	SLC2A14	TCOF1	IPO4	SLC7A1	ABCC3	SLC6A4	SLC6A8	OSTalpha	OCA2	ABCB6	SLC39A5	MCFD2	SLC1A1	RHBG	SLC11A2	ATP8B2	AQP10	NUP107	SLC26A2	SLC17A4	SLC7A5	SLC2A8	SLC26A6	CSE1L	APOA4	SORL1	SLC1A3	MRS2L	SLC27A2	SLC30A1	SLC23A3	SL							
99	PANTHER_MF_ALL	MF00141:Hydrolase	58	0.0749	6.62869E-06	ANK3	EPB41L4B	TFF3	ANPEP	MAN2A1	ORC6L	LGR4	CAPN13	AIG1	ATAD3A	FUCA1	PDGFC	AQP10	HMBS	BCAT1	FIGNL1	DPYSL3	GAA	BPHL	SMPDL3A	ACY1	EPHX2	PNLIPRP2	GUSB	ASPA	RBM28	PPT1	GLS	CKS1B	SI	SLC3A1	HMGB3	CAT	SLC5A9	SAE1	RAD51	MOSC2	F		
100	PANTHER_MF_ALL	MF00123:Oxidoreductase	44	0.0568	6.89619E-06	DAO	AKR1C1	CRYL1	ME1	PAM	MCF2L	C5orf4	F10	HEPH	PYCR1	GPX3	SCP2	NRP1	BRCA1	DECR1	CYP2C9	GPX4	PH-4	RRM1	CYP3A7	NOXA1	ACOX2	GLRX	PHYH	HSD17B2	AKR1C3	HGD	PON3	BBOX1	MAOB	PRODH	CYP27A1	C16orf33	PHF19	CBR1	IMPDH1	PTGS2	MGC41		
101	PANTHER_MF_ALL	MF00131:Transferase	100	0.1292	8.33298E-06	STMN1	UGT2B17	CHPT1	KIAA1984	PRSS3	ACE2	MT1B	GSTA2	DGAT2	HS6ST2	DPYSL3	NETO2	UGT2B10	DPP4	TGM2	ESCO2	GSTA4	BXDC2	ST6GAL1	STMN3	PRSS2	OAT	GNPTG	HMGB3	HOMER1	TKT	ME1	MCF2L	ADAMTS13	MT1L	UGT2B15	SLC11A2	NEU1	C15orf21	ABAT	P				
102	PANTHER_MF_ALL	MF00212:Other G-protein modulator	145	0.1873	3.73523E-05	RAB11FIP5	PAM	NBR1	CHPT1	PUS1	SLC6A8	AVPI1	KIAA1984	CAPN13	NRP1	HMMR	MT1B	HMGB2	PDGFC	CKB	FJX1	DGAT2	NCOA7	HS6ST2	RBKS	IGSF9	CALD1	TCP1	MEP1A	CCT5	LRP1	ST6GAL1	STMN3	RPL15	CHAF1B	LMBRD1	MCM2	SLC3A1	CHTF18	WHSC1	PNRC1	CA			
103	PANTHER_MF_ALL	MF00127:Reductase	26	0.0336	0.001558971	C16orf35	AKR1C1	FADS1	DENR	RRM2	FZD4	FREQ	PYCR1	MT1B	DKK1	RRM1	CYP3A7	MUC20	ACY1	FGA	AKR1C3	ACY3	ALDH18A1	ASPA	TIMM23	AP1S3	EZH2	CBR1	GLULD1	WHSC1	MORC4														
104	PANTHER_MF_ALL	MF00262:Non-motor actin binding protein	128	0.1654	0.002306338	FAM54A	PAM	VIPR1	CENPA	TMC4	KIAA1984	FAIM	NRP1	HMMR	PDGFC	FIGNL1	NCOA7	SLC7A5	UBE2S	CALD1	TGM2	GLRX	NEDD4L	GEMIN4	NY-SAR-48	BBX	PEA15	GLS	CHAF1B	PRSS2	LMBRD1	SLC3A1	WHSC1	PNRC1	PAOX	MPZL1	HOMER1	MOSC2	CDCA8	MCF2L	DENR				
105	PANTHER_MF_ALL	MF00098:Large G-protein	37	0.0478	0.008491367	PSAT1	GPA33	PHYHIPL	MCF2L	GNG4	TFAM	APOB	MXI1	ABCB6	FARP1	POU4F1	TACC2	F7	PRSS3	CD59	C2	FZD2	HNMT	DGKD	SLC17A4	DKFZP564J	UNC93A	SLC35F2	MUC20	GSTA4	SLC7A6	SLC2A5	EPB41L2	GSN	NPPB	PDCD4	CKS1B	SI	WHSC1	OS9	CAT	UBE2C			
106	PANTHER_MF_ALL	MF00137:Glycosyltransferase	51	0.0659	0.009991678	UGT2B17	ASNS	CAPN13	KAZALD1	MGST1	HSPC111	UGT2B10	SLC27A2	LYAR	PON3	ASPA	SFRS7	ST6GAL1	BCL2L12	CKS1B	SUSD2	AKAP9	TP53AP1	MGC4172	GALNT10	C6orf173	DNAJC15	OIP5	TCOF1	C1orf115	ME1	UGT2B15	PERLD1	PHLDB2	C2	FCGRT	P2RX4	TSPAN12							
107	PANTHER_MF_ALL	MF00088:Apolipoprotein	15	0.0194	0.022376784	APOA4	APOA1	APOM	MCM3	APOB	APOC3	MUC13	SELENBP1	APOE	PHLDB2	APOH	ARHGEF10	ALB	BMP7	RAD51																									
108	PANTHER_MF_ALL	MF00078:Chaperonin	7	0.009	0.040848432	HSPD1	TCP1	FZD2	FZD4	CCT2	ATP5L	CCT5																																	
109	PANTHER_SUBFAMILY	PTHR11571:SF4~GLUTATHIONE S-TRANSFERASE CLASS ALPHA	5	0.0065	1.29642E-05	GSTA5	GSTA2	GSTA4	GSTA3	GSTA1																																			
110	PANTHER_SUBFAMILY	PTHR11783:SF13~SULFOTRANSFERASE SULT1A, PHENOL-PREFERRING	3	0.0039	0.002811403	SULT1A2	SULT1A1	SULT1A4																																					
111	PIR_SUPERFAMILY	PIRSF002564:metallothionein	6	0.0078	0.000162393	MT2A	MT1H	MT1X	MT1B	MT1E	MT1L																																		
112	PIR_SUPERFAMILY	PIRSF000503:glutathione transferase	5	0.0065	0.0116144	GSTA5	GSTA2	GSTA4	GSTA3	GSTA1																																			
113	PIR_SUPERFAMILY	PIRSF005678:glucuronosyltransferase	5	0.0065	0.024615015	UGT2B10	UGT2B17	UGT2B7	UGT2B15	UGT2B11																																			
114	PIR_SUPERFAMILY	PIRSF002367:apolipoprotein A-I	3	0.0039	0.038190753	APOE	APOA1	APOC3																																					
115	SP_PIR_KEYWORDS	disease mutation	98	0.1266	1.31409E-08	SLC25A22	SERPINA1	PUS1	SLC6A8	FGB	GK	GAA	PEPD	ACY1	ESCO2	APOA1	SERPINA6	GUSB	CCT5	TIMP3	ASPA	PPT1	CYP27A1	OAT	TRPM6	LDLR	SLC3A1	AMN	RAD51	MSH6	DKC1	TCOF1	BLM	ETHE1	LMNB2	FBLN5	APOB	ADAMTS13	OCA2	MCFD2	NEU1	SLC11A2	F7		
116	SP_PIR_KEYWORDS	signal	157	0.2028	1.31966E-05	AMICA1	TFF3	GPA33	UGT2B17	SERPINA1	PAM	VIPR1	EREG	RCN1	CDH17	PRSS3	CD59	ACE2	TNFRSF14	DKK1	FGB	LRRC19	EFNA1	DEFB1	GAA	IGSF9	NETO2	SMPDL3A	UGT2B10	AFP	RNASE4	ZG16	MEP1A	APOA1	ASAHL	SERPINA6	EDN1	GUSB	TIMP3	KREMEN2	CDH16				
117	SP_PIR_KEYWORDS	lipid binding	7	0.009	4.26208E-05	APOA4	APOE	FABP1	APOH	APOA1	APOB	VCL																																	
118	SP_PIR_KEYWORDS	intestine	8	0.0103	4.56035E-05	APOA4	TFF3	GAL	VIPR1	APOA1	APOB	APOC3	FABP6																																
119	SP_PIR_KEYWORDS	metal binding	7	0.009	6.02453E-05	MT2A	MT1H	MT1X	MT1B	AFP	MT1E	MT1L																																	
120	SP_PIR_KEYWORDS	copper	11	0.0142	8.4586E-05	MT1H	MT1X	MT1B	AFP	PAM	ALB	HEPH	MT1E	LOX	MT1L	ABP1																													
121	SP_PIR_KEYWORDS	cadmium	5	0.0065	0.00014131	MT1H	MT1X	MT1B	MT1E	MT1L																																			
122	SP_PIR_KEYWORDS	Secreted	84	0.1085	0.00019606	TFF3	SERPINA1	PAM	EREG	GPX3	PRSS3	ACE2	KAZALD1	COCH	TFF2	DKK1	FGB	DEFB1	SMPDL3A	APOA4	MST1	DPP4	AFP	RNASE4	ZG16	FGA	PNLIPRP2	APOA1	SERPINA6	PON3	MUC13	EDN1	CYR61	GSN	TIMP3	NPPB	IGFL2	ST6GAL1	PRSS2	FGG	LGI4	GNPTG	MGC417		
123	SP_PIR_KEYWORDS	transferase	81	0.1047	0.000314828	PSAT1	SAT2	POLE3	UGT2B17	CDC2L6	TST	CHPT1	SULT1A2	SULT1A4	CKB	MGST1	TPK1	GSTA2	UMPS	HMBS	BCAT1	METTL1	HS6ST2	GSG2	GK	RBKS	SNF1LK	UGT2B10	PFKFB4	TGM2	ESCO2	GSTA4	GRK5	ALDH18A1	KHK	GATM	NME2	ST6GAL1	CHEK1	VRK1	OAT	TRPM6			
124	SP_PIR_KEYWORDS	chylomicron	5	0.0065	0.000398196	APOA4	APOE	APOH	APOB	APOC3																																			
125	SP_PIR_KEYWORDS	oxidoreductase	39	0.0504	0.000844823	DAO	AKR1C1	FADS1	ME1	PAM	RRM2	HEPH	LOX	PYCR1	GPX3	FTH1	DECR1	CYP2C9	GPX4	RRM1	PH-4	CYP3A7	ACOX2	PHYH	NOS2A	HSD17B2	AKR1C3	HGD	ALDH18A1	BBOX1	MTHFD2	MAOB	CYP27A1	CBR1	IMPDH1	PTGS2	MGC4172	CAT	PAOX	DHRS3	ABP1	NDUFC2	RDH5		
126	SP_PIR_KEYWORDS	microsome	11	0.0142	0.009511665	PTRF	UGT2B10	MGST1	UGT2B17	SYNCRIP	UGT2B7	PTGS2	CYP2C9	UGT2B15	UGT2B11	CYP3A7																													
127	SP_PIR_KEYWORDS	transport	73	0.0943	0.014978007	SLC26A3	SLC2A14	SLC25A22	KPNA2	RAB11FIP5	SLC7A1	OSBPL3	SNX4	SLC6A8	HEPH	ABCB6	CDH17	RAN	AQP10	SLC7A5	APOA4	GLRX	SLC7A6	APOA1	ATP5L	SERPINA6	RBM8A	SLC40A1	PEA15	SLC3A1	TRPM6	LDLR	SLC5A9	RAB37	FADS1	IGF2R	TCOF1	IPO4	FABP1	A					
128	SP_PIR_KEYWORDS	lipid metabolism	11	0.0142	0.019913446	SORL1	SOAT2	ACOX2	SLC27A2	LDLR	SULT1A2	SCARB1	APOB	APOC3	SULT1A1	SULT1A4																													
129	SP_PIR_KEYWORDS	calcium	41	0.053	0.020672257	S100A11	F10	FBLN5	APOB	FREQ	RCN1	ADAMTS13	MCFD2	CDH17	F7	PRSS3	CAPN12	RGN	ANXA4	PH-4	PLA2G12B	ANXA1	ASGR1	SULF2	EHD4	SLC26A6	MYL7	FAM20C	TGM2	NOS2A	MYL5	F2	ARSE	GSN	CDH16	LRP1	CRELD1	PRSS2	FGG	TRPM6	ITGA7	GALNT10	DNASE		
130	SP_PIR_KEYWORDS	cholesterol metabolism	5	0.0065	0.028053477	SORL1	SOAT2	LDLR	APOA1	APOB																																			
131	SP_PIR_KEYWORDS	peroxisome	8	0.0103	0.036271784	SCP2	ACOX2	DAO	SLC27A2	EPHX2	PHYH	CAT	PAOX																																
132	SP_PIR_KEYWORDS	transmembrane protein	35	0.0452	0.041006509	IGF2R	ANPEP	HPN	PAM	SLC6A4	PROCR	VIPR1	GJB1	SLC6A8	ACE2	UGT2B15	SCARB1	CD68	TM4SF1	ERBB2	MGST1	SLC7A5	CYP2C9	FXYD3	ASGR1	CYP3A7	UGT2B10	DPP4	UGT2B7	MEP1A	KITLG	SLC2A5	LRP1	ST6GAL1	CYP27A1	GUCY2C	LDLR	SLC3A1	ITGA7	AREG					
133	UP_SEQ_FEATURE	metal ion-binding site:Calcium	7	0.009	0.049474531	PRSS3	TGM2	PRSS2	PLA2G12B	ARSE	SULF2	TXT																																	

Supplementary Table 2. List of the genes of LD cells showing at least 1.5-fold increase or decrease with respect to the HD cells

First column reports the gene symbol, the second the gene description, the third the RefSeq number and the last column reports the values of LD/HD ratio.

Supplementary Table 2

GeneSymbol	Description	RefSeq	LD/HD
PFKFB3	6-phosphofructo-2-kinase/fructose-2,6-biphosphatase 3	NM_004566	0.12
LOC253012	hypothetical protein LOC253012	NM_198151	0.32
CYBRD1	cytochrome b reductase 1	NM_024843	0.32
A_32_P7974			0.34
ITLN1	intelectin 1 (galactofuranose binding)	NM_017625	0.39
BU561469	Transcribed locus		0.40
GNG13	guanine nucleotide binding protein (G protein), gamma 13	NM_016541	0.42
PRAP1	proline-rich acidic protein 1	NM_145202	0.46
SIGLEC11	sialic acid binding Ig-like lectin 11	NM_052884	0.48
AK128714	Similar to embigin homolog		0.50
G0S2	G0/G1switch 2	NM_015714	0.50
SERPINA6	serpin peptidase inhibitor, clade A (alpha-1 antiproteinase, antitrypsin), member 6	NM_001756	0.51
SAMD9L	sterile alpha motif domain containing 9-like	NM_152703	0.51
KLHL13	kelch-like 13 (Drosophila)	NM_033495	0.51
APOH	apolipoprotein H (beta-2-glycoprotein I)	NM_000042	0.51
AL049990	Chromosome 4 open reading frame 31		0.52
LOC124220	similar to common salivary protein 1	NM_145252	0.54
SI	sucrase-isomaltase (alpha-glucosidase)	NM_001041	0.54
IF	complement factor I	NM_000204	0.54
FGA	fibrinogen alpha chain	NM_021871	0.54
SPON1	spondin 1, extracellular matrix protein	NM_006108	0.55
MIA2	melanoma inhibitory activity 2	NM_054024	0.55
CPA2	carboxypeptidase A2 (pancreatic)	NM_001869	0.55
FLJ23191	chromosome 4 open reading frame 31	NM_024574	0.55
CR603982	MRNA; cDNA DKFZp313B1017 (from clone DKFZp313B1017)		0.56
IF	complement factor I	NM_000204	0.56
THC2406147	BF476310 naa21a07.x1 NCI_CGAP_Pr28 Homo sapiens cDNA clone IMAGE:3255444 3' similar to contains Alu repetitive element;contains element MIR MIR repetitive element ;, mRNA sequence [BF476310]		0.56
THC2437430	ALU7_HUMAN (P39194) Alu subfamily SQ sequence contamination warning entry, partial (17%) [THC2437430]		0.56
REN	renin	NM_000537	0.56
ICAM2	intercellular adhesion molecule 2	NM_000873	0.56
ENST00000361681			0.56
ADH4	alcohol dehydrogenase 4 (class II), pi polypeptide	NM_000670	0.57
AFP	alpha-fetoprotein	NM_001134	0.57
C9orf125	chromosome 9 open reading frame 125	NM_032342	0.57
CYBRD1	cytochrome b reductase 1	NM_024843	0.57
BCDO2	beta-carotene dioxygenase 2	NM_031938	0.58
U52054	S6 H-8 mRNA expressed in chromosome 6-suppressed melanoma cells		0.58
PRKACB	protein kinase, cAMP-dependent, catalytic, beta	NM_002731	0.58
FRAS1	Homo sapiens Fraser syndrome 1 (FRAS1), transcript variant 2, mRNA [NM_206841]	NM_206841	0.59
MAN1A1	mannosidase, alpha, class 1A, member 1	NM_005907	0.59
MAN1A1	mannosidase, alpha, class 1A, member 1	NM_005907	0.60
PKIB	protein kinase (cAMP-dependent, catalytic) inhibitor beta	NM_181795	0.61
COL5A2	collagen, type V, alpha 2	NM_000393	0.62
A_24_P508946			0.62
F3	coagulation factor III (thromboplastin, tissue factor)	NM_001993	0.62
AK128714	Similar to embigin homolog		0.63
GALNTL1	UDP-N-acetyl-alpha-D-galactosamine:polypeptide N-acetylgalactosaminyltransferase-like 1	NM_020692	0.63
TFF2	trefoil factor 2 (spasmolytic protein 1)	NM_005423	0.63
YAP1	Yes-associated protein 1, 65kDa	NM_006106	0.63
ENST00000305820			0.64
C1S	complement component 1, s subcomponent	NM_001734	0.65
LOC339483	Homo sapiens hypothetical protein LOC339483 (LOC339483), mRNA [NM_178546]	NM_178546	0.65
THC2434747	1P3K_A Chain A, Crystallographic Studies Of Nucleosome Core Particles Containing Histone 'sin' Mutants. (Xenopus laevis;) , partial (30%) [THC2434747]		1.09
SLCO4A1	solute carrier organic anion transporter family, member 4A1	NM_016354	1.52
AJ293393	MRNA differentially expressed in malignant melanoma, clone MM D3		1.52
ADAM19	ADAM metallopeptidase domain 19 (meltrin beta)	NM_033274	1.53
P8	nuclear protein 1	NM_012385	1.54
CD104030	Transcribed locus		1.55
F2	coagulation factor II (thrombin)	NM_000506	1.55
TOP2A	topoisomerase (DNA) II alpha 170kDa	NM_001067	1.56
ARHGAP22	Rho GTPase activating protein 22	NM_021226	1.57
C20orf55	family with sequence similarity 110, member A	NM_207121	1.57
APOM	apolipoprotein M	NM_019101	1.57
BRCA1	breast cancer 1, early onset	NM_007295	1.57
EGLN3	egl nine homolog 3 (C. elegans)	NM_022073	1.57
LEPREL1	leprecan-like 1	NM_018192	1.58
NNMT	nicotinamide N-methyltransferase	NM_006169	1.58
KIAA1102	hypothetical protein	NM_014988	1.58
ATP1B1	ATPase, Na+/K+ transporting, beta 1 polypeptide	NM_001677	1.58
ITGB3BP	integrin beta 3 binding protein (beta3-endonexin)	NM_014288	1.59
ANXA1	annexin A1	NM_000700	1.59
CEACAM7	carcinoembryonic antigen-related cell adhesion molecule 7	NM_006890	1.59
XAGE3	X antigen family, member 3	NM_130776	1.60
CDCA1	NUF2, NDC80 kinetochore complex component, homolog (S. cerevisiae)	NM_145697	1.60
KIAA1181	endoplasmic reticulum-golgi intermediate compartment (ERGIC) 1		1.60
GDPD2	glycerophosphodiester phosphodiesterase domain containing 2	NM_017711	1.60
OXCT1	3-oxoacid CoA transferase 1	NM_000436	1.61
SLC12A2	solute carrier family 12 (sodium/potassium/chloride transporters), member 2	NM_001046	1.61
ANP32A	acidic (leucine-rich) nuclear phosphoprotein 32 family, member A	NM_006305	1.61
CENPH	centromere protein H	NM_022909	1.62
CSF1R	colony stimulating factor 1 receptor, formerly McDonough feline sarcoma viral (v-fms) oncogene homolog	NM_005211	1.62
BIRC5	baculoviral IAP repeat-containing 5 (survivin)	NM_001012271	1.62
FLJ39647	chromosome 17 open reading frame 78	NM_173625	1.63
FAM64A	family with sequence similarity 64, member A	NM_019013	1.64
TMEM42	transmembrane protein 42	NM_144638	1.64
SLC2A14	solute carrier family 2 (facilitated glucose transporter), member 14		1.64
PBK	PDZ binding kinase	NM_018492	1.64
DLG7	discs, large homolog 7 (Drosophila)	NM_014750	1.64
KIF15	kinesin family member 15	NM_020242	1.65
GSG2	germ cell associated 2 (haspin)		1.66
MT2A	metallothionein 2A	NM_005953	1.66
CCNB1	cyclin B1	NM_031966	1.66
ASNS	asparagine synthetase	NM_001673	1.67
LAMA1	laminin, alpha 1	NM_005559	1.67
CHMP4B	chromatin modifying protein 4B	NM_176812	1.67
CEACAM6	carcinoembryonic antigen-related cell adhesion molecule 6 (non-specific cross reacting antigen)	NM_002483	1.68
AK098511	CDNA FLJ25645 fis, clone SYN00113		1.68
THC2279735			1.69
SLA	Src-like-adaptor	NM_006748	1.69
CD24	CD24 molecule	NM_013230	1.69
BMP7	bone morphogenetic protein 7 (osteogenic protein 1)	NM_001719	1.69
LFNG	Homo sapiens lunatic fringe homolog (Drosophila) (LFNG), mRNA [NM_002304]	NM_002304	1.69
AL581048	Aldehyde dehydrogenase 18 family, member A1		1.69
GAJ	meiotic nuclear divisions 1 homolog (S. cerevisiae)	NM_032117	1.69
PPP3R1	protein phosphatase 3 (formerly 2B), regulatory subunit B, alpha isoform	NM_000945	1.69
ESRRG	estrogen-related receptor gamma	NM_206594	1.70
LMNB1	lamin B1	NM_005573	1.70
UBE2C	ubiquitin-conjugating enzyme E2C	NM_181803	1.70
INHBB	inhibin, beta B (activin AB beta polypeptide)	NM_002193	1.71
ZC3H7B	zinc finger CCCH-type containing 7B	NM_017590	1.72
RRM2	ribonucleotide reductase M2 polypeptide	NM_001034	1.72
LAMA1	laminin, alpha 1	NM_005559	1.73
CDC2	cell division cycle 2, G1 to S and G2 to M	NM_001786	1.74
PTTG2	pituitary tumor-transforming 2	NM_006607	1.74
CEACAM7	carcinoembryonic antigen-related cell adhesion molecule 7	NM_006890	1.76
CEACAM6	carcinoembryonic antigen-related cell adhesion molecule 6 (non-specific cross reacting antigen)		1.76
DPEP1	dipeptidase 1 (renal)	NM_004413	1.76
KRT20	keratin 20	NM_019010	1.76
KNTC2	NDC80 homolog, kinetochore complex component (S. cerevisiae)	NM_006101	1.78
DNAJC15	DnaJ (Hsp40) homolog, subfamily C, member 15	NM_013238	1.78
IGFBP2	insulin-like growth factor binding protein 2, 36kDa	NM_000597	1.78
FKSG14	centromere protein K	NM_022145	1.79
DHRS2	dehydrogenase/reductase (SDR family) member 2	NM_182908	1.79
C3	complement component 3	NM_000064	1.79
MTHFD2	methylenetetrahydrofolate dehydrogenase (NADP+ dependent) 2, methenyltetrahydrofolate cyclohydrolase	NM_006636	1.79
FLJ36031	hypothetical protein FLJ36031	NM_175884	1.79
PLB1	phospholipase B1		1.80
SLC17A4	solute carrier family 17 (sodium phosphate), member 4	NM_005495	1.81
ST6GALNAC1	ST6 (alpha-N-acetyl-neuraminyl-2,3-beta-galactosyl-1,3)-N-acetylgalactosaminide alpha-2,6-sialyltransferase 1	NM_018414	1.82
MLF1IP	MLF1 interacting protein	NM_024629	1.83
TSPAN5	tetraspanin 5	NM_005723	1.83
ALPPL2	alkaline phosphatase, placental-like 2	NM_031313	1.84
CHMP4B	chromatin modifying protein 4B	NM_176812	1.86
PTPRR	protein tyrosine phosphatase, receptor type, R	NM_002849	1.87
GNRH2	gonadotropin-releasing hormone 2	NM_178332	1.88
TRIM55	tripartite motif-containing 55	NM_184086	1.88
DHRS2	dehydrogenase/reductase (SDR family) member 2	NM_182908	1.90
SPBC25	SPC25, NDC80 kinetochore complex component, homolog (S. cerevisiae)	NM_020675	1.91
DPYSL3	dihydropyrimidinase-like 3	NM_001387	1.98
S100P	S100 calcium binding protein P	NM_005980	1.98
PLSCR4	phospholipid scramblase 4	NM_020353	1.99
GPX7	glutathione peroxidase 7	NM_015696	1.99
BCAT1	branched chain aminotransferase 1, cytosolic	NM_005504	2.00
PPP2R2B	protein phosphatase 2 (formerly 2A), regulatory subunit B, beta isoform	NM_004576	2.01
IGFBP1	insulin-like growth factor binding protein 1	NM_000596	2.01
GNRH2	gonadotropin-releasing hormone 2	NM_001501	2.06
CPE	carboxypeptidase E	NM_001873	2.07
SLC39A2	solute carrier family 39 (zinc transporter), member 2	NM_014579	2.08
CP	ceruloplasmin (ferroxidase)	NM_000096	2.08
TSPAN5	tetraspanin 5		2.09
LAMA1	laminin, alpha 1	NM_005559	2.14
IL1B	interleukin 1, beta	NM_000576	2.15
SPARC	secreted protein, acidic, cysteine-rich (osteonectin)	NM_003118	2.22
KRT23	Homo sapiens keratin 23 (histone deacetylase inducible) (KRT23), transcript variant 2, mRNA [NM_173213]	NM_173213	2.24
MMP1	matrix metallopeptidase 1 (interstitial collagenase)	NM_002421	2.25
SOX2	SRY (sex determining region Y)-box 2	NM_003106	2.27
KIAA1102	hypothetical protein	NM_014988	2.37
SOCS2	suppressor of cytokine signaling 2	NM_003877	2.38
SULF2	sulfatase 2	NM_018837	2.50
THC2439829			2.53
GSTM3	glutathione S-transferase M3 (brain)	NM_000849	3.19
PAGE4	P antigen family, member 4 (prostate associated)	NM_007003	3.44
GSTM3	glutathione S-transferase M3 (brain)	NM_000849	3.68

Supplementary Table 3. List of the genes found at the intersection of the sets of differentially expressed genes obtained from the "Diff/Cycl" and the "LD/HD" experiments.

First column reports the gene symbol, the second the gene description, the third the RefSeq number. Fourth and fifth columns report the Log2 Diff/Cycl and Log2 LD/HD ratios, respectively. Last column indicates the quadrant of the scatter plot of Figure 5 in which the gene matches.

Supplementary Table 3

GeneSymbol	Description	RefSeq	Log2 Diff/Cycl	Log2 LD/HD	Quadrant
SOCS2	suppressor of cytokine signaling 2	NM_003877	**-3.55**	**1.25**	**a**
MT2A	metallothionein 2A	NM_005953	**-3.01**	**0.73**	**a**
ANXA1	annexin A1	NM_000700	**-2.85**	**0.67**	**a**
DPYSL3	dihydropyrimidinase-like 3	NM_001387	**-2.84**	**0.98**	**a**
BIRC5	baculoviral IAP repeat-containing 5 (survivin)	NM_001012271	**-2.82**	**0.69**	**a**
CCNB1	cyclin B1	NM_031966	**-2.77**	**0.73**	**a**
MTHFD2	methylenetetrahydrofolate dehydrogenase (NADP+ dependent) 2, methenyltetrahydrofolate cyclohydrolase	NM_006636	**-2.77**	**0.84**	**a**
UBE2C	ubiquitin-conjugating enzyme E2C	NM_181803	**-2.73**	**0.77**	**a**
SLC2A14	solute carrier family 2 (facilitated glucose transporter), member 14		**-2.55**	**0.71**	**a**
CDC2	cell division cycle 2, G1 to S and G2 to M	NM_001786	**-2.30**	**0.80**	**a**
SPBC25	SPC25, NDC80 kinetochore complex component, homolog (S. cerevisiae)	NM_020675	**-2.27**	**0.93**	**a**
BCAT1	branched chain aminotransferase 1, cytosolic	NM_005504	**-2.26**	**1.00**	**a**
ASNS	asparagine synthetase	NM_001673	**-2.22**	**0.74**	**a**
KNTC2	NDC80 homolog, kinetochore complex component (S. cerevisiae)	NM_006101	**-2.01**	**0.83**	**a**
RRM2	ribonucleotide reductase M2 polypeptide	NM_001034	**-1.98**	**0.78**	**a**
DLG7	discs, large homolog 7 (Drosophila)	NM_014750	**-1.83**	**0.72**	**a**
FAM64A	family with sequence similarity 64, member A	NM_019013	**-1.83**	**0.71**	**a**
BMP7	bone morphogenetic protein 7 (osteogenic protein 1)	NM_001719	**-1.82**	**0.75**	**a**
DNAJC15	DnaJ (Hsp40) homolog, subfamily C, member 15	NM_013238	**-1.76**	**0.83**	**a**
TOP2A	topoisomerase (DNA) II alpha 170kDa	NM_001067	**-1.75**	**0.64**	**a**
PBK	PDZ binding kinase	NM_018492	**-1.74**	**0.71**	**a**
BRCA1	breast cancer 1, early onset	NM_007295	**-1.73**	**0.65**	**a**
PTTG2	pituitary tumor-transforming 2	NM_006607	**-1.70**	**0.80**	**a**
MLF1IP	MLF1 interacting protein	NM_024629	**-1.62**	**0.87**	**a**
GSG2	germ cell associated 2 (haspin)		**-1.57**	**0.73**	**a**
CDCA1	NUF2, NDC80 kinetochore complex component, homolog (S. cerevisiae)	NM_145697	**-1.44**	**0.68**	**a**
SLC12A2	solute carrier family 12 (sodium/potassium/chloride transporters), member 2	NM_001046	**-1.42**	**0.69**	**a**
GAJ	meiotic nuclear divisions 1 homolog (S. cerevisiae)	NM_032117	**-1.32**	**0.76**	**a**
FKSG14	centromere protein K	NM_022145	**-1.13**	**0.84**	**a**
KIF15	kinesin family member 15	NM_020242	**-1.02**	**0.73**	**a**
DHRS2	dehydrogenase/reductase (SDR family) member 2	NM_182908	**-0.88**	**0.93**	**a**
G0S2	G0/G1switch 2	NM_015714	**4.99**	**-1.00**	**c**
SERPINA6	serpin peptidase inhibitor, clade A (alpha-1 antiproteinase, antitrypsin), member 6	NM_001756	**2.31**	**-0.98**	**c**
KLHL13	kelch-like 13 (Drosophila)	NM_033495	**1.21**	**-0.97**	**c**
APOH	apolipoprotein H (beta-2-glycoprotein I)	NM_000042	**3.33**	**-0.97**	**c**
SI	sucrase-isomaltase (alpha-glucosidase)	NM_001041	**4.12**	**-0.89**	**c**
FGA	fibrinogen alpha chain	NM_021871	**1.05**	**-0.88**	**c**
SPON1	spondin 1, extracellular matrix protein	NM_006108	**1.36**	**-0.87**	**c**
CR603982	MRNA; cDNA DKFZp313B1017 (from clone DKFZp313B1017)		**2.77**	**-0.85**	**c**
AFP	alpha-fetoprotein	NM_001134	**3.36**	**-0.82**	**c**
PKIB	protein kinase (cAMP-dependent, catalytic) inhibitor beta	NM_181795	**1.70**	**-0.72**	**c**
COL5A2	collagen, type V, alpha 2	NM_000393	**1.11**	**-0.70**	**c**
A_24_P508946			**3.29**	**-0.69**	**c**
TFF2	trefoil factor 2 (spasmolytic protein 1)	NM_005423	**3.05**	**-0.67**	**c**
ENST00000305820			**1.13**	**-0.65**	**c**
LOC339483	Homo sapiens hypothetical protein LOC339483 (LOC339483), mRNA [NM_178546]	NM_178546	**0.86**	**-0.62**	**c**
F2	coagulation factor II (thrombin)	NM_000506	**2.14**	**0.63**	**b**
APOM	apolipoprotein M	NM_019101	**4.76**	**0.65**	**b**
FLJ39647	chromosome 17 open reading frame 78	NM_173625	**2.82**	**0.71**	**b**
SLA	Src-like-adaptor	NM_006748	**2.01**	**0.75**	**b**
IGFBP2	insulin-like growth factor binding protein 2, 36kDa	NM_000597	**3.07**	**0.83**	**b**
SLC17A4	solute carrier family 17 (sodium phosphate), member 4	NM_005495	**2.52**	**0.86**	**b**
PTPRR	protein tyrosine phosphatase, receptor type, R	NM_002849	**2.02**	**0.91**	**b**
GNRH2	gonadotropin-releasing hormone 2	NM_178332	**1.59**	**0.91**	**b**
GNRH2	gonadotropin-releasing hormone 2	NM_001501	**1.69**	**1.04**	**b**
SULF2	sulfatase 2	NM_018837	**1.79**	**1.32**	**b**

Appendix II

Mechanisms of defence from Fe(II) toxicity in human intestinal Caco-2 cells

Manuela Natoli [a,*], Armando Felsani [a], Simonetta Ferruzza [b], Yula Sambuy [b], Raffaella Canali [b], Maria Laura Scarino [b]

a CNR, Institute of Neurobiology and Molecular Medicine, Via del Fosso di Fiorano 64, 00143 Rome, Italy

b National Research Institute on Food and Nutrition (INRAN), Via Ardeatina 546, 00178 Rome, Italy

Iron is used to cure iron-deficient anaemia but can also be toxic to the intestine. Fe(II) toxicity was investigated using differentiated human intestinal Caco-2 cells treated with 15 and 50 μM of Fe(II)/ascorbate for 2 h (acute phase), and followed for 24 h after iron removal and replacement of complete culture medium (late phase). During the acute phase damage to tight junctions occurred as demonstrated by an increase in cell monolayer permeability and by partial delocalization of the tight junction protein claudin 4 from the plasma membrane to an intracellular compartment. At the end of the late phase, cells treated with 15 μM Fe(II) showed full restoration of claudin 4 localization to the plasma membrane and their tight junction permeability returned to values close to those of control cells. Conversely, cells treated with 50 μM Fe(II) showed sustained and irreversible damage to the tight junctions, accompanied by apoptosis and necrosis. Activation of NF-jB occurred at both Fe(II) concentrations after 30 min of Fe(II) treatment, followed, at the end of the acute phase, by a strong induction of mRNA coding for heat shock protein 70 and metallothionein 2A. Our results indicate that intestinal cells respond to iron toxicity by strongly activating two genes involved in cell response to stress, although the outcome in terms of cell survival is different depending on the dose of treatment, namely almost complete restoration of epithelial permeability and cell survival at 15 μM Fe(II), and progressive and irreversible cytotoxicity leading to apoptosis and necrosis at 50 μM Fe(II).

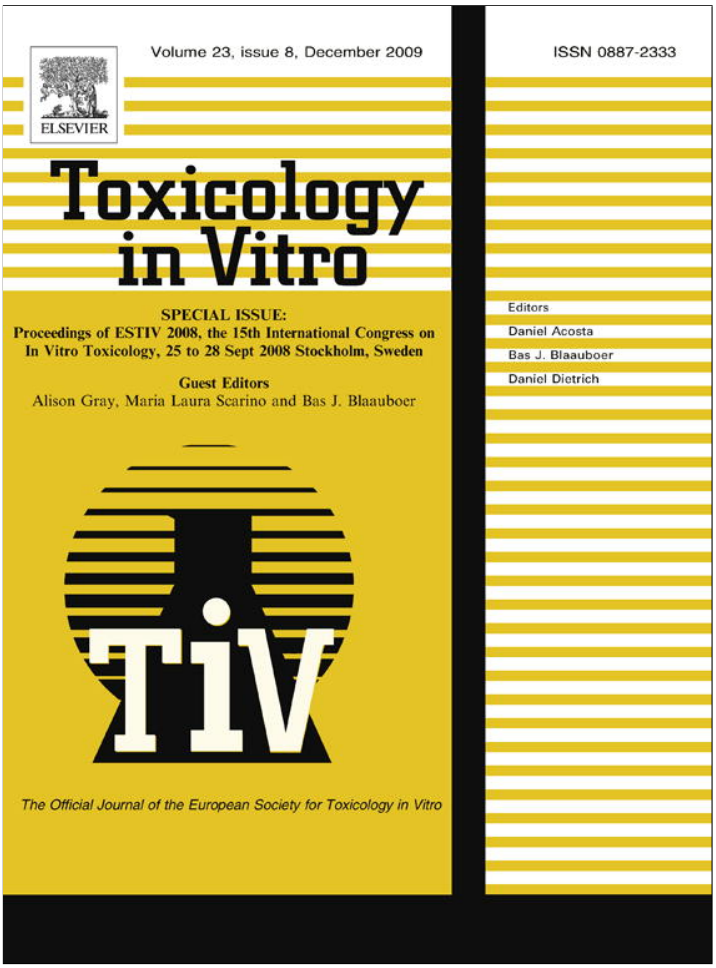

Toxicology in Vitro 23 (2009) 1510–1515

Contents lists available at ScienceDirect

Toxicology in Vitro

journal homepage: www.elsevier.com/locate/toxinvit

Mechanisms of defence from Fe(II) toxicity in human intestinal Caco-2 cells

Manuela Natoli [a,*], Armando Felsani [a], Simonetta Ferruzza [b], Yula Sambuy [b], Raffaella Canali [b], Maria Laura Scarino [b]

[a] CNR, Institute of Neurobiology and Molecular Medicine, Via del Fosso di Fiorano 64, 00143 Rome, Italy
[b] National Research Institute on Food and Nutrition (INRAN), Via Ardeatina 546, 00178 Rome, Italy

ARTICLE INFO

Article history:
Received 1 November 2008
Accepted 15 June 2009
Available online 18 June 2009

Keywords:
Apoptosis
Claudin 4 delocalization
Epithelial permeability
Necrosis
Oxidative stress
Phenol red passage
Trans-epithelial resistance
RT-PCR

ABSTRACT

Iron is used to cure iron-deficient anaemia but can also be toxic to the intestine. Fe(II) toxicity was investigated using differentiated human intestinal Caco-2 cells treated with 15 and 50 μM of Fe(II)/ascorbate for 2 h (acute phase), and followed for 24 h after iron removal and replacement of complete culture medium (late phase). During the acute phase damage to tight junctions occurred as demonstrated by an increase in cell monolayer permeability and by partial delocalization of the tight junction protein claudin 4 from the plasma membrane to an intracellular compartment. At the end of the late phase, cells treated with 15 μM Fe(II) showed full restoration of claudin 4 localization to the plasma membrane and their tight junction permeability returned to values close to those of control cells. Conversely, cells treated with 50 μM Fe(II) showed sustained and irreversible damage to the tight junctions, accompanied by apoptosis and necrosis. Activation of NF-κB occurred at both Fe(II) concentrations after 30 min of Fe(II) treatment, followed, at the end of the acute phase, by a strong induction of mRNA coding for heat shock protein 70 and metallothionein 2A. Our results indicate that intestinal cells respond to iron toxicity by strongly activating two genes involved in cell response to stress, although the outcome in terms of cell survival is different depending on the dose of treatment, namely almost complete restoration of epithelial permeability and cell survival at 15 μM Fe(II), and progressive and irreversible cytotoxicity leading to apoptosis and necrosis at 50 μM Fe(II).

1. Introduction

Iron is the most abundant transition metal in the body and it is an essential micronutrient required for many important biological processes, however, when in excess, it can generate oxidative stress due to the production of reactive oxygen species (ROS) in aqueous solutions (Puntarulo, 2005). Tightly regulated cellular mechanisms have evolved to govern the absorption, utilization and sequestration of iron (Hentze et al., 2004). In mammals, there is no pathway for iron excretion and whole body iron homeostasis is almost exclusively regulated through its absorption at the level of the intestinal mucosa (Sharp and Srai, 2007). However, since iron absorption in humans ranges from 1% to 30% of the whole quantity ingested with the diet and daily iron requirements are relatively high (11–12 mg/day), iron deficiency is still a public health concern worldwide (Tapiero et al., 2001). To fight iron-deficient anaemia, especially in children and in women in the reproductive age, this metal is frequently prescribed as a supplement or it is used to fortify food. However, in addition to the well known toxic effects of iron overload (Puntarulo, 2005), even iron supplementation can cause damage and increased permeability of the intestinal mucosa, as demonstrated by a recent follow-up study in African schoolchildren (Nchito et al., 2006).

Using the human intestinal Caco-2 cell line as an *in vitro* model of human absorptive small intestine (Sambuy et al., 2005), we have previously shown that Fe(II) ascorbate can cause a biphasic cytotoxic effect indicated by an early increase in tight junction permeability and disorganization of the perijunctional F-actin cytoskeleton (during iron treatment), followed by a delayed toxicity leading to apoptosis and necrosis (during the 24 h that followed iron treatment), and that this latter phase was mediated by the generation of ROS (Ferruzza et al., 2002, 2003). In the present paper, we therefore aimed at better characterizing the mechanisms underlying the observed iron cytotoxic effects in Caco-2 cells.

Briefly, we have shown that during Fe(II) treatment the increase in tight junction permeability was accompanied by delocalization of the tight junction protein claudin 4 and by activation of the redox-sensitive transcription factor NF-κB. This led, at both concentration tested, to increased transcription of genes coding for proteins involved in stress response, namely heat shock protein 70 (HSPA1A) and metallothionein 2A, (MT2A). After 24 h from treatment with 15 μM Fe(II), tight junction permeability returned

Abbreviations: HEPES, N-2-hydroxyethyl piperazine-N-4-butanesulfonic acid; MES, morpholinoetanesulfonic acid; Papp, apparent permeability; PI, propidium iodide; qRT-PCR, quantitative reverse transcription-PCR; ROS, reactive oxygen species; TEER, trans-epithelial electrical resistance.

* Corresponding author.
E-mail address: manuela.natoli@inmm.cnr.it (M. Natoli).

0887-2333/$ - see front matter © 2009 Elsevier Ltd. All rights reserved.
doi:10.1016/j.tiv.2009.06.016

to values close to control and claudin 4 localization at the plasma membrane was restored. Conversely, at 50 μM Fe(II) in spite of additional increase in transcription of genes involved in ROS and iron detoxification, namely HSPA1A, MT2A, Mn-superoxide dismutase (SOD2) and ferritin heavy chain (FTH1), apoptosis was activated leading, at the end of the late phase, to irreversible cytotoxic damage and extensive cell death.

2. Materials and methods

2.1. Cell culture

The human intestinal Caco-2 cell line was originally obtained from Prof. Alan Zweibaum (INSERM, Villejuif, France). Cells were routinely subcultured when they reached 50% density and were maintained at 37 °C in a 90% air/10% CO_2 atmosphere in DMEM containing 25 mM glucose, 3.7 g/L $NaHCO_3$ and supplemented with 4 mM L-glutamine, 1% non essential amino acids, 100 U/L penicillin, 100 μg/L streptomycin, and 10% heat-inactivated foetal calf serum (Gibco) (complete medium). Immunofluorescence and gene expression experiments were performed on cells seeded on polyethylene-terephthalate filter inserts (0.4 μm pore diameter, 4.71 cm^2; Becton-Dickinson), while permeability studies were performed on cells seeded on polycarbonate filter inserts (Transwell, 0.4 μm pore diameter, 1.13 cm^2; Corning). Cells were seeded on filters at a density of $3{\cdot}10^5$ cell/cm^2 and maintained for 21 days in complete medium; the medium was changed three times a week.

2.2. Iron treatment

Caco-2 cells were treated for 2 h (acute treatment) from the apical side with 15 and 50 μM Fe(II)/ascorbate in Balanced Salt Solution (BSS) (137 mM NaCl, 5.36 mM KCl, 0.44 mM KH_2PO_4, 1 mM $CaCl_2$, 1 mM $MgCl_2$, 5.6 mM glucose) containing 20 mM morpholinoetanesulfonic acid (MES) pH 6.0 while the basolateral compartment contained BSS complemented with 20 mM N-2-hydroxyethyl piperazine-N-4-butanesulfonic acid (HEPES), pH 7.4. The Fe(II)/ascorbate complex was freshly prepared as previously described (Ferruzza et al., 2003). During acute treatment, the permeability of the cell monolayer was monitored by measuring the trans-epithelial electrical resistance (TEER) at 37 °C, using a commercial apparatus (Millicell ERS, Millipore). At the end of the experiment, cells were washed with phosphate buffered saline containing 1 mM $CaCl_2$ and 1 mM $MgCl_2$ (PBS^{++}) and either immediately utilized to measure phenol red permeability, or transferred to complete culture medium in the incubator at 37 °C for 24 h to follow the late phase effects of Fe(II) treatment. Phenol red permeability was also measured at the end of late phase as previously described and expressed as apparent permeability (Papp) in cm/s (Ferruzza et al., 2003).

2.3. Cell imaging

For ZO-1 and claudin 4 localization, cells were processed by standard immunofluorescence techniques as previously described (Ferruzza et al., 2002). Briefly, ZO-1 and claudin 4 were localized on methanol-fixed cells with commercially available mouse monoclonal antibodies (antibody to ZO-1 clone 1A12 antibody to claudin 4 clone 3E2C1 respectively; Zymed Laboratories). Apoptotic cells were stained by immunofluorescence with a mouse monoclonal antibody against cytokeratine 18 fragments (clone M30, Roche Diagnostics) on methanol-fixed cells as previously described (Ranaldi et al., 2007). The secondary antibody utilized was Alexa Fluor 488 goat anti-mouse IgG (Invitrogen). For propidium iodide staining of necrotic cells, they were washed twice in PBS^{++}, treated for 5 min with 0.001% propidium iodide (Sigma–Aldrich) in PBS^{++}, washed again and fluorescence immediately viewed without mounting medium.

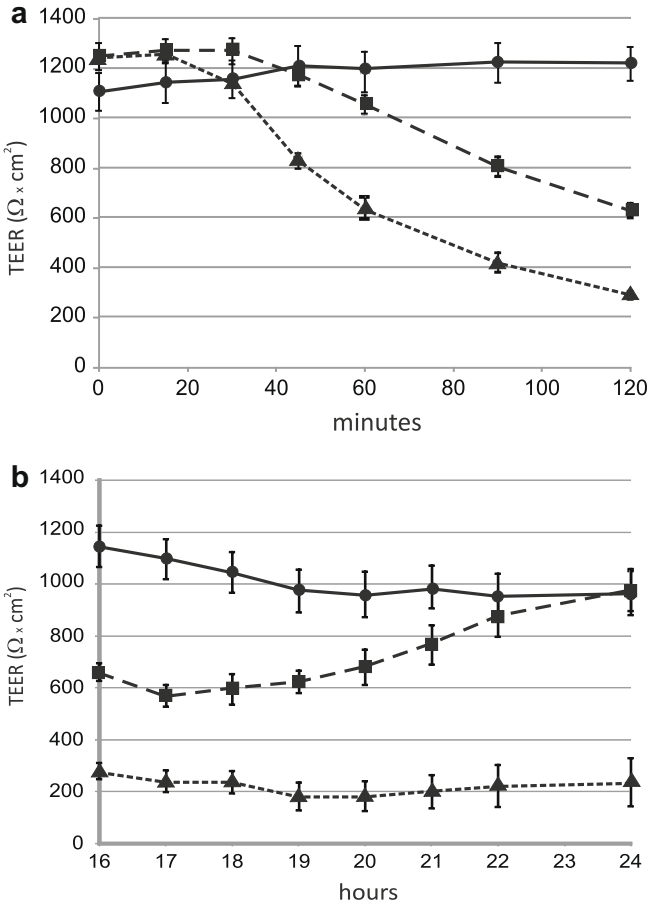

Fig. 1. Effects of Fe(II) exposure on tight junction permeability in Caco-2 cells. (a) Time course of TEER changes in Caco-2 cells treated from the apical side with 0, 15 and 50 μM Fe(II) for 2 h (acute phase). (b) Time course of TEER changes measured from 16 to 24 h after Fe(II) removal and transfer of the cells to complete medium (late phase). Data from a representative experiment performed in triplicate are shown as mean ± SD.

Table 1
Sequences of the primers and hydrolysis probes used for qRT-PCR of transcripts coding for ferritin heavy chain (FTH1), claudin 4 (CLDN4), heat shock protein 70 (HSPA1A), Mg-superoxide dismutase (SOD2), metallothionein 2A (MT2A) and glyceraldehyde-3-phosphate hydrogenase (GAPDH).

Gene symbol	Accession No.	Sense primer	Antisense primer	Hydrolysis probe
FTH1	NM_002032	GCCAGAACTACCACCAGGAC	ACATCATCGCGGTCAAAGTA	CCTGGAGC
CLDN4	NM_005073	TCCGCCAAGTATTCTGCTG	CGTGGCACCTTACACGTAGTT	CTGCTGCC
HSPA1A	NM_005345	AAGGACCGAGCTCTTCTCG	GCTCGGCTCTGAGATTGG	TCCAGTGT
SOD2	NM_000636	CTGGACAAACCTCAGCCCTA	TGATGGCTTCCAGCAACTC	TGGTGGAG
MT2A	NM_005953	CTCTAGCCGCCTCTTCAGC	ACTCTTTGCATTTGCAGGAAC	CTGCTCCT
GAPDH	NM_002046	AGCCACATCGCTCAGACA	GCCCAATACGACCAAATCC	TGGGGAAG

2.4. Electrophoretic mobility shift assay

Nuclear extracts of control and Fe(II)-treated cells were incubated with a radioactively labelled oligonucleotide probe which contains the specific recognition sequence for NF-κB (AGTTGAGGGGACTTTCCCAGG). Specificity of the binding was tested by adding a 10-fold excess of unlabelled cold probe as non-specific competitor DNA in the sample treated with 50 μM Fe(II) using standard conditions (25 mM Hepes pH 8, 0.5 mM EDTA, 0.5 mM DTT, 1% Nonidet P-40, 4 mM NaCl, 20% (v/v) glycerol, and 0.2 μg of poly(dI-dC). Samples were separated on a non-denaturating polyacrylamide gel and bands were detected by autoradiography.

2.5. Gene expression analysis

Total cell RNA was isolated using silica columns (NucleoSpin RNA II, Macherey-Nagel) and its quality checked using a Bioanalyzer 2100 (Agilent Technologies). The RNA was retro-transcribed using standard conditions and the cDNA was then subjected to real time PCR analysis with an Applied Biosystems 7900HT thermal cycler, using the FastStart Universal Probe Master Mix (Roche Diagnostics) and the sequence specific primers and hydrolysis probes from the Universal Probe Library (Roche Diagnostics), as described in Table 1. The different gene expression data were normalized using the GAPDH expression values.

2.6. Data presentation and statistical analysis

Data presented in Figs. 1 and 2 were analyzed by one–way ANOVA followed by Tukey's post-hoc test to determine significant differences among the means (STATISTICA for Windows software, Stat.Soft. Inc.). The significance of expression data (Fig. 5b) were analyzed by a two tailed paired *t*-test on the normalized threshold cycle value (ΔCt), using the Prism GraphPad software. The standard deviation of ΔCt were incorporated into the fold-difference of gene expression as indicated in the Applied Biosystems 7900HT Manual cms042380.

3. Results

3.1. Effects of Fe(II) on tight junction permeability

The time course of TEER changes during Fe(II) treatment for 2 h (Fig. 1a) and from 16 to 24 h following Fe(II) removal and transfer of cells to complete medium (Fig. 1b) showed a gradual decrease in TEER during iron treatment that was more pronounced at 50 μM

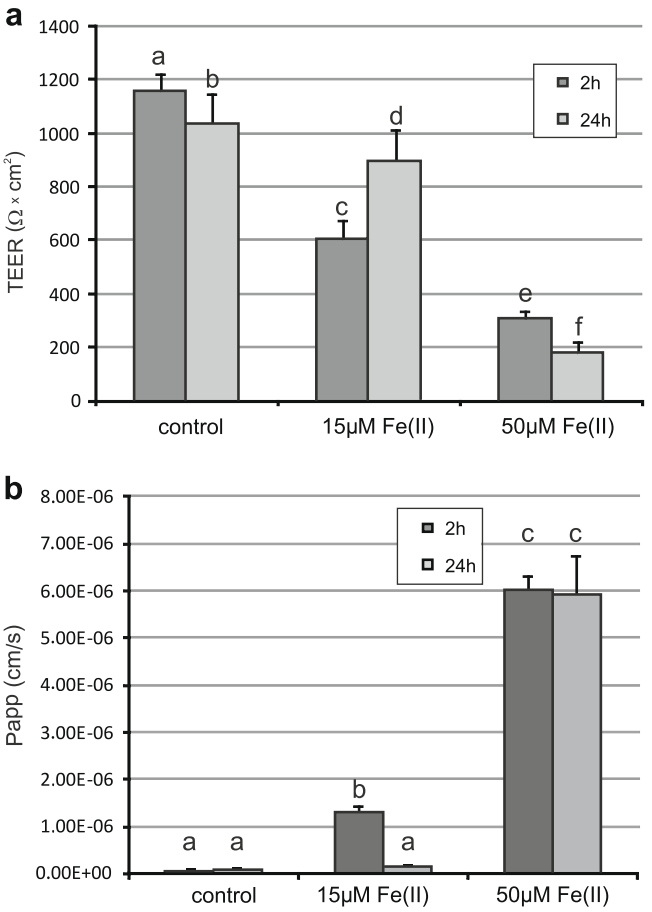

Fig. 2. Permeability of Caco-2 cells treated with Fe(II) measured by TEER (a) and phenol red Papp (b). (a) TEER values of cells treated with 0 (control), 15 and 50 μM Fe(II) after 2 h of treatment (end of acute phase) and after 24 h from Fe(II) removal and transfer to complete medium (end of late phase). Data are the mean ± SD of four experiments ($n = 14$). (b) Phenol red Papp of cells treated with 0, 15 and 50 μM Fe(II) after 2 h of treatment (end of acute phase) and after 24 h from Fe(II) removal and transfer to complete medium (end of late phase). Data are the mean ± SD of two experiments ($n = 6$). Different letters above error bars indicate significant ($P < 0.01$) differences between groups calculated by one way ANOVA followed by Tukey's post-hoc test.

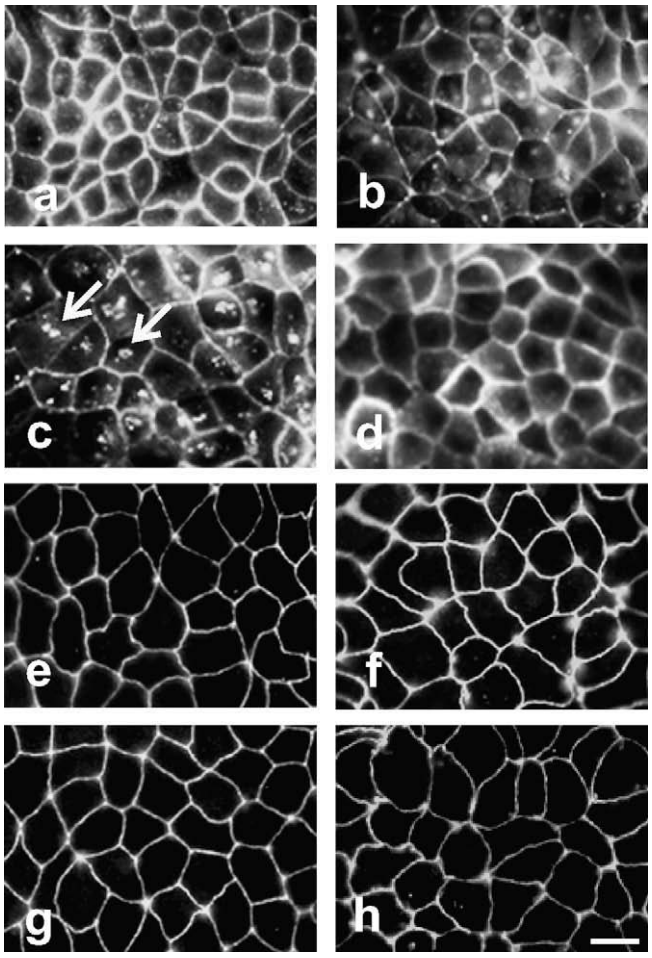

Fig. 3. Claudin 4 and ZO-1 localization in Caco-2 cells exposed to Fe(II). Immunofluorescence of claudin 4 (a–d) in untreated (control) cells (a) and in cells treated with 15 μM Fe(II) at the end of 2 h of acute treatment (b) and after 3 h (c), and 24 h (d) from Fe(II) removal. Arrows indicate cytoplasmic localization of claudin 4. Immunofluorescence of ZO-1 (e–h) in untreated (control) cells (e) and in cells treated with 15 μM Fe(II) at the end of acute treatment (f) and after 3 h (g), and 24 h (h) from Fe(II) removal. Scale bar: 20 μm.

than at 15 μM (Fig. 1a). Upon iron removal and transfer of the cells to complete culture medium for 24 h (late phase) (Fig. 1b), TEER values of cells treated with 15 μM gradually returned to the levels of control cells from 16 to 24 h, while they remained low in cells that had been treated with 50 μM (II). TEER values (Fig. 2a) and phenol red permeability (Fig. 2b) at the end of iron treatment and following transfer to complete medium for 24 h indicated a significant effect on TEER and Papp values after the 2 h of treatment at both iron concentrations, that was almost completely reversed during the 24 h of the late phase, but only in cells treated with 15 μM iron. At the end of the late phase, cells treated with 15 μM showed TEER values similar to control cells, even if still significantly different. Conversely, Papp values at the end of late phase were not statistically different from those measured in control cells. Taken together, all these results demonstrate that cells treated with 15 μM Fe (II) were able to recover during the late phase from the increased tight junction permeability caused by iron treatment during the acute phase. TEER and Papp values of cells treated with 50 μM Fe(II) cells were significantly different from those of control cells, both at the end of acute phase and at the end of the late phase, indicating that the damage occurring during the acute phase of iron treatment was irreversible and led to extensive cytotoxicity, apoptosis and necrosis.

3.2. Morphological effects of Fe(II) treatment

Treatments leading to changes in epithelial monolayer permeability are frequently associated with structural changes at the levels of the tight junctions and of the cytoskeleton. The localization of the tight junction proteins claudin 4 (Fig. 3a–d) and ZO-1 (Fig. 3e–h) was analyzed by immunofluorescence in cells treated with 15 μM Fe(II) at the end of the acute treatment and during the late phase (after 3 and 24 h following iron removal). Claudin 4 localization in control cells was restricted to the cell periphery (Fig. 3a) but it partially delocalized to an intracellular compartment, as shown by dot-like staining in the cytoplasm, after acute treatment with 15 μM Fe(II) (Fig. 3b) and after 3 h of the late phase (Fig. 3c). At the end of the late phase, claudin 4 localization was restored to the plasma membrane (Fig. 3d), similar to that of control cells. At the same time, another tight junction protein, ZO-1 did not change its plasma membrane localization after the treatment with 15 μM Fe(II), nor during the late phase compared to control cells (Fig. 3e–h). In cells treated with 50 μM Fe(II), claudin 4 internalization was also observed at the end of acute phase and this was accompanied by gross alterations to cell morphology as also shown by extensive F-actin disorganization (data not shown).

3.3. Cell death: apoptosis and necrosis after Fe(II) treatment

Only few sparse necrotic and apoptotic cells were detected at the end of the acute phase in cells treated with 15 μM Fe(II) (Fig. 4a and b) and their number remained stable during the late phase, up to 24 h after iron removal (Fig. 4c–h). Conversely, their number increased from the end of the acute phase (Fig. 3i and j) and during the late phase (Fig. 3 k–n) in cells treated with 50 μM Fe(II), leading at the end of the 24 h to massive necrosis, as shown by chromatin staining with propidium iodide of non-permeabilized cells (Fig. 3o).

3.4. Gene regulation in Caco-2 cells following Fe(II) treatment

Activation of the transcription factor NF-κB was detected by band shift assay performed using protein from nuclei collected from cells after the first 30 min of the acute phase. Treatment with Fe(II) for 30 min caused activation and migration of NF-κB to the nuclei (Fig. 5a), as shown by the increase in the amount of the protein bands identified as NF-κB in nuclear extracts of cells treated with both iron concentrations as compared to control untreated cells (Fig. 5a). The expression of mRNAs coding for a number of genes involved in response to stress and in iron metabolism was

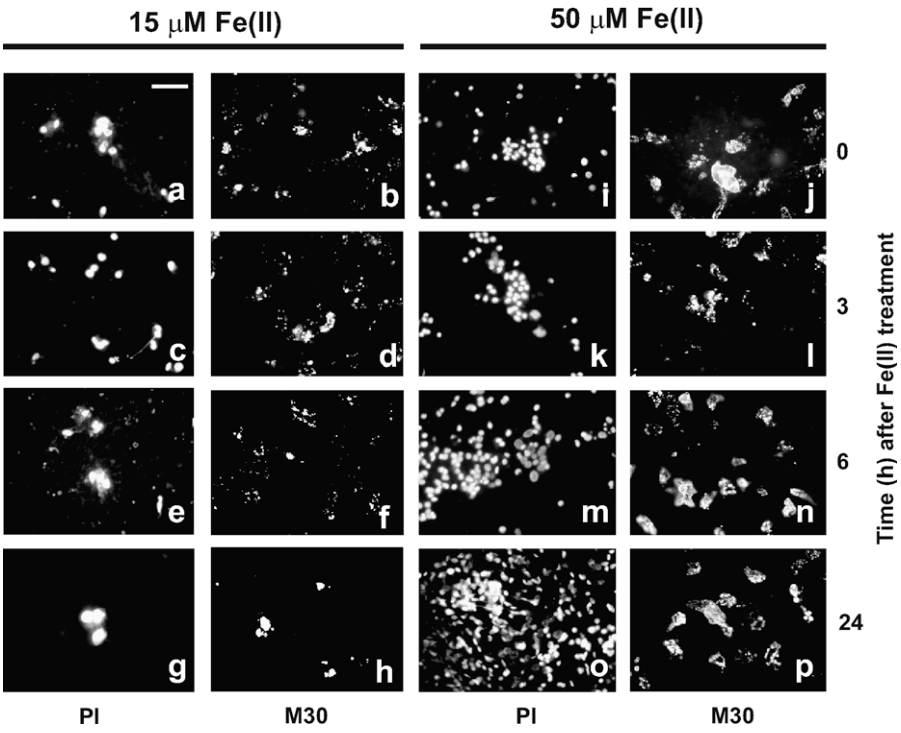

Fig. 4. Apoptosis and necrosis in Caco-2 cells exposed to Fe(II). Propidium iodide (PI) staining indicating necrosis, and cytokeratine 18 fragments (M30) immunofluorescence, indicating apoptosis, of cells treated with 15 μM Fe(II) (a–h) and 50 μM Fe(II) (i–p) at the end of acute treatment (a, b, i, j) and after 3 h (c, d, k, l), 6 h (e, f, m, n) and 24 h (g, h, o, p) from iron removal (late phase). Scale bar: 60 μm.

quantified by RT-PCR technique at the end of acute phase (Fig. 5b). The genes examined were chosen among those involved in cellular response to stress (HSPA1A and MT2A), in ROS detoxification (SOD2), in iron metabolism (FTH1) and in tight junction structure (CLDN4) (Fig. 5b). The expression of MT2A and HSPA1A showed the strongest induction among all the genes tested at both Fe(II) concentrations. FTH1 and SOD2 were also induced, but to a much lesser extent, and only in cells treated with 50 μM Fe(II). Claudin 4 gene expression did not change at both iron concentrations as compared to controls.

4. Discussion

To investigate the mechanisms involved in iron toxicity in human intestinal Caco-2 cells, two concentrations of Fe(II) were employed, one leading to recovery of tight junction integrity (15 μM for 2 h) and another leading to irreversible loss of barrier function and to cellular death (50 μM for 2 h). Both conditions led to an increase in tight junctions permeability of Caco-2 cells after the acute phase that was proportional to the dose applied, as shown by two independent assays: TEER (a measure of the paracellular conductance of the cell monolayer) and trans-epithelial passage of phenol red (a measure of paracellular permeability to small extracellular solutes). Changes in epithelial permeability represent an early and sensitive indicator of sub-lethal toxicity and TEER values and phenol red permeability are useful indicators of these changes *in vitro*. In the Caco-2 cell model, recovery of TEER values and restoration of paracellular permeability to control levels after removal of a toxic insult have been reported to depend upon dose and time of treatment for different types of stimuli including the heavy metals copper and iron (Ferruzza et al., 1999, 2003), ethanol (Catalioto et al., 2009), mycotoxins (Ranaldi et al., 2007), polycations (Ranaldi et al., 2002), and heat (Dokladny et al., 2006). Such changes in Caco-2 monolayer permeability have been shown to be accompanied by movement of the tight junction proteins claudins away from the plasma membrane to intracellular compartments as shown for claudin 1 in cells treated with the drug miltefosine (Menez et al., 2006), for claudin 4 in cells exposed to ochratoxin A (Lambert et al., 2007; Ranaldi et al., 2007). Claudin 7 delocalization was also observed in cultured monolayers of alveolar pneumocytes obtained from ethanol-treated rats (Fernandez et al., 2007). Such changes represent an early response to agents altering tight junction permeability and they and can be reversed upon removal of the inducing agent. Claudin 4 belongs to a family of trans-membrane proteins responsible for size- and charge-selectivity of epithelial tight junctions (Krause et al., 2008) and, along the intestine, it is predominantly expressed in the upper villi/surface (Holmes et al., 2006). The data presented indicate that claudin 4 movement during iron treatment and its return to the plasma membrane did not require *de novo* transcription of its gene CLDN4 and was concomitant to almost complete restoration of monolayer permeability. On the other hand, the irreversible delocalization of claudin 4 accompanied by extensive F-actin disorganization after treatment with 50 mM Fe(II) is likely to have been due to the occurrence of progressive cytotoxicity during the late phase, as clearly indicated by the large number of apoptotic (M30 staining) and of necrotic (PI staining) cells (Fig. 4).

In addition to the morphological changes accompanying alteration of the permeability of the cell monolayer, a strong induction of MT2A gene upon iron treatment was observed at both concentrations employed. Metallothioneins are small cystein-rich proteins that can be induced by both heavy metals and oxidative stress (Andrews, 2000) and act by scavenging ROS in a similar way to reduced glutathione (Thornalley and Vasàk, 1985), thus playing an important role in the prevention of oxidative damage. A role for MT2A in anti-oxidative defence is suggested by a study reporting that over-expression of metallothionein 2A isoform in Hela cells treated with rotenone to elicit increased ROS production, improved cell viability, reducing or delaying apoptosis (Reinecke et al., 2006). Another gene that was strongly induced upon iron treatment was HSPA1A, coding for Hsp70, a protein, that responds to heat and oxidative stress (Gebhardt et al., 1999) and to heavy metals like cadmium (Kusakabe et al., 2008). Hsp70 over-expression in MDCK cells was shown to reduce oxidative stress by enhancing the activity of the anti-oxidative enzymes glutathione peroxidase and reductase (Guo et al., 2007). A protective role of

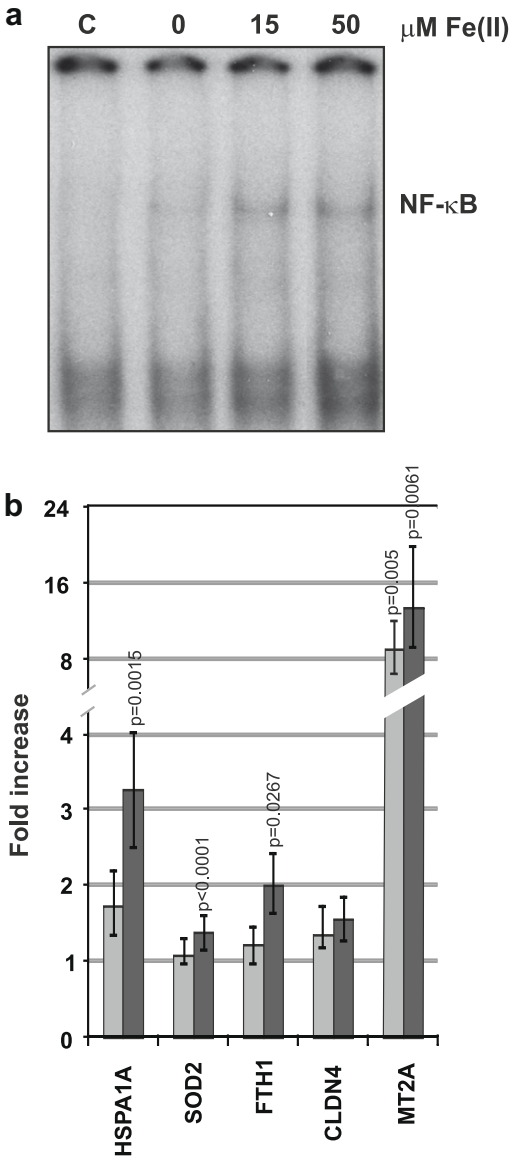

Fig. 5. Gene regulation and expression in Caco-2 cells exposed to Fe(II). (a) Electrophoretic mobility shift assay of the transcriptional factor NF-κB after 30 min of control (lane 0) 15 μM (lane 15) and 50 μM (lane 50) Fe(II) treatment. Lane C shows the 50 μM Fe(II) nuclear extract with a 10-fold excess of unlabelled probe. (b) Gene expressions measurement by qRT-PCR of heat shock protein 70 (HSPA1A), manganese superoxide dismutase (SOD2), ferritin heavy chain (FTH1), claudin 4 (CLDN4) and metallothionein 2A (MT2A) at the end of 2 h of 15 and 50 μM Fe(II) treatment. For each gene, grey and dark bars represent, respectively, the gene-expression fold increase of 15 and 50 μM Fe(II)-treated cells relative to control cells. The data represent the average of four different measurements and the *P*-values above the bars indicate the significance of gene increase versus control and were calculated by a two tailed paired *t*-test using the normalized threshold cycle value (ΔCt). The error bars were calculated as indicated in Section 2.

heat shock proteins from conditions altering tight junction permeability was also suggested in a study of Caco-2 cells exposed to a moderate increase in temperature (Dokladny et al., 2006). The induction of MT2A and HSPA1A genes may thus have contributed to the ability of Caco-2 cells to recover from the effects of 15 μM Fe(II) treatment.

After 30 min of the acute phase, the ROS sensitive transcription factor NF-κB was translocated to the nuclei of cells treated with both iron concentrations. This transcription factor has been reported to trigger two opposite cellular responses to ROS: to survive or to succumb (Papa et al., 2004). In fact, NF-κB activation can stimulate cell death by apoptosis (Perkins and Gilmore, 2006), enhancing the role of ROS in the induction of cell damage (Haddad, 2004). Activation of NF-κB in Caco-2 cells has also been implicated in cytoskeletal derangements associated to barrier dysfunction after oxidant-induced iNOS upregulation (Banan et al., 2004) or ethanol treatment (Banan et al., 2007). On the other hand, the pro-survival action of NF-κB can act through ROS suppression, with a key role played by upregulation of SOD2 and FTH1 (Bubici et al., 2006). However, in our study, upregulation of SOD2 and FTH1, genes that are transcriptionally controlled by NF-κB, was only observed after treatment with 50 μM Fe(II), a condition that led to apoptosis and necrosis. It has to be pointed out that the lack of recovery and survival after treatment with 50 μM Fe(II), despite a strong induction of genes coding for potentially protective proteins, may have been due to the inability of the cells to proceed to protein synthesis and expression of their protective functions given the early onset of apoptosis and necrosis.

In conclusion, the induction of HSPA1A and MT2A could have contributed to the defence from iron-induced oxidative stress, enabling cells to survive to treatment with 15 μM Fe(II) and re-establish tight junction function. An irreversible temporal checkpoint for redox recovery has previously been suggested in Caco-2 cells beyond which prevention of the progression of apoptosis to its biological end point cannot be stopped (Wang et al., 2000). This would further support the inability to recover after treatment with the higher iron concentration, where the strong induction of genes involved in oxidative defence was unable to stop progression to overt cytotoxicity and cell death.

Acknowledgement

This work has been supported by European Union, EU FP6 Project "LIINTOP" Contract No. LSHB-CT-2006-037499.

References

Andrews, G.K., 2000. Regulation of metallothionein gene expression by oxidative stress and metal ions. Biochemical Pharmacology 59, 95–104.

Banan, A., Zhang, L.J., Shaikh, M., Field, J.Z., Farhadi, A., Keshavarzian, A., 2004. Novel effect of NF-kappaB activation: carbonylation and nitration injury to cytoskeleton and disruption of monolayer barrier in intestinal epithelium. American Journal of Physiology, Cell Physiology 287, C1139–C1151.

Banan, A., Keshavarzian, L., Zhang, L., Shaikh, M., Forsyth, C.B., Tang, Y., Fields, J.Z., 2007. NF-kB activation as a key mechanism in ethanol-induced disruption of the F-actin cytoskeleton and monolayer barrier integrity in intestinal epithelium. Alcohol 41, 447–460.

Bubici, C., Papa, S., Dean, K., Franzoso, G., 2006. Mutual cross-talk between reactive oxygen species and nuclear factor-kappa B: molecular basis and biological significance. Oncogene 25, 6731–6748.

Catalioto, R.M., Festa, C., Triolo, A., Altamura, M., Maggi, C.A., Giuliani, S., 2009. Journal of Pharmaceutical Sciences 98, 713–727.

Dokladny, K., Moseley, P.L., Ma, T.Y., 2006. Physiologically relevant increase in temperature causes an increase in intestinal epithelial tight junction permeability. American Journal of Physiology, Gastrointestinal Liver Physiology 290, G204–G212.

Fernandez, A.L., Koval, M., Fan, X., Guidot, D.M., 2007. Chronic alcohol ingestion alters claudin expression in the alveolar epithelium of rats. Alcohol 41, 371–379.

Ferruzza, S., Scarino, M.L., Rotilio, G., Ciriolo, M.R., Santaroni, P., Onetti-Muda, A., Sambuy, Y., 1999. Copper treatment alters the permeability of tight junctions in cultured human intestinal Caco-2 cells. American Journal of Physiology, Gastrointestinal Liver Physiology 277, G1138–G1148.

Ferruzza, S., Scacchi, M., Scarino, M.L., Sambuy, Y., 2002. Iron and copper alter tight junction permeability in human intestinal Caco-2 cells by distinct mechanisms. Toxicology In Vitro 16, 399–404.

Ferruzza, S., Scarino, M.L., Gambling, L., Natella, F., Sambuy, Y., 2003. Biphasic effect of iron on human intestinal Caco-2 cells: early effect on tight junction permeability with delayed onset of oxidative cytotoxic damage. Cellular and Molecular Biology 49, 89–99.

Gebhardt, B.R., Ries, J., Caspary, W.F., Boehles, H., Stein, J., 1999. Superoxide: a major factor for stress protein induction in reoxygenation injury in the intestinal cell line Caco-2. Digestion 60, 238–245.

Guo, S., Wharton, W., Moseley, P., Shi, H., 2007. Heat shock protein 70 regulates cellular redox status by modulating glutathione-related enzyme activities. Cell Stress Chaperones 12, 245–254.

Haddad, J.J., 2004. Redox and oxidant-mediated regulation of apoptosis signaling pathways: immuno-pharmaco-redox conception of oxidative siege versus cell death commitment. International Immunopharmacology 4, 475–493.

Hentze, M.W., Muckenthaler, M.U., Andrews, N.C., 2004. Balancing acts: molecular control of mammalian iron metabolism. Cell 117, 285–297.

Holmes, J.L., Van Itallie, C.M., Rasmussen, J.E., Anderson, J.M., 2006. Claudin profiling in the mouse during postnatal intestinal development and along the gastrointestinal tract reveals complex expression patterns. Gene Expression Patterns 6, 581–588.

Krause, G., Winkler, L., Mueller, S.L., Haseloff, R.F., Piontek, J., Blasig, I.E., 2008. Structure and function of claudins. Biochimica et Biophysica Acta 1778, 631–645.

Kusakabe, T., Nakajima, K., Nakazato, K., Suzuki, K., Takada, H., Satoh, T., Oikawa, M., Arakawa, K., Nagamine, T., 2008. Changes of heavy metal, metallothionein and heat shock proteins in Sertoli cells induced by cadmium exposure. Toxicology In Vitro 22, 1469–1475.

Lambert, D., Padfield, P.J., McLaughlin, J., Cannell, S., O'Neill, C.A., 2007. Ochratoxin A displaces claudins from detergent resistant membrane microdomains. Biochemical and Biophysical Research Communications 358, 632–636.

Menez, C., Buyse, M., Chacun, H., Farinotti, R., Barratt, G., 2006. Modulation of intestinal barrier properties by miltefosine. Biochemical Pharmacology 71, 486–496.

Nchito, M., Friis, H., Michaelsen, K.F., Mubila, L., Olsen, A., 2006. Iron supplementation increases small intestine permeability in primary schoolchildren in Lusaka, Zambia. Transactions of the Royal Society of Tropical Medicine and Hygiene 100, 791–794.

Papa, S., Zazzeroni, F., Pham, C.G., Bubici, C., Franzoso, G., 2004. Linking JNK signaling to NF-kappaB: a key to survival. Journal of Cell Science 117, 5197–5208.

Perkins, N.D., Gilmore, T.D., 2006. Good cop, bad cop: the different faces of NF-kappaB. Cell Death and Differentiation 13, 759–772.

Puntarulo, S., 2005. Iron, oxidative stress and human health. Molecular Aspects of Medicine 26, 299–312.

Ranaldi, G., Marigliano, I., Vespignani, I., Perozzi, G., Sambuy, Y., 2002. The effect of chitosan and other polycations on tight junction permeability in the human intestinal Caco-2 cell line. Journal Nutritional Biochemistry 13, 157–167.

Ranaldi, G., Mancini, E., Ferruzza, S., Sambuy, Y., Perozzi, G., 2007. Effects of red wine on ocratoxin A toxicity in intestinal Caco-2/TC7 cells. Toxicology In Vitro 21, 204–210.

Reinecke, F., Levanets, O., Olivier, Y., Louw, R., Semete, B., Grobler, A., Hidalgo, J., Smeitink, J., Olckers, A., Van der Westhuizen, F.H., 2006. Metallothionein isoform 2A expression is inducible and protects against ROS-mediated cell death in rotenone-treated HeLa cells. Biochemical Journal 395, 405–415.

Sambuy, Y., De Angelis, I., Ranaldi, G., Scarino, M.L., Stammati, A., Zucco, F., 2005. The Caco-2 cell line as a model of the intestinal barrier: influence of cell and culture-related factors on Caco-2 cell functional characteristics. Cell Biology and Toxicology 21, 1–26.

Sharp, P., Srai, S.K., 2007. Molecular mechanisms involved in intestinal iron absorption. World Journal of Gastroenterology 13, 4716–4724.

Tapiero, H., Gate, L., Tew, K.D., 2001. Iron: deficiencies and requirements. Biomedicine and Pharmacotherapy 55, 324–332.

Thornalley, P.J., Vasàk, M., 1985. Possible role for metallothionein in protection against radiation-induced oxidative stress. Kinetics and mechanism of its reaction with superoxide and hydroxyl radicals. Biochimica et Biophysica Acta 827, 36–44.

Wang, T.G., Gotoh, Y., Jennings, M.H., Rhoads, C.A., Aw, T.Y., 2000. Lipid hydroperoxide-induced apoptosis in human colonic Caco-2 cells is associated with an early loss of cellular redox balance. FASEB Journal 14, 1567–1576.